

AD-A063 306

UNIVERSAL ENERGY SYSTEMS INC DAYTON OHIO

F/G 20/10

EXPERIMENTAL MEASUREMENTS OF CUMULATIVE EXCITATION AND IONIZATION--ETC(U)

DEC 77 M L LAKE

F33615-75-C-1082

AFAPL-TR-77-84

NL

UNCLASSIFIED

1 OF 2

AD
A063306



AFAPL-TR-77-84

②

LEVEL

DDC
RECEIVED
JAN 16 1979
C

AD A063306

DDC FILE COPY

EXPERIMENTAL MEASUREMENTS OF CUMULATIVE EXCITATION AND IONIZATION IN ATOMIC AND MOLECULAR GASES

MAX L. LAKE

*UNIVERSAL ENERGY SYSTEMS, INC.
3195 PLAINFIELD ROAD
DAYTON, OHIO 45432*

DECEMBER 1977

TECHNICAL REPORT AFAPL-TR-77-84
Final Report for Period 9 December 1974 – 16 May 1977

Approved for public release; distribution unlimited.

AIR FORCE WRIGHT AERONAUTICAL LABORATORIES
AIR FORCE SYSTEMS COMMAND
AIR FORCE AERO PROPULSION LABORATORY
WRIGHT-PATTERSON AIR FORCE BASE, OHIO 45433

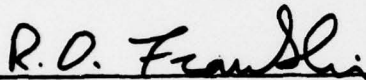
169 01 10 007

NOTICE

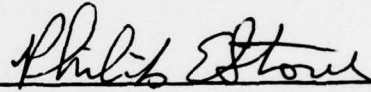
When Government drawings, specifications, or other data are used for any purpose other than in connection with a definitely related Government procurement operation, the United States Government thereby incurs no responsibility nor any obligation whatsoever; and the fact that the government may have formulated, furnished, or in any way supplied the said drawings, specifications, or other data, is not to be regarded by implication or otherwise as in any manner licensing the holder or any other person or corporation, or conveying any rights or permission to manufacture, use, or sell any patented invention that may in any way be related thereto.

This report has been reviewed by the Information Office (OI) and is releasable to the National Technical Information Service (NTIS). At NTIS, it will be available to the general public, including foreign nations.

This technical report has been reviewed and is approved for publication.



RICHARD D. FRANKLIN, Capt, USAF
Project Engineer



PHILIP E. STOVER
Chief, High Power Branch

FOR THE COMMANDER



JAMES D. REAMS
Chief, Aerospace Power Division

"If your address has changed, if you wish to be removed from our mailing list, or if the addressee is no longer employed by your organization please notify AFAPL/POD-2, W-PAFB, OH 45433 to help us maintain a current mailing list".

Copies of this report should not be returned unless return is required by security considerations, contractual obligations, or notice on a specific document.

SECURITY CLASSIFICATION OF THIS PAGE (When Data Entered)

REPORT DOCUMENTATION PAGE		READ INSTRUCTIONS BEFORE COMPLETING FORM
1. REPORT NUMBER 18 AFAPL-TR-77-84	2. GOVT ACCESSION NO.	3. RECIPIENT'S CATALOG NUMBER
4. TITLE (and Subtitle) 6 EXPERIMENTAL MEASUREMENTS OF CUMULATIVE EXCITATION AND IONIZATION IN ATOMIC AND MOLECULAR GASES	5. TYPE OF REPORT & PERIOD COVERED 9 Final Report. 9 Dec 74 - 16 May 77	
7. AUTHOR(s) 10 Max L./Lake	8. CONTRACT OR GRANT NUMBER(s) 15 F33615-75-C-1082	
9. PERFORMING ORGANIZATION NAME AND ADDRESS Universal Energy Systems, Inc. 3195 Plainfield Road Dayton, Ohio 45432	10. PROGRAM ELEMENT, PROJECT, TASK AREA & WORK UNIT NUMBERS 16 2301-52-78 17 52	
11. CONTROLLING OFFICE NAME AND ADDRESS Air Force Aero Propulsion Laboratory (POD) Air Force Systems Command Wright-Patterson AFB, Ohio 45433	12. REPORT DATE 1 December 1977	
14. MONITORING AGENCY NAME & ADDRESS (if different from Controlling Office) 12 125p	13. NUMBER OF PAGES 123	
15. SECURITY CLASS. (of this report) Unclassified		15a. DECLASSIFICATION/DOWNGRADING SCHEDULE
16. DISTRIBUTION STATEMENT (of this Report) Approved for Public Release; Distribution Unlimited		
17. DISTRIBUTION STATEMENT (of the abstract entered in Block 20, if different from Report)		
18. SUPPLEMENTARY NOTES		
19. KEY WORDS (Continue on reverse side if necessary and identify by block number) Cross Section Excitation from Metastable States Two Step Excitation Electron Impact Excitation Cumulative Excitation		
20. ABSTRACT (Continue on reverse side if necessary and identify by block number) This work described an experimental effort to determine the electron collision excitation and ionization cross sections of metastable atoms and molecules. The ionization cross section measurements were not successful. Excitation cross section studies were productive, and a number of direct and two-step cross sections were obtained. Measurements of several direct excitation cross sections of xenon in the range from 6000 Å to 9000 Å were made. These relative excitation functions compare favorably to data in the literature where it exists, and offer some insight to the lasing processes of the 5d levels.		

DD FORM 1 JAN 73 1473 EDITION OF 1 NOV 65 IS OBSOLETE

SECURITY CLASSIFICATION OF THIS PAGE (When Data Entered)

390 743 79 01 15 007

Gu

Measurements on the cross sections from the helium 2^3S state to the 3^3S , 3^3P , 3^3D , 4^3S , and 4^3D states were obtained. Results indicate that the 3^3D level has the largest cross section. The apparent $Q_{2^3S \rightarrow 3^3D}$ is $1.6 \times 10^{-15} \text{ cm}^2$ at 21 eV, as compared to Flannery's calculations for the level $Q_{2^3S \rightarrow 3^3D}$ of $3.5 \times 10^{-16} \text{ cm}^2$ at 20 eV by the Eikonal method. Evidence for the existence of the two-step cross section in Krypton has also been observed, but there is insufficient direct cross section data available to estimate the magnitude of the two-step process. An experimental investigation was performed to determine the cross sections of the relevant transitions. Excitation functions of several $5p$, $6p$, $7s$ and $5d$ states of Krypton have been measured.

ACCESSION for	Write Section	<input checked="" type="checkbox"/>
NTIS	Write Section	<input type="checkbox"/>
DDC	Write Section	<input type="checkbox"/>
UNANNOUNCED		
DATE		
BY	DISTRIBUTION/AVAILABILITY CODES	
	SPECIAL	

A

TABLE OF CONTENTS

SECTION		PAGE
I	INTRODUCTION.	1
II	CUMULATIVE EXCITATION-IONIZATION.	7
	1. Cross Section Formula.	7
	2. Linearity Tests.	11
	3. Ion Collection Efficiency.	15
	4. Results.	16
	5. Conclusions.	30
III	EXCITATION OF XENON SINGLE ELECTRON IMPACT.	36
	1. Background.	36
	2. Results.	39
IV	TWO-STEP EXCITATION IN HELIUM.	52
	1. Two Beam Experiment.	52
	2. Experimental Technique.	52
	3. Results.	58
	4. Modifications.	58
	5. Linearity Tests and Sources for Misinterpretation.	62
	6. Single Beam Experiment.	71
V	EXCITATION OF KRYPTON BY SINGLE ELECTRON IMPACT.	83
	1. Background.	83
	2. Results.	85
	3. Calibration of the Optical Detection System.	101
	REFERENCES.	112

LIST OF ILLUSTRATIONS

FIGURE		PAGE
1	Electron Beams	4
2	Crossed Beam System Components	6
3	Crossed Beam Device.	10
4	Signal vs. Current	13
5	Direct Ionization Cross Section of Helium.	17
6	Helium Ionization Cross Section.	18
7	Ionization Function and In-phase Signal Below Threshold.	19
8	Helium Metastable Excitation Function.	20
9	Helium Metastable Excitation Function.	21
10	Helium Metastable Excitation Function.	22
11	N ₂ Metastable Excitation Function	24
12	N ₂ Metastable Excitation Function.	25
13	Total Metastable Excitation Function in Neon	27
14	Xenon Metastable Excitation Function	28
15	Xenon Metastable Signal in Selected Channels	31
16	Xenon Metastable Excitation Function	32
17	Xenon Excitation Function as a Function of Pressure.	33
18	N ₂ Metastable Excitation Function at 10Khz Chopping Frequency.	34
19	Quantum Efficiency of Detection System vs. Wavelength	41
20	Xe 8819Å 6s[3/2] ₂ - 6p[3/2] ₃	45
21	Xe 8231Å 6s[3/2] ₂ - 6p[3/2] ₂	46
22	Xe 7336Å 6p[5/2] ₂ - 5d'[5/2] ₃	47

FIGURE		PAGE
23	Xe 8346Å 6s'[1/2] ₁ - 6p'[3/2] ₂	48
24	Xe 8280Å 6s[3/2] ₁ - 6p[1/2] ₀	49
25	Xe 7887Å 6s'[1/2] - 6p[1/2] ₀	50
26	Energy Level Diagram of Xenon	51
27	Comparison of Raw Two-Step Excitation Data With the Function of the Electron Gun Current vs. Accelerating Voltage.	54
28	Helium 2 ³ S → 3 ³ N	59
29	Modification of Electron Gun.	61
30	Helium 3889Å.	64
31	Helium 3889Å.	66
32	Beam Current vs. Energy	67
33	Helium 3889Å.	68
34	Voltage Configuration of Electron Beam.	70
35	Helium 3889Å.	72
36	Helium 3889Å.	73
37	Excitation Function of the He 4471Å (4 ³ D → 2 ³ P) Line.	75
38	Apparent 2 ³ S → 3 ³ P Cross Section of This Experiment Com- pared to the Level Cross Sections of Flannery and McCann Using the Eikonal Approximation and of Flannery et al. Using the Born and VPS Approximations	80
39	Apparent 2 ³ S → 3 ³ D Cross Section of This Experiment Com- pared to the Level Cross Sections of Flannery and McCann Using the Eikonal Approximation and of Flannery et al. Using the Born and VPS Approximations	81
40	Electron Impact Cross Sections.	84
41	Energy Levels in Krypton.	86
42	Fel'tsan Data	87

FIGURE		PAGE
43	Kr 8508 $5p'[3/2]_1 \rightarrow 5s'[1/2]$	88
44	Kr 8263 $5p'[3/2]_2 \rightarrow 5s'[1/2]_1$	89
45	Kr 5871 $5p'[3/2]_2 \rightarrow 5s[3/2]_1$	91
46	Kr 5570 $5p'[1/2]_1 \rightarrow 5s[3/2]_2$	92
47	Kr 8112 $5p[5/2]_3 \rightarrow 5s[3/2]_2$	93
48	Kr 8298 $5p[3/2]_1 \rightarrow 5s[3/2]_1$	94
49	Kr 8190 $5p[3/2]_2 \rightarrow 5s[3/2]_1$	95
50	Kr 8776 $5p[5/2]_2 \rightarrow 5s[3/2]_1$	96
51	Krypton Measurements by Fel'tsan	97
52	Kr 7982 $7s[3/2]_2 \rightarrow 5p[3/2]_2$	99
53	Kr 7913 $5d[1/2]_1 \rightarrow 5p[1/2]_1$	100
54	Kr 4812 $4f[3/2]_1 \rightarrow 5s_1[1/2]_0$	102
55	Spectral Radiance of the Standard Lamp	109
56	Spectral Sensitivity of the Optical Detection System . .	110

LIST OF TABLES

TABLE		PAGE
1	Relative Cross Sections in Xenon.	42
2	Comparison of Apparent Cross Sections of This Experiment with Apparent Cross Sections Constructed from the Born Approximation Values of Ton That et al. . .	77
3	Relative Intensity of Krypton Lines at 20 eV (This Experiment)	103
4	Fel'tsan Data	106

ACCESS for	
NTIS	<input checked="" type="checkbox"/>
DOC	<input type="checkbox"/>
UNCLASSIFIED	<input type="checkbox"/>
J. B. HANLEY	
DISTRICT ADMINISTRATIVE SERVICES	
OFF. OF CIVIL	
A	

SUMMARY

This work describes an experimental effort to determine the electron collision excitation ionization cross sections of metastable atoms and molecules using a dual electron beam apparatus. In this experiment, the first electron beam was used to produce the metastables, and the second was used to excite or ionize the metastables. Cross sections are inferred from decay radiation or from a determination of the ions produced. Although the ionization cross section measurements were not immediately successful, excitation cross section studies were productive, and a number of direct and two-step cross sections were obtained.

Measurements of several direct excitation cross sections of xenon in the range from 6000\AA to 9000\AA were made. These relative excitation functions compare favorably to data in the literature where it exists, and offer some insight into the lasing processes of the $5d$ levels.

Effects of cumulative excitation from the helium 2^3S state were observed in decay radiation from the helium 3^3P state. Analysis of this data and a comparison of the inferred $2^3S - 3^3P$ cross section with theory was performed. By assuming that the ratio of metastables to neutrals in the molecular beam when it encounters the second electron beam is the same as in the first (metastable creating) beam, a lower limit on the cross section for the $2^3S \rightarrow 3^3P$ states was obtained. The value obtained was an order of magnitude lower than the theoretical predictions. Subsequent work proved this assumption to be poor, however.

The electron guns in the crossed beam system were then modified to yield an improvement in the signal-to-noise ratio of a factor of ten over the signal to noise ratio before modification.

A parameter study of the electron guns in the crossed beam system was performed. Results indicated that the system will operate in the conditions for highest sensitivity without fear of spurious signal only if limits on the voltage of certain electron gun elements are observed.

Measurements on the cross sections from the helium 2^3S state were then extended to the 3^3S , 3^3P , 3^3D , 4^3S , and 4^3D states. Results indicate that the 3^3D level has the largest cross section. The apparent $Q_{2^3S \rightarrow 3^3D}$ is $1.6 \times 10^{-15} \text{ cm}^2$ at 21 eV, as compared to Flannery's calculations for the level $Q_{2^3S \rightarrow 3^3D}$ of $3.5 \times 10^{-16} \text{ cm}^2$ at 20 eV by the Eikonal method. Evidence for the existence of the two-step cross section in krypton has also been observed, but there is insufficient direct cross section data available to estimate the magnitude of the two-step process. An experimental investigation was performed to determine the cross sections of the relevant transitions. Excitation functions of several 5p, 6p, 7s and 5d states have been measured.

The absolute spectral sensitivity of the crossed beam optical detection system was measured over the range from 5500\AA to 9200\AA . This spectral region contains a majority of the most prominent transitions in krypton, and the spectral sensitivity measurement enabled the previously measured cross sections in krypton to be placed on an relative scale.

SECTION I

INTRODUCTION

This work is a continuation of an effort at the U.S. Air Force Aerospace Research Laboratory, and subsequently at the Aero Propulsion Laboratory, aimed at measuring electron impact excitation and ionization cross sections of atoms and molecules which are in excited states. Although a large body of information exists for electron impact excitation and ionization of atoms and molecules in the ground state,¹ relatively little is known about the cross sections of atoms or molecules in excited states. Since a significant fraction of the atoms or molecules in a plasma are in excited states it is necessary to consider the influence of the excited state constituents on the characteristics of the plasma. In a low density plasma, a majority of the excited states will decay in a time much shorter than the reciprocal of the average collision frequency, so that ground state cross sections offer an accurate description of energy channeled into short-lived states. However, the metastable states in general have lifetimes longer than the average time between collisions with either electrons or other atoms, so that this channel of energy transfer must be considered further. The metastable states are much closer to the ionization threshold than the ground state, and in addition, have a different quantum configuration than the ground state. Two observations may therefore be made. First, the metastables may be ionized by a collision with an electron of much lower energy than that which would be required to ionize a ground state atom. Consequently the ionization rate for many gases can be governed by the ionization cross section of the

metastable specie. Second, the probability for a transition from one state to another state depends on the quantum configurations of both the initial and final states. As a result the dominant channels of energy transfer from metastable levels to other excited states could be radically different from the dominant transitions from ground state atoms to those same excited states. These two observations lead to the conclusion that the fundamental characteristics of a plasma may change in the case where substantial metastable atom or molecule densities may develop, and further, in order to accurately model plasmas of this nature, an accounting of the ionization and excitation cross sections from metastable levels must be made.

The first measurements of cross sections for collisions of electrons with excited atoms were for superelastic collisions with metastable Hg atoms. These were performed in 1930 by Latyscheff and Leipunsky.² In 1953 Phelps and Molnar³ measured the cross section for $\text{He } 2^1\text{S} \rightarrow 2^3\text{S}$ by electron impact using an absorption technique applied to a helium microwave discharge afterglow. A measurement of the total cross section of the $\text{He } 2^3\text{S}$ metastable was made by Neynaber et al.⁴ in 1964, and a measurement of the relative shape of the helium $2^3\text{S} \rightarrow 3^3\text{P}$ cross section was made in 1974 by Mityureva and Penkin.⁵ No absolute measurements of the cross section from metastable states to upper levels other than this work are known to exist. Somewhat more attention has recently been given to measurements of the ionization cross section of metastable atoms. Fite and Brackman⁶ reported a measurement of the ionization cross section of helium metastable levels in 1963, as did Vriens et al.⁷ in 1968, Koller⁸ in 1969,

Long and Geballe⁹ in 1970, Shearer-Izumi and Botter¹⁰ in 1974, and Dixon et al.¹¹ in 1976. The earlier of these measurements were limited by the small ratio of metastables-to-neutrals to the energy region below the ionization threshold, and the results differed widely among themselves. The more recent papers (Long and Geballe, Dixon et al.) show reasonable agreement with each other and with recent theoretical calculations (Ton That et al.¹²).

This experiment employs a dual electron beam device which perpendicularly intercepts a neutral particle beam of thermal energy (room temperature). The apparatus is described in detail in P.D. Tannen's Ph.D. dissertation,¹³ and, with the exception of any significant modifications, will receive only a brief description here.

In the experiment, the first electron beam is set to have an energy only sufficient to excite the lowest metastable level of the subject atom or molecule (see Figure 1). Metastables so produced flow out of the first electron beam and into the second electron beam where they may be excited to higher levels or ionized by electrons with energies much lower than the threshold energy for direct excitation of ionization. One of the electron beams is modulated so that any signal arising from this two-step process is modulated. In this way noise picked up by the detection system may be discriminated against.

Signals may be detected as decay radiation from the excited states, or by the collection of ions by a charged particle counter. The signals are amplified and recorded by an SSR dual channel counting system (see Figure 2). The crossed beam apparatus features high stability electronics

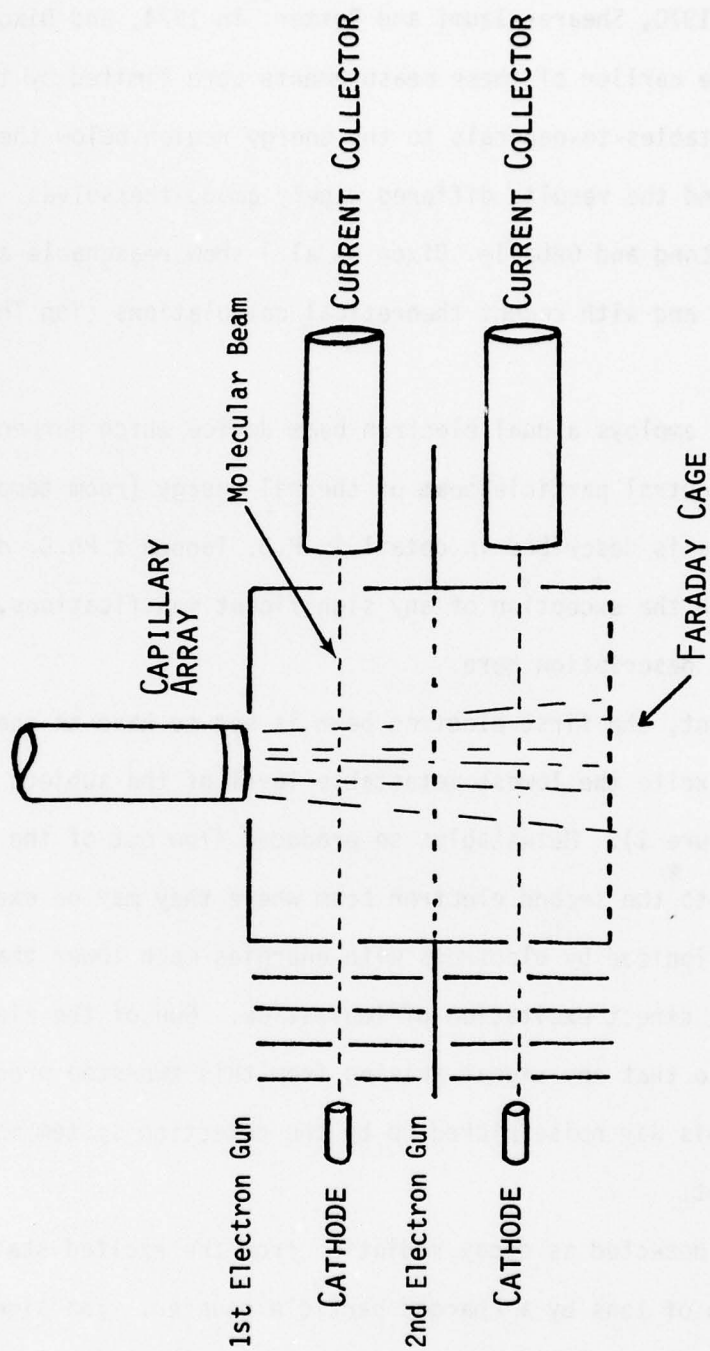


FIGURE 1 - Electron beams

in the electron gun control power supplies, and is equipped with an automatic pressure control system.

The objective of the first experiment undertaken was to measure the total ionization cross section of a selected metastable state. This experiment was less than successful. The next measurements included direct excitation cross section measurements for xenon, and two-step excitation cross sections in helium. These two preliminary experiments both showed promise, and the latter was selected for pursuit as being the most useful to the USAF scientific community. The remainder of the time on the contract was devoted to the two-step excitation experiment. The following chapters present an account of the experiments undertaken and the results obtained.

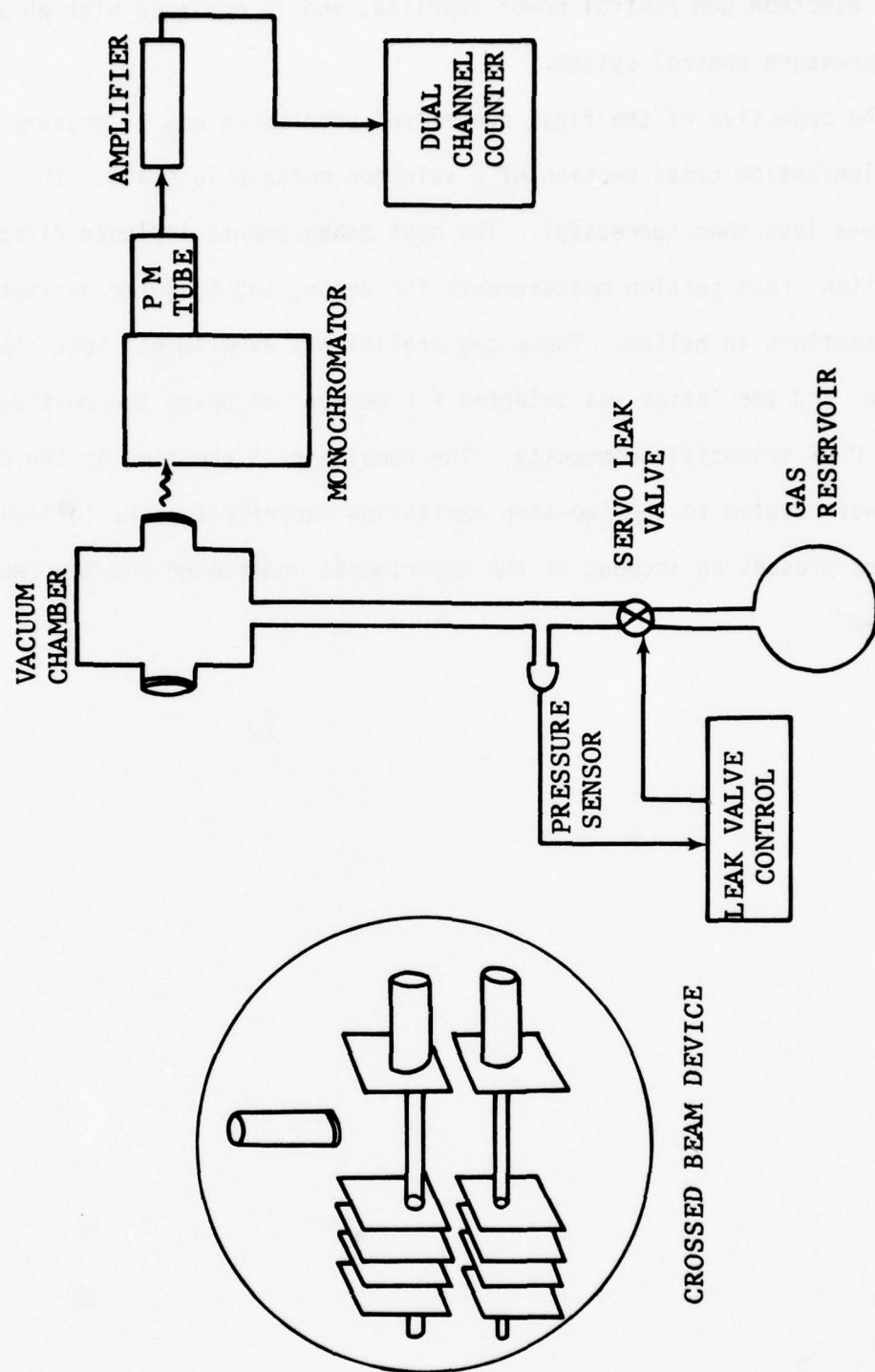


FIGURE 2 - Crossed beam system components

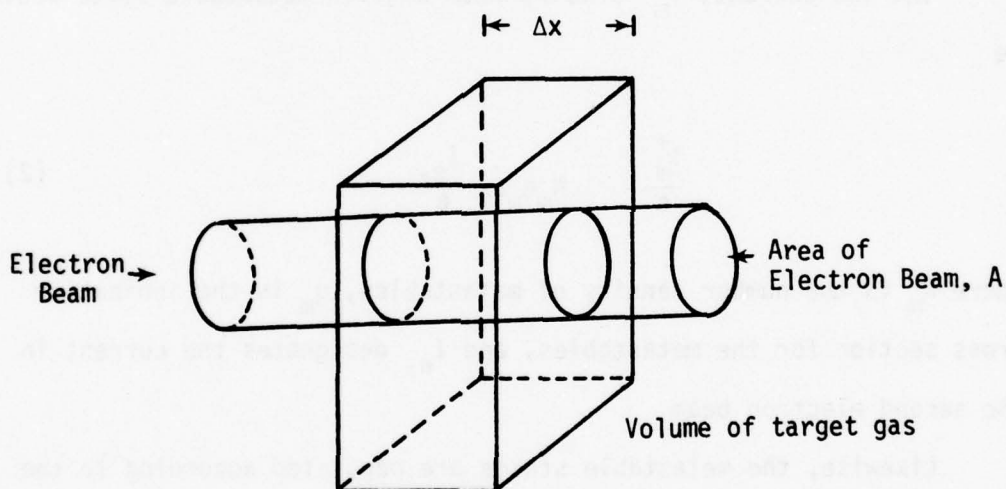
SECTION II

CUMULATIVE EXCITATION-IONIZATION

1. CROSS SECTION FORMULA

Electron impact ionization cross sections relate to the probability of stripping an orbital electron off of a molecule by electron bombardment. The method of obtaining ionization cross sections is dictated by parameters arrived at in the following way.

Consider a volume of gas at thermal energy (300°K) through which a beam of electrons is passed. The molecules in the gas are subjected to collisions with electrons.



The interaction volume is given by $A\Delta x$, where A is the cross sectional area of the electron beam, and Δx is the path length of electrons through the gas.

Each molecule obscures a fractional part of the total cross sectional area and this cross section is given by q/A , where q is the area cross section of molecule for electron impact ionization. The cross section can be determined, as follows, from its relation to the ion current produced from the aforementioned configuration.

$$\frac{i^+}{e} = \frac{NA \Delta x q I_e}{A e} \quad (1)$$

Where N is the number of molecules per cm^3 , $A\Delta x$ is the interaction volume, I_e is the electron beam current, i^+ is the ion current, and e is the electronic charge.

The ion current, i_m^+ arising from a given metastable state would be

$$\frac{i_m^+}{e} = N_m q_m \Delta x \frac{I_{e_2}}{e} \quad (2)$$

where N_m is the number density of metastables, q_m is the ionization cross section for the metastables, and I_{e_2} designates the current in the second electron beam.

Likewise, the metastable states are populated according to the rate

$$\frac{dN_m}{dt} = NQ_m \Delta x \frac{I_{e_1}}{e} - N_m \bar{v}A' \quad (3)$$

if conditions are maintained so that the excited state population comes only from electron bombardment and loss comes only from flow

losses. In Equation (3), N is the ground state number density, Q_m is the cross section for direct excitation to the metastable state, \bar{v} is the average velocity of the molecules I_{e_1} is the electron current in the first electron gun, and A' is the exit area for the metastables. The metastable number density produced thereby is:

$$N_m = \frac{NQ_m \Delta x I_{e_1}}{e \bar{v} A'} \quad (4)$$

The crossed beam device (see Figure 3) uses two parallel electron beams on which a perpendicular molecular beam is imposed. A metastable density given by Equation (4) is produced in the first electron beam and a portion of these, $k_1 N_m$, are subjected to electron bombardment in a second electron beam. The cumulative ion current rate collected by the SEM detector is given by combining Equation (2) and (4), yielding:

$$\frac{i_m^+}{e} = \frac{k_1 N Q_m \Delta x}{\bar{v} A'} \frac{I_{e_1}}{e} q_m \Delta x \frac{I_{e_2}}{e} \quad (5)$$

However, a portion of the ion signal is lost due to geometric factors and detector sensitivity, so that a collection efficiency relates the measured signal to the total signal produced.

$$i_{(\text{collected})}^+ = (i^+)(k_2) \quad (6)$$

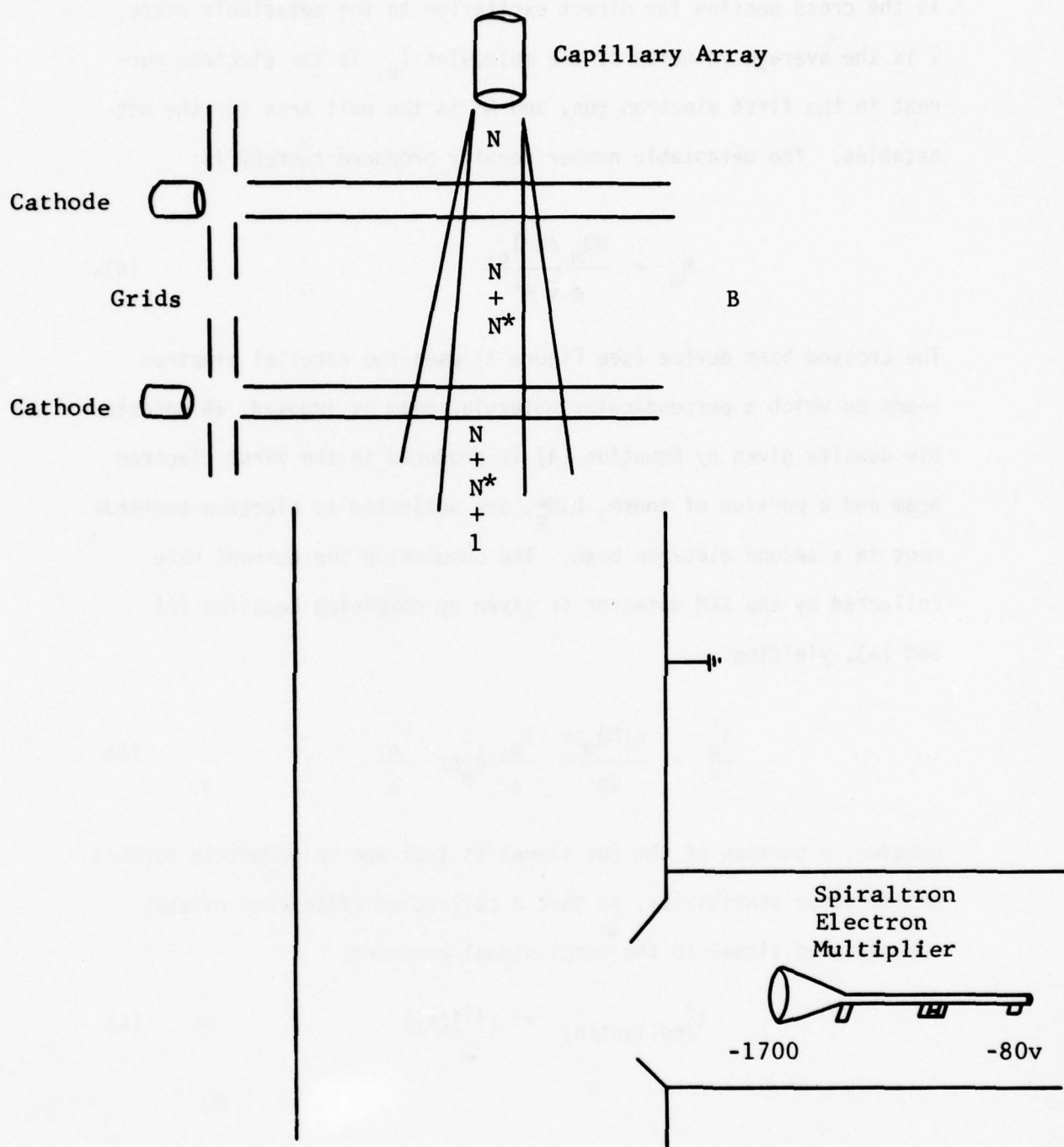


FIGURE 3 - Crossed beam device

The cumulative ionization cross section is then related to the measured signal as follows:

$$q_m = \frac{i_m^+(\text{coll}) \bar{v} A' e}{k_1 k_2 N Q_m \Delta x_1 I_{e_1} \Delta x_2 I_{e_2}} \quad (7)$$

2. LINEARITY TESTS

In order to ascertain that the observed signal arises only for the desired phenomenon, it is necessary to conduct tests to determine the relationship between the signal and its governing parameters. As seen, the ion or metastable signal must be a linear function of the electron current, target number density, and interaction volume. Furthermore, conditions must be maintained such that only the desired population mechanisms are occurring. Finally, tests must be performed to determine the collection efficiency of the detection system. These determinations are made as follows: The signal as a function of electron current is determined by holding the pressure, accelerating voltage, and all other parameters constant while changing the current by varying the drawout potential of the electron gun. Figure 4 gives signal response for a modulated electron beam over typical operating currents. In this case the signal monitored was the total metastable excitation cross section in xenon, measured by intercepting the metastable beam with a Channel Electron Multiplier.

In order to infer that the measured optical signal arises from an electron-atom collision where the electron energy is known, it is necessary that the electrons have suffered no other collisions either

in the interaction volume or in the region where the accelerating potential is developed. For this purpose the following criterion is imposed: If less than one percent of the electrons in the beam experience inelastic collisions, then only an insignificant number of energy degraded electrons contribute to the excitation process, and also, only an insignificant fraction of the current is lost through scattering. We have

$$I \text{ (collisions)} = N \Delta x Q I \text{ (total)} \quad (8)$$

where Q is the total scattering cross section and $I \text{ (collisions)}$ is the portion of the total current, $I \text{ (total)}$, which impacts an atom. For the criterion that less than one percent error is induced by multiple collisions or scattering:

$$\frac{I \text{ (collisions)}}{I} \leq .01 \quad (9)$$

or

$$N \Delta x Q \leq .01 \quad (10)$$

Assuming $Q = 10^{-15} \text{ cm}^2$ and $\Delta x = 1 \text{ cm}$, then $N = 10^{13} / \text{cm}^3$ is the maximum number density which can be used without observing a non-linear signal as current response. Similar arguments apply to atom-atom collisional quenching, but the simplest method of determining the onset of pressure dependent non-linearities is to monitor the desired transition as a function of pressure.

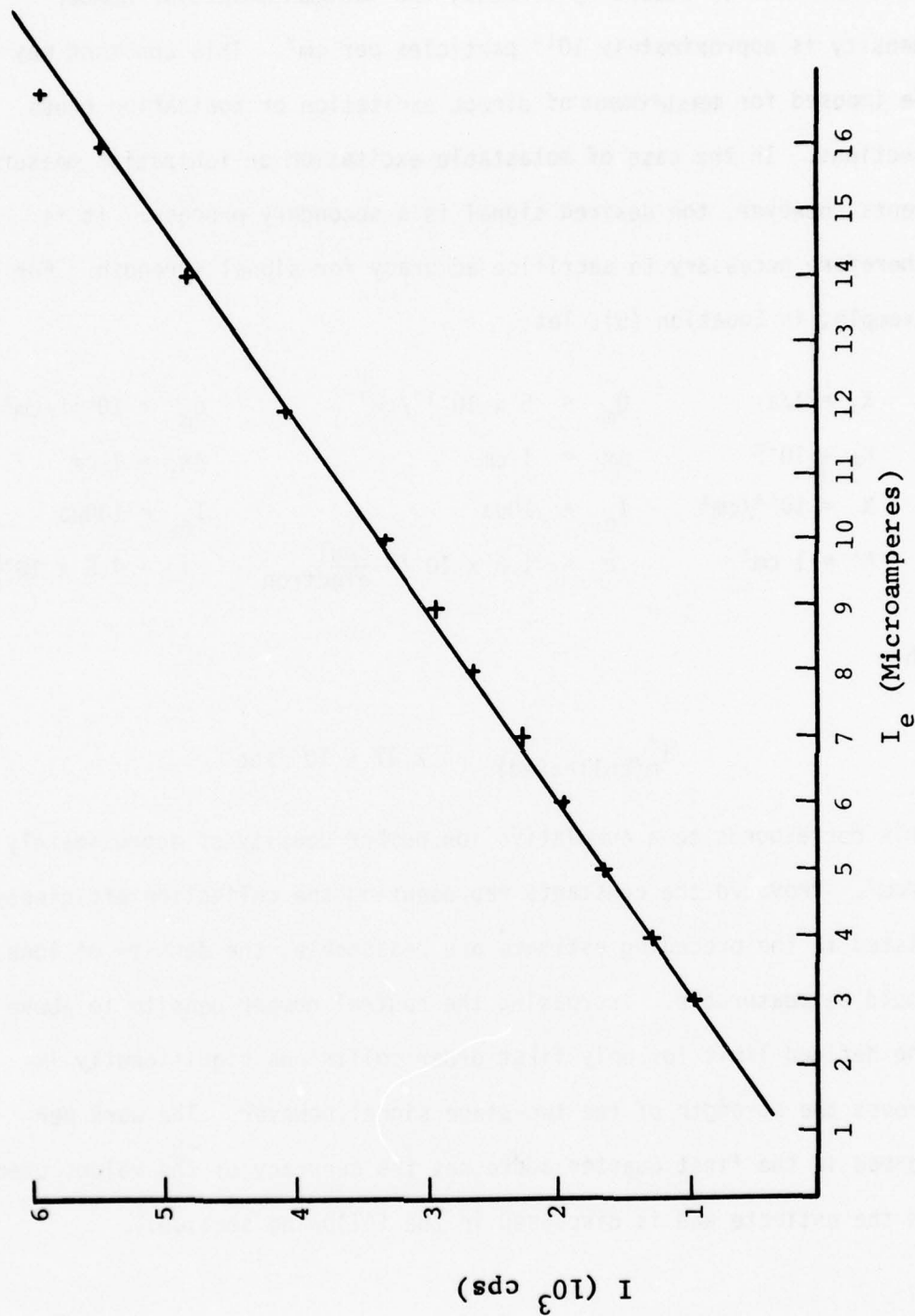


FIGURE 4 - Signal vs. current

These arguments lead to the conclusion that to avoid significant errors from secondary effects, the maximum molecular number density is approximately 10^{13} particles per cm^3 . This constant may be imposed for measurement of direct excitation or ionization cross sections. In the case of metastable excitation or ionization measurements, however, the desired signal is a secondary process. It is therefore necessary to sacrifice accuracy for signal strength. For example, in Equation (5), let

$$\begin{array}{lll}
 K_1 = 1/2 & Q_m = 5 \times 10^{-17}/\text{cm}^2 & q_m = 10^{-15}/\text{cm}^2 \\
 K_2 = 10^{-2} & \Delta x_1 = 1 \text{ cm} & \Delta x_2 = 1 \text{ cm} \\
 N = 10^{13}/\text{cm}^3 & I_{e_1} = 10 \mu\text{a} & I_{e_2} = 100 \mu\text{a} \\
 A' = 1 \text{ cm}^2 & e = 1.6 \times 10^{-19} \frac{\text{coul}}{\text{electron}} & \bar{v} = 4.5 \times 10^4 \frac{\text{cm}}{\text{sec}}
 \end{array}$$

then

$$i_m^+(\text{collected}) = 2.17 \times 10^3/\text{sec}$$

This corresponds to a cumulative ion number density of approximately $5/\text{cm}^3$. Provided the constants representing the collection efficiency listed in the preceding estimate are reasonable, the density of ions would be measurable. Increasing the neutral number density to above the defined limit for only first order collisions significantly improves the strength of the two-stage signal, however. The work performed in the first quarter addresses the accuracy of the values used in the estimate and is discussed in the following section.

3. ION COLLECTION EFFICIENCY

Equation (7), the expression for the two-stage ionization cross section, calls for a determination of density, the density attenuation between the first and second electron beams, and the collection efficiency of the detector for ions. The quantities are measured by means of the direct ionization cross section. From Equations (1) and (6), the collected ion current from the second beam is:

$$\frac{i^+(\text{coll})}{e} = K_2 N_2 \Delta x_2 q \frac{I'_{e_2}}{e} \quad (11)$$

The density attenuation, measured optically, is

$$K_1 = \frac{N_1}{N_2} \propto \frac{F_{ij}(\Omega)_1}{F_{ij}(\Omega)_2} \quad (12)$$

where $F_{ij}(\Omega)_1$ and $F_{ij}(\Omega)_2$ are the photon fluxes per steradian from the first and second electron beams respectively. Then

$$\frac{(i^+)(\text{coll})}{e} = (K_1 K_2 N \Delta x_2) q \frac{I'_{e_2}}{e} \quad (13)$$

and Equation (7) becomes

$$q_m = \frac{i_m \bar{v} A' e I'_{e_2} q(\text{direct})}{i(\text{coll}) q_m \Delta x_1 I_{e_1} I_{e_2}} \quad (14)$$

4. RESULTS

The first step necessary for measurement of cumulative ionization cross section is to calibrate the detector from the direct ionization curves. This is performed by sweeping the lower electron gun in energy while monitoring the ion count rate from a spiraltron electron multiplier (SEM). Figure 5 shows a preliminary direct ionization curve for helium taken without correction for current vs. accelerating voltage. Note the appearance of signal at 20 eV. The count rate stays in the low hundreds per second until the electron energy reaches 23.5 eV, whereupon it rises into the thousands. Subsequent careful direct ionization cross section measurements corrected for current show a function which does not compare well with those of Rapp and Englander-Golden,¹⁴ as seen in Figure 6. The curves are normalized at 50 eV. The data also shows an in-phase signal below the threshold for ionization (Figure 7). The threshold for this signal corresponds approximately to 20 volts after correcting for the contact potential, and was presumed to arise from metastable and/or UV radiative transitions. In order to verify this as the source, the bias on the SEM was shifted so that the entrance cone was at ground potential. The result was a curve bearing a great similarity to the helium metastable excitation function measured by Borst¹⁵ (Figures 8 and 9). A direct comparison with Borst's curve shows that the metastable curve produced on this system is higher than Borst's at higher energies (Figure 10). The cause for this difference at higher energies was not immediately apparent. Previous to the particle counting work, optical excitation functions of various

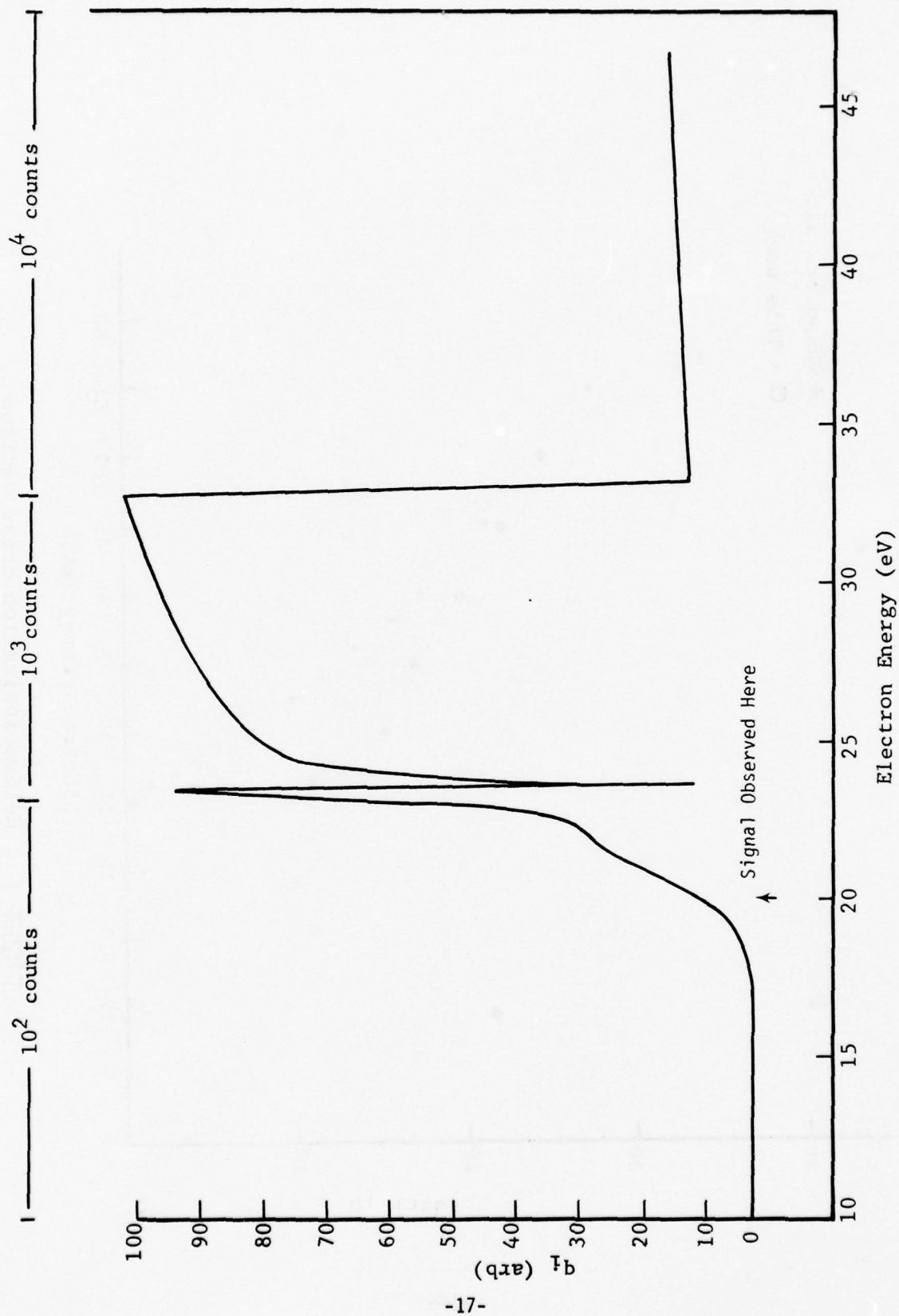


FIGURE 5 - Direct ionization cross section of helium

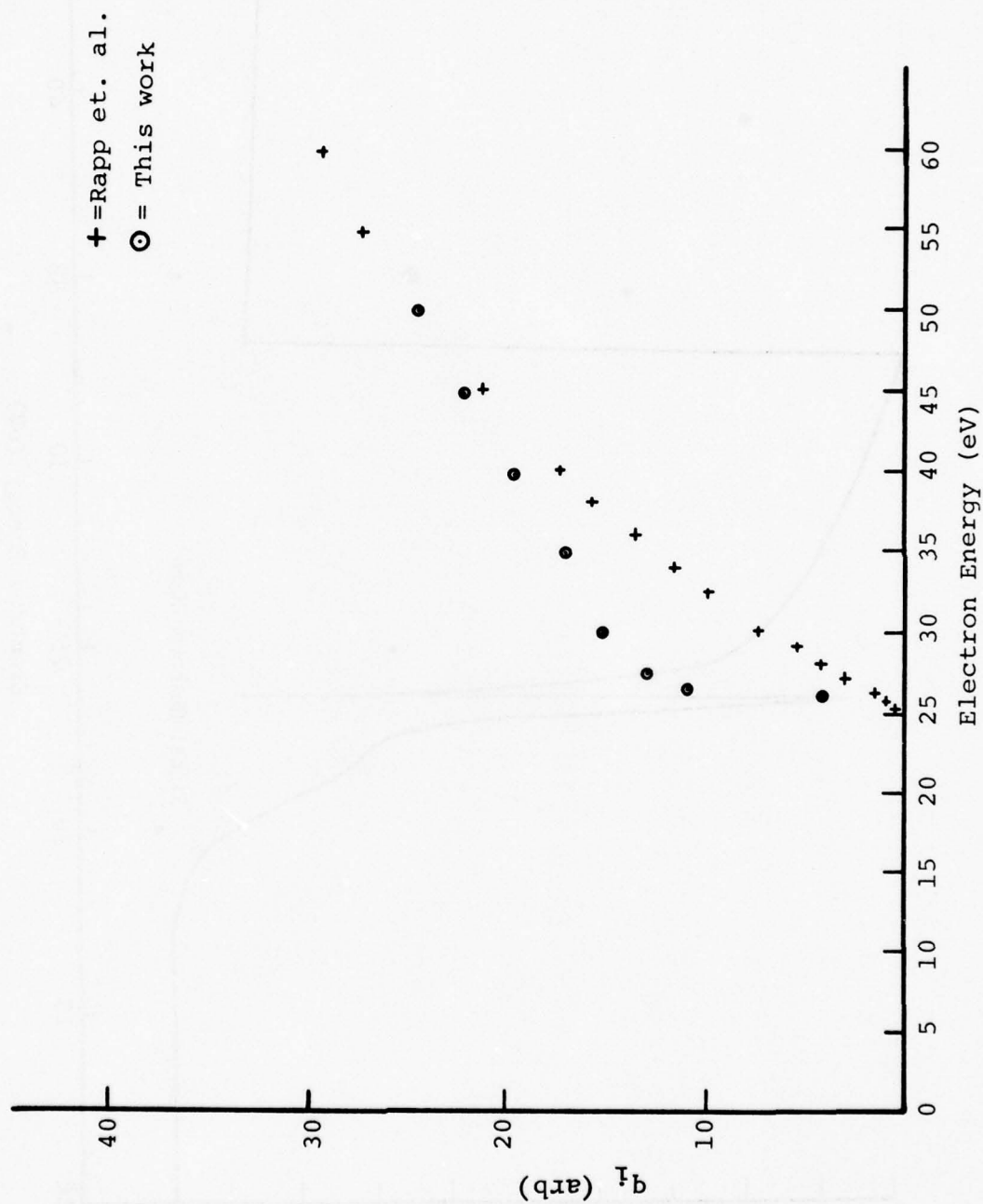


FIGURE 6 - Helium ionization cross section

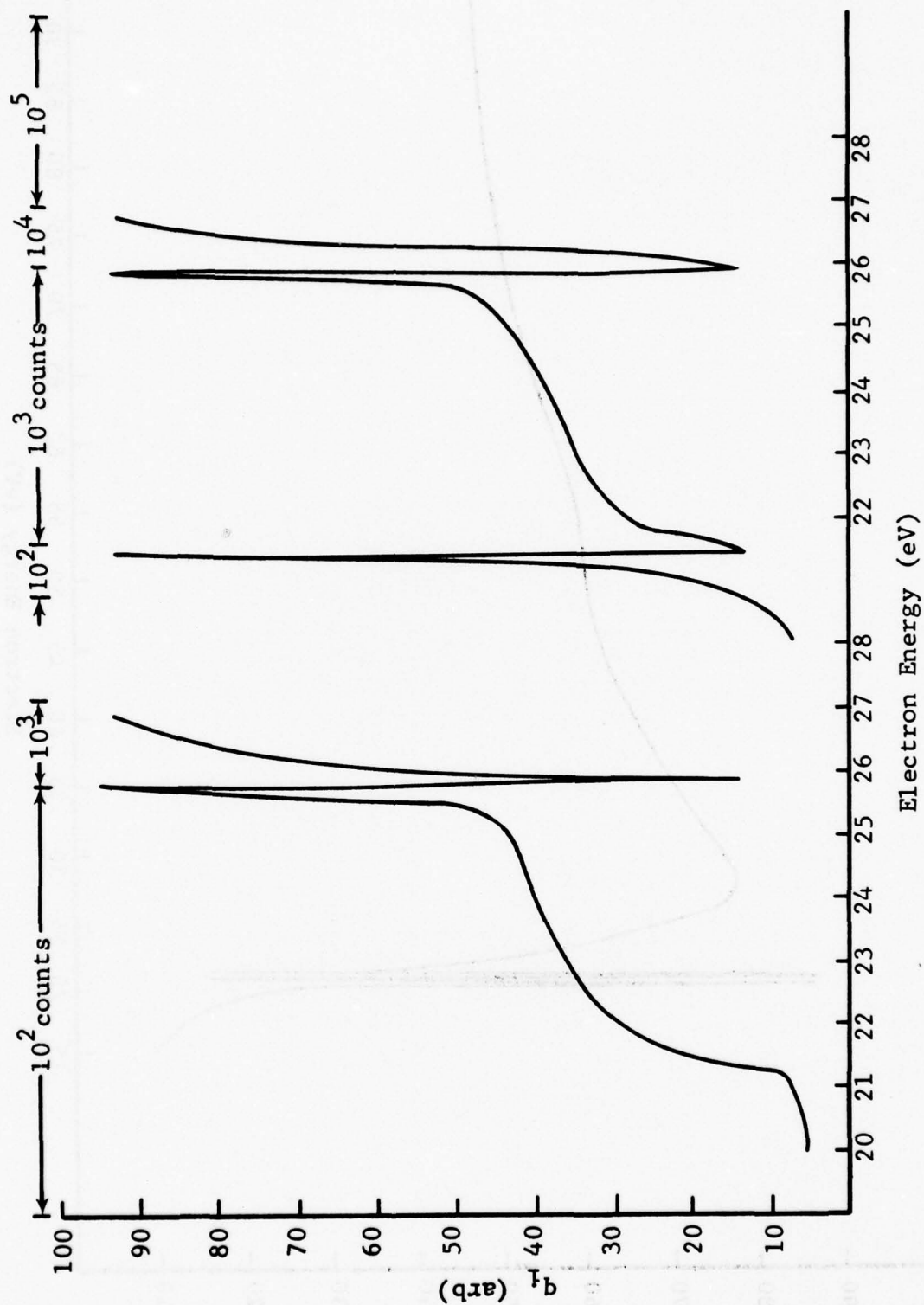


FIGURE 7 - Ionization function and in-phase signal below threshold

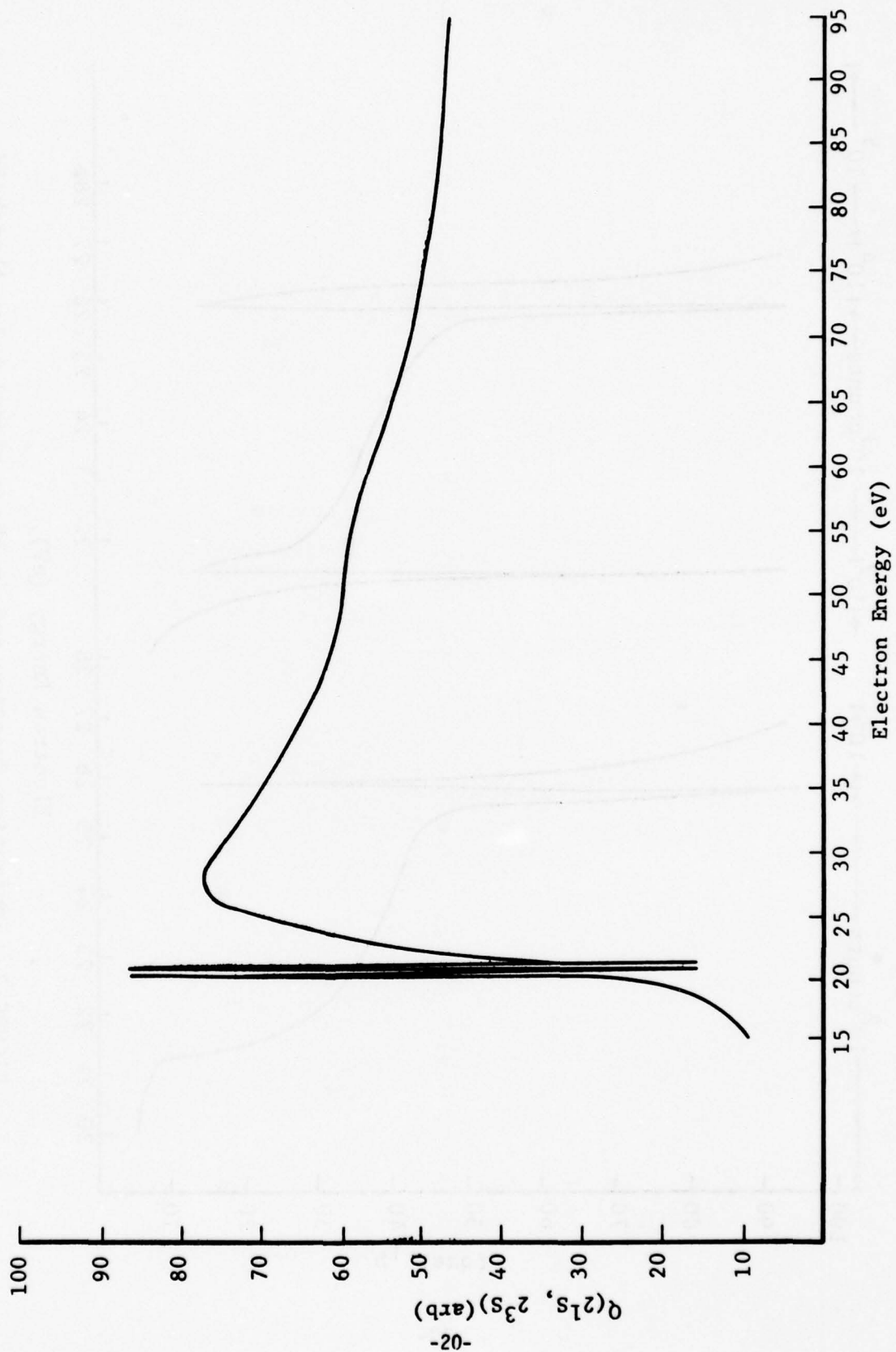


FIGURE 8 - Helium metastable excitation function

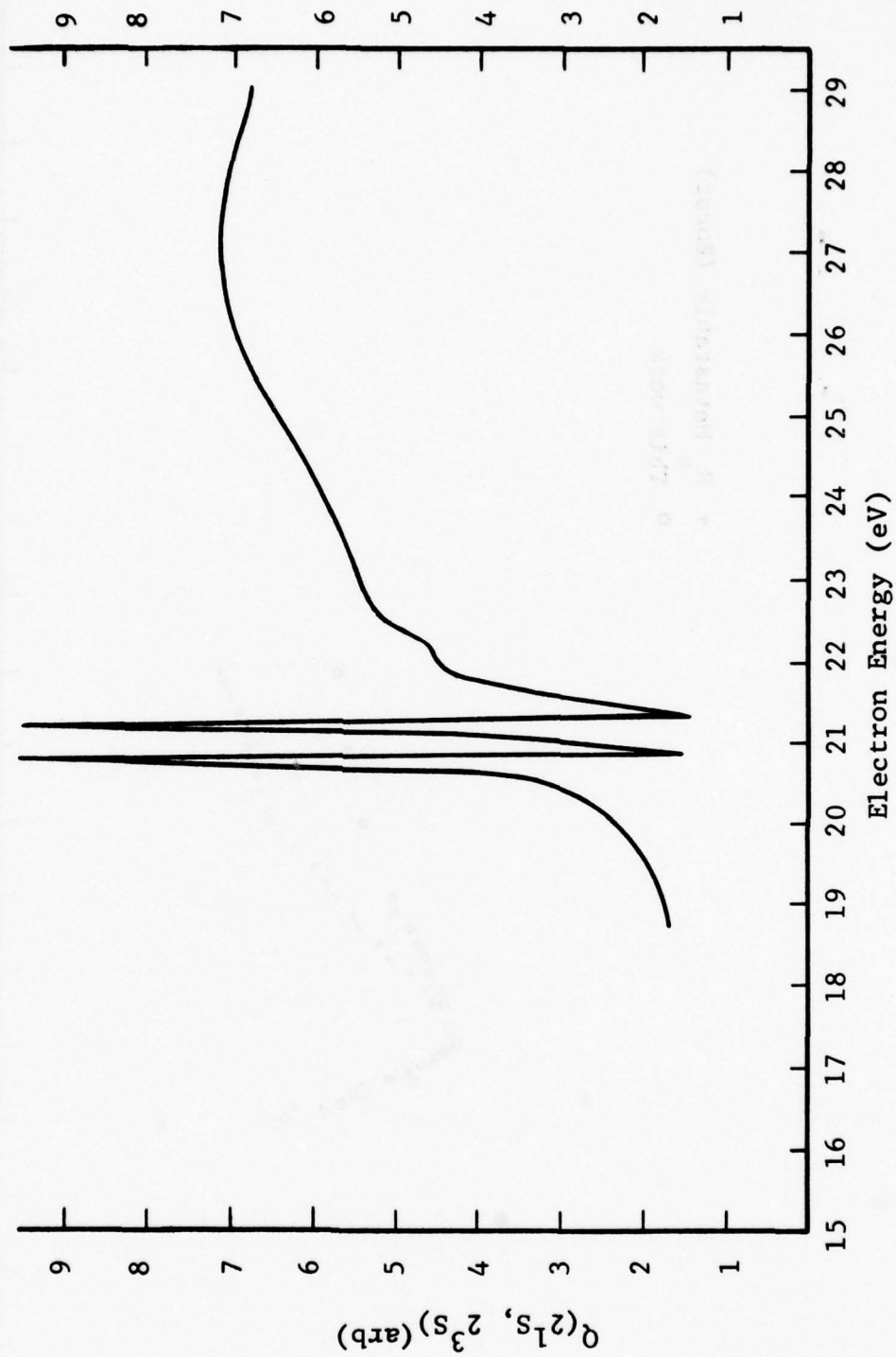


FIGURE 9 - Helium metastable excitation function

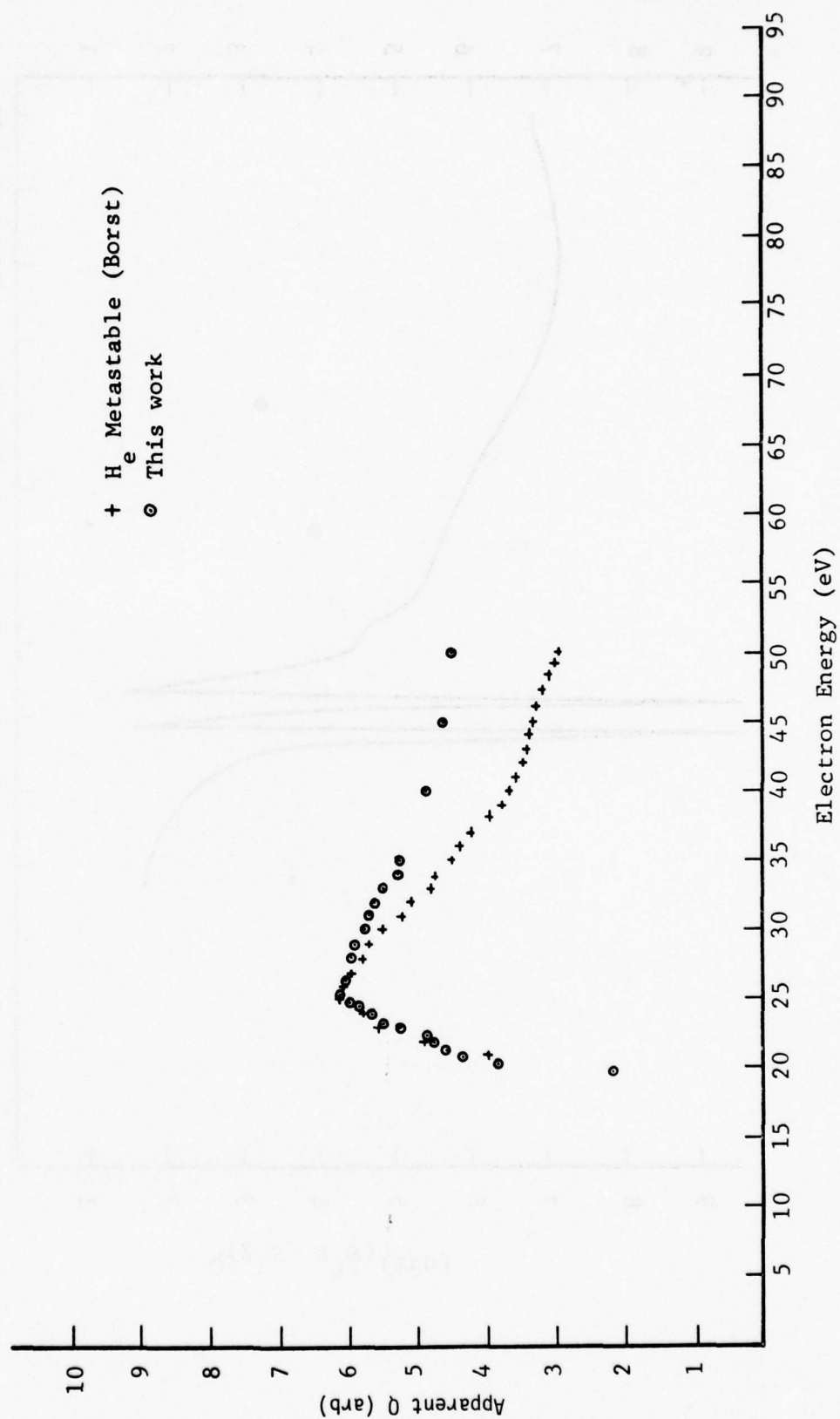


FIGURE 10 - Helium metastable excitation function

helium excitation functions were obtained, and it was found that cavalier assignments of draw-out voltages were not sufficient to produce a well-defined accelerating potential for the electronically chopped electron beam. If the beam is not entirely biased off during the off cycle, signal can develop from electrons which have a much higher average energy than when the electron beam is on. At accelerating voltages where the cross section is changing rapidly the error is large. However, the limits of the voltages yielding well-defined optical signals were established, and these limits were obeyed for particle counting as well.

In order to positively identify the observed signal as being the sum of all metastable levels excited at a given electron energy, nitrogen was substituted for helium. Sweeping the energy of the electron guns in an identical way should produce an excitation function of the N_2 total metastable cross section, which could also be compared to similar measurements by Borst. Figures 11 and 12 show what is apparently the total metastable excitation function of N_2 . These curves compare favorably in shape to the measurements of Borst, with the added feature of better energy resolution. The curves do contain a disparity from Borst's measurements which becomes more apparent at higher energies. Figure 12 shows the curve produced from both guns normalized at 16 eV.

The function from the second gun is actually rising above 50 eV. Neon was also examined. The resulting excitation function compared well with earlier measurements of the relative excitation

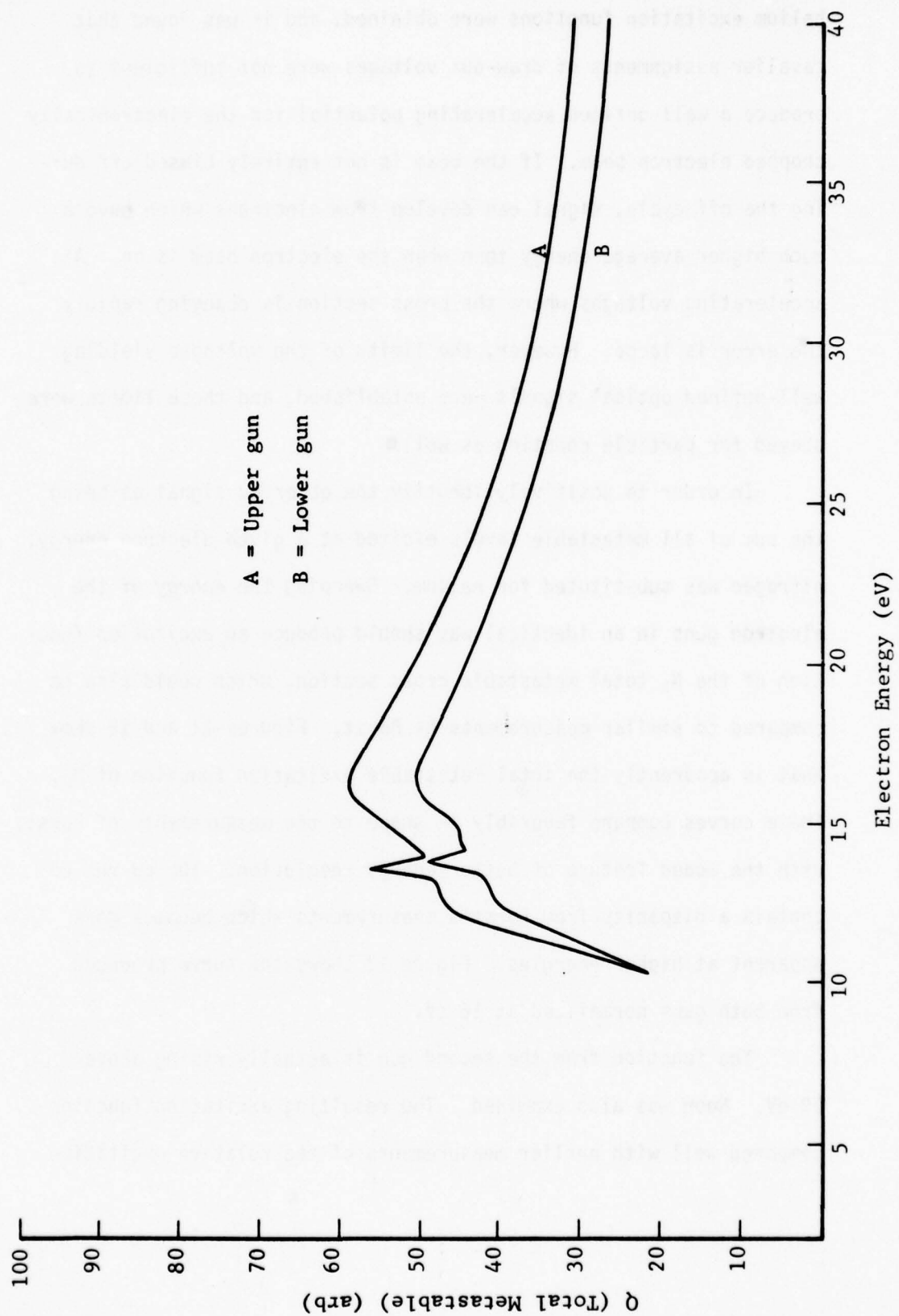


FIGURE 11 - N_2 metastable excitation function

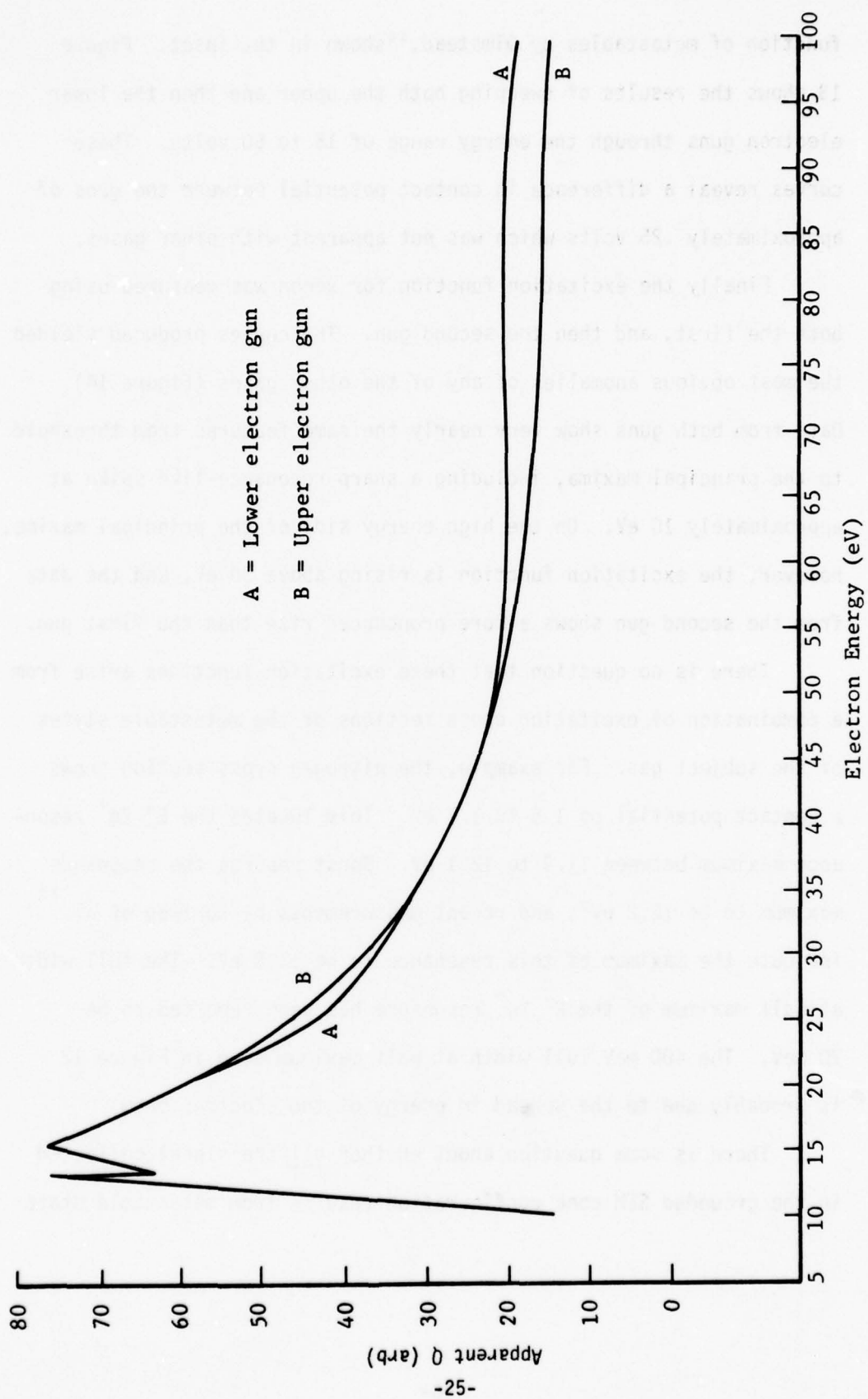


FIGURE 12 - N_2 metastable excitation function

function of metastables by Olmstead,¹⁶ shown in the inset. Figure 13 shows the results of sweeping both the upper and then the lower electron guns through the energy range of 15 to 50 volts. These curves reveal a difference in contact potential between the guns of approximately .25 volts which was not apparent with other gases.

Finally the excitation function for xenon was measured using both the first, and then the second gun. The curves produced yielded the most obvious anomalies of any of the other gases (Figure 14). Data from both guns show very nearly the same features from threshold to the principal maxima, including a sharp resonance-like spike at approximately 10 eV. On the high energy side of the principal maxima, however, the excitation function is rising above 30 eV, and the data from the second gun shows a more pronounced rise than the first gun.

There is no question that these excitation functions arise from a combination of excitation cross sections of the metastable states of the subject gas. For example, the nitrogen cross section shows a contact potential of 1.5 to 1.7 eV. This locates the $E^3 \Sigma g^+$ resonance maximum between 11.9 to 12.1 eV. Borst reports the resonance maximum to be 12.2 eV³, and recent measurements by Kurzweg et al.¹⁷ indicate the maximum of this resonance to be 11.8 eV. The full width at half maximum of the $E^3 \Sigma g^+$ resonance has been reported to be 70 meV. The 400 meV full width at half maximum seen in Figure 12 is probably due to the spread in energy of the electron beam.

There is some question about whether all the signal collected in the grounded SEM cone configuration results from metastable state

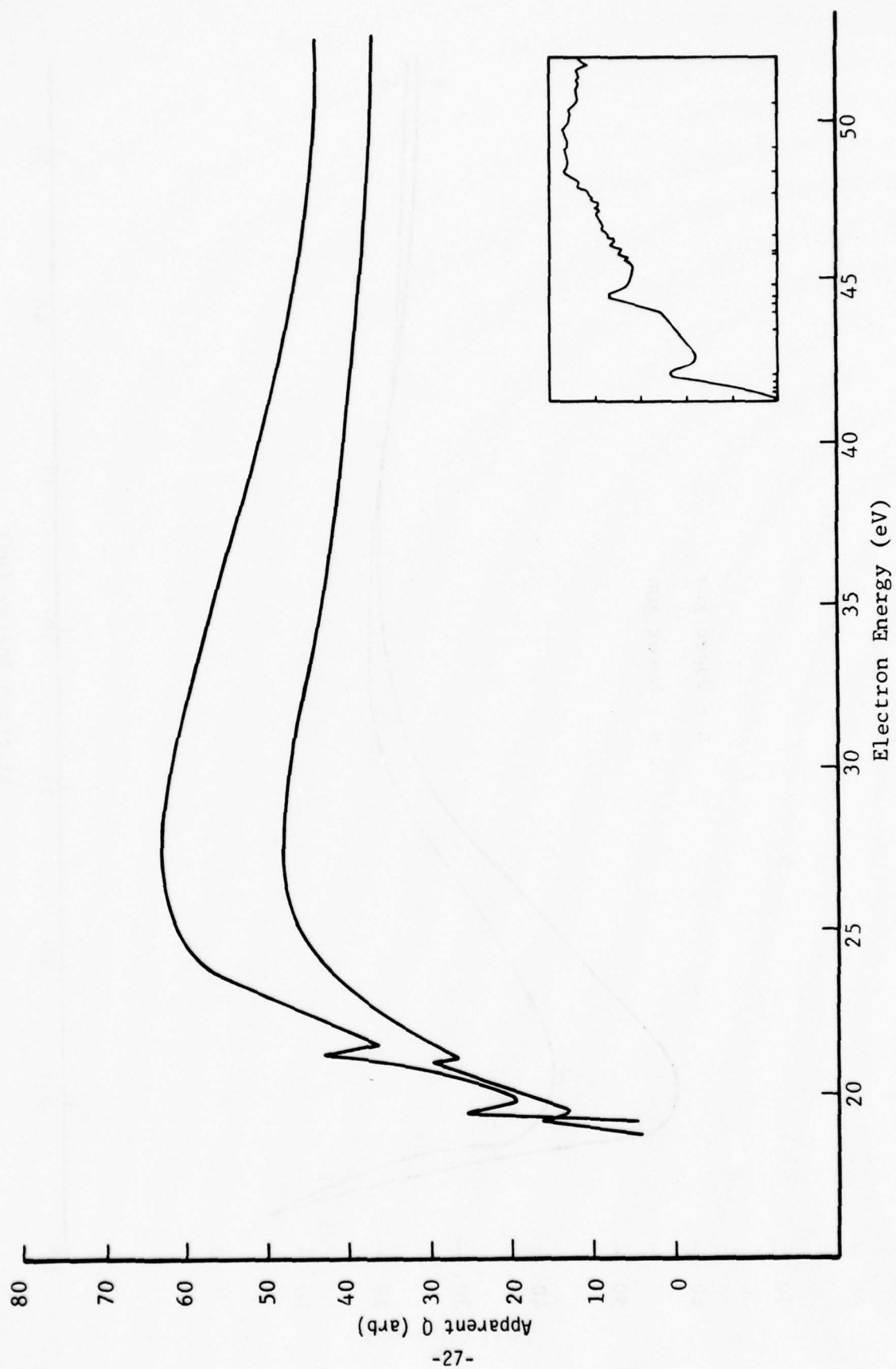


FIGURE 13 - Total metastable excitation function in neon

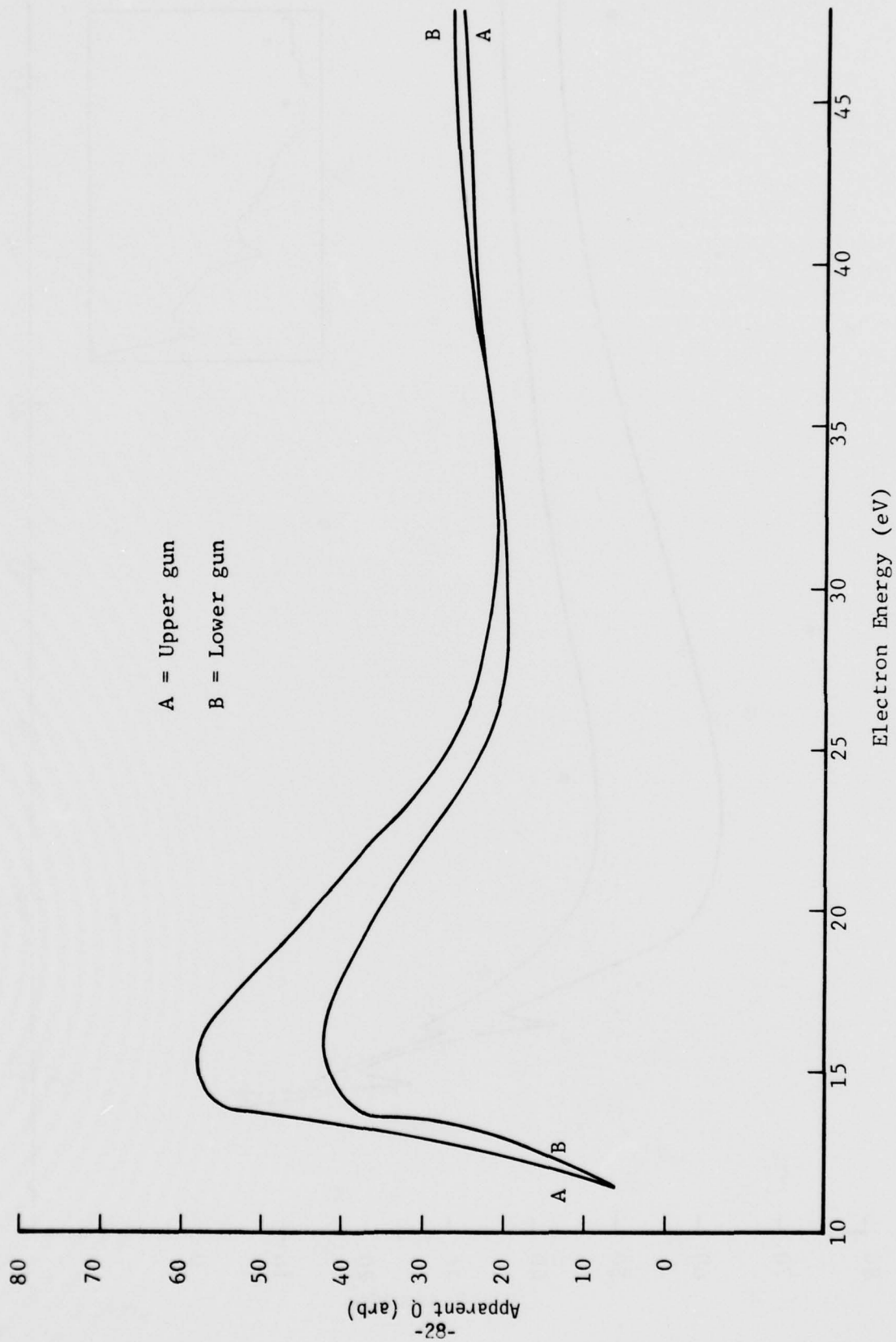


FIGURE 14 - Xenon metastable excitation function

excitation, however. There is nothing to exclude collection of scattered ultraviolet radiation from UV radiation transitions, since the SEM is sensitive to energy above 6 eV. In order to discriminate between the metastable signal and possible UV or ion collection, the electron gun chopping frequency was increased to 5 kHz, so that the length of a half cycle corresponded roughly to the time of flight between the electron gun and SEM, and the SEM cone was biased 20 V positive with respect to ground. This frequency might jeopardize the energy resolution since the guns and electronics were not designed for rapid cut off. By selecting data from a portion of the time when the gun is biased off, however, the data collected by the detector must arise from metastable excitation. Figure 15 shows xenon signal thereby measured for: the gun on (curve A), the gun off (curve C) and the difference (curve B). The difference curve indicates that a significant portion, but not all of the rising signal, is apparently due to prompt emission, possibly resulting from ion transitions. The remaining bump at approximately 41 eV is evidently due to electron beam focussing since its shape shifts with respect to the principal maximum as a function of magnetic field (Figure 16). The source of the anomalous signal appears not to be electron scattering, since the bump scales with pressure the same as the principal maximum (Figure 17). The nitrogen excitation function taken at 10 kHz shows little difference from the earlier curves taken without time discrimination, except that the extra bump is peaked at 24 eV (Figure 18). It would be

tempting to ascribe the bump to delayed emission of the $C^3\pi_\mu$ state populated from the $E^3\Sigma_g^+$, but Kurzweg et al. observed this process to peak at 22 eV, and any difference in the portion of signal sampled between Kurzweg's and this work, or any difference in chopping lengths, should not change the position of the maximum.

The conclusion is that the anomalous bump is a result of the way in which the data is collected. Recalling Equation (1), the signal is a function of the current number density, and electron path length. One candidate for the error is the reflected electrons which re-enter the interaction volume (due to the confining magnetic field) and therefore produce a signal, but are not collected and measured as current.

The direct ionization curves obtained indicate that the collection efficiency for ions produced in the lower electron beam is approximately 10^{-4} . This, coupled with the large in-phase signal from direct metastable excitation have precluded measurement of the two-step ionization cross sections.

5. CONCLUSIONS

The experiments for two-step ionization and two-step excitation in helium were repeated in the pressure range of 1 to 100 millitorr to explore possible signal-to-noise enhancement at higher pressure and to confirm the earlier negative results obtained with the spiraltron electron multiplier (SEM) for ion counting.

The basic conclusions drawn from these experiments are as follows: For ion counting, operating the electron guns in a

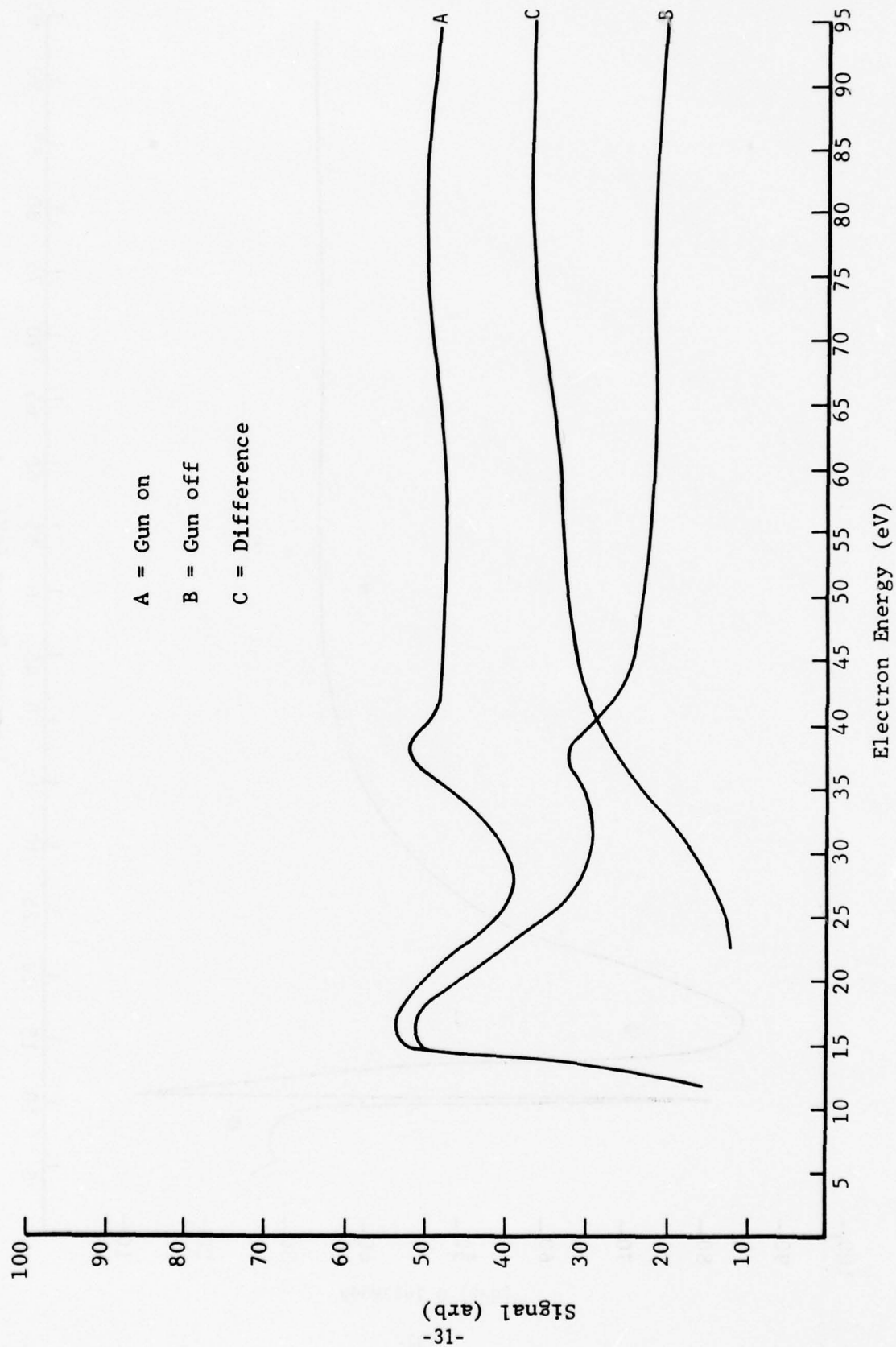


FIGURE 15 - Xenon metastable signal in selected channels

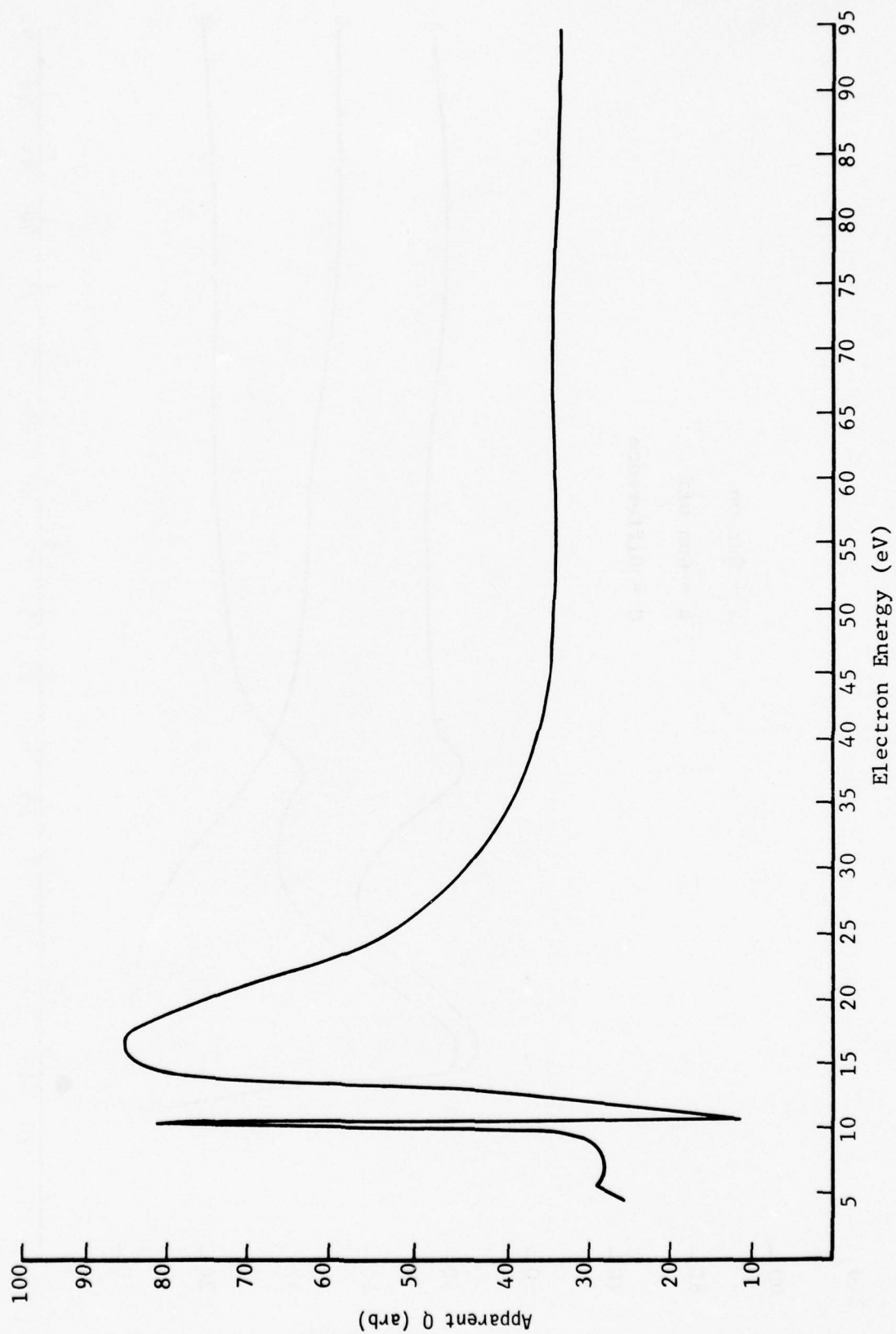


FIGURE 16 - Xenon metastable excitation function

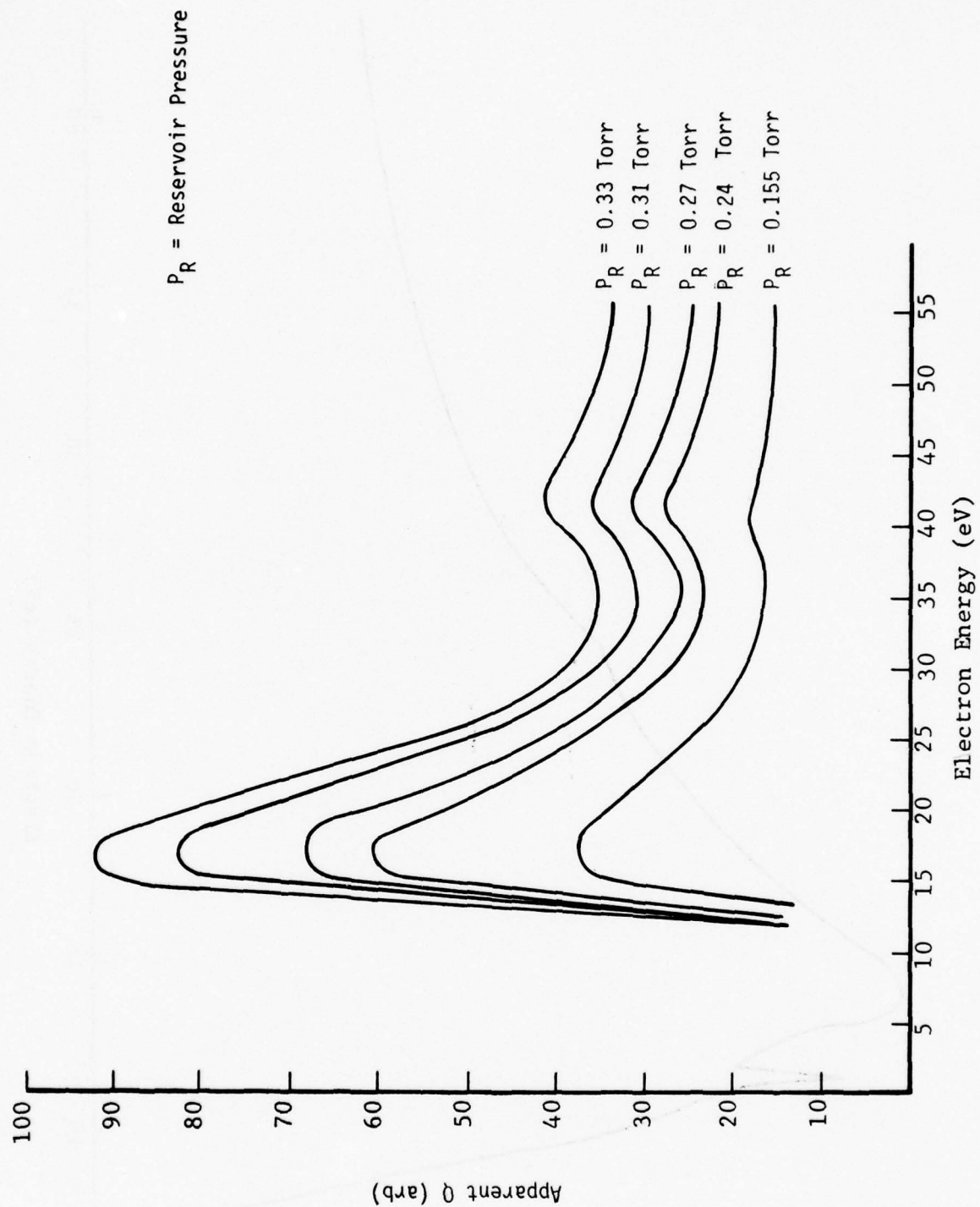


FIGURE 17 - Xenon excitation function as a function of pressure

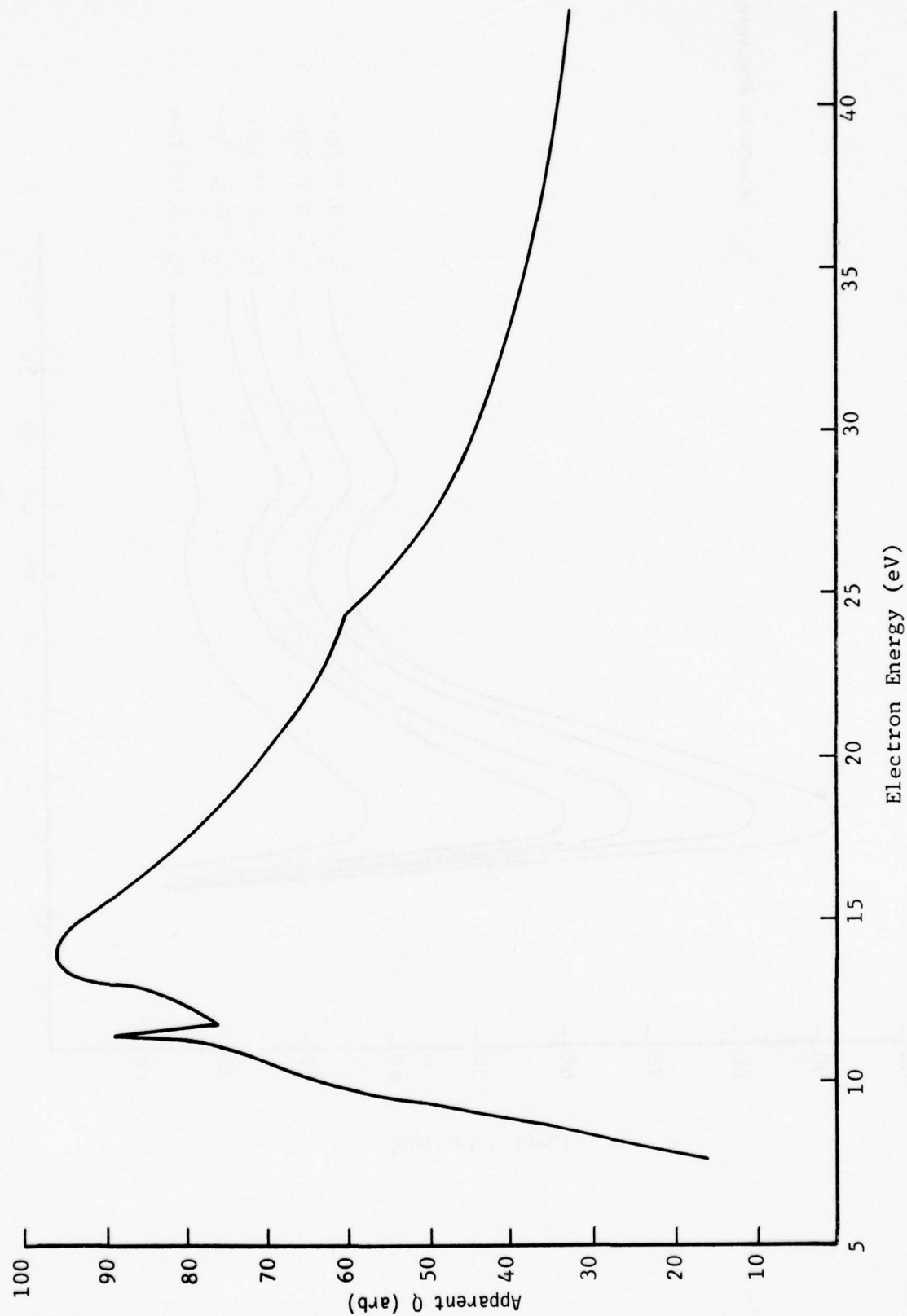


FIGURE 18 - N_2 metastable excitation function at 10Khz chopping frequency

reasonable parameter range (as determined experimentally) leads to an expected difference of approximately six orders of magnitude between the predicted cumulative signal and the direct ion signal. Since the observed direct ion signal is strong enough to saturate the detector even at pressures of one millitorr, the cumulative ion signal should lie within the dynamic range of the crossed beam system. However, the detector is fairly efficient for detecting metastable atoms, having a collection efficiency of approximately one-fifteenth that of ions. This leads to a noise source which totally obscures signals less than four orders of magnitude smaller than the direct ion signal. The solution to the problem is to isolate the detector from the metastable signal but still retain a high collection efficiency for ions. Possible means for achieving this result are (1) placing the SEM in an ion extraction network, or (2) replacing the SEM with a quadrupole mass analyzer with an off-axis electron multiplier wired for ion counting.

SECTION III

EXCITATION OF XENON BY SINGLE ELECTRON IMPACT

1. BACKGROUND

Following the results obtained for two-stage ionization cross section measurement through ion counting, an investigation into means of measuring metastable cross sections was initiated. This led to the design and construction of a large diameter electron beam for use in obtaining infrared xenon excitation cross sections.

A survey experiment in xenon was performed in order to establish the feasibility of making measurements of decay radiation which was in the infrared. Optical cross sections of several xenon transitions in the near infrared were obtained, and spectra in the range of 6000Å to 4000Å obtained at three different electron impact energies were used to evaluate the relative magnitudes of the cross sections.

In order to predict the possibility of lasing in a gas medium where the primary excitation mechanism is collisional excitation, an analysis considering certain atomic and molecular properties must be made. The properties are contained in the expression for the absorption coefficient, α_0 , at the center of a radiative transition:¹⁹

$$\alpha_0 = \frac{2\sqrt{\pi \ln 2} \frac{e^2}{mc}}{\Delta \nu_0} f_{21} \left(N_1 - \frac{g_1}{g_2} N_2 \right) \quad (15)$$

where e = electron charge

m = electron mass

f_{21} = oscillator strength for transition from states 2 to 1

c = speed of light

$\Delta\nu_0$ = Doppler width of the transition

N_1 = number density of atoms in lower state 1

N_2 = number density of atoms in upper state 2

g_1 = degeneracy factor for state 1

g_2 = degeneracy factor for state 2

Notice that the absorption coefficient becomes negative for

$$\frac{g_1}{g_2} N_2 > N_1 \quad (16)$$

Situations for which these non-equilibrium conditions exist are illuminated by examining the rate equations for the selected states.

$$\frac{dN_1}{dt} = N_0 \Delta x Q_1 \frac{I_e}{e} + \sum_j A_{j1} N_j - \frac{N_1}{\tau_1} \quad (17)$$

$$\frac{dN_2}{dt} = N_0 \Delta x Q_2 \frac{I_e}{e} + \sum_j A_{j2} N_j - \frac{N_2}{\tau_2} \quad (18)$$

where N_0 = ground state number density

Δx = electron path length through the medium

Q_1, Q_2 = cross sections for collisional excitation by electrons

I_e/e = electron flux through the medium

A_{j1}, A_{j2} = spontaneous emission probability of transition from state j into states 1 and 2

N_j = number density in state j

τ_1, τ_2 = lifetimes of states 1 and 2

Equations (17) and (18) assume that excitation arises primarily from electron collision and subsequent cascade. As an example, simplify the analysis by further assuming that the system has reached steady state:

$$\frac{dN_1}{dt} = 0 = N_0 \Delta x Q_1 \frac{I_e}{e} + A_{21} N_2 - \frac{N_1}{\tau_1} \quad (19)$$

$$\frac{dN_2}{dt} = 0 = N_0 \Delta x Q_2 \frac{I_e}{e} - \frac{N_2}{\tau_2} \quad (20)$$

then

$$N_1 = \tau_1 N_0 \Delta x Q_1 \frac{I_e}{e} + \tau_1 A_{21} N_2 \quad (21)$$

$$N_2 = \tau_2 N_0 \Delta x Q_2 \frac{I_e}{e} \quad (22)$$

The condition for gain is then

$$N_0 \Delta x \frac{I_e}{e} \left(\frac{g_1}{g_2} \tau_2 Q_2 - \tau_2 Q_1 \right) - \tau_1 A_{21} N_2 > 0 \quad (23)$$

Other parameters, such as oscillator strength, line width, and single pass losses must be considered, but Equation (23) indicates that the level cross sections and lifetimes are key parameters to lasing action from electron pumping.

Xenon is a lasing medium for which the primary means of excitation is apparently electron collision. Strong laser lines have been observed from all of the 5d levels, which terminate on one of the 6p levels. (see Figure 26)

Although lifetimes, oscillator strengths, transition probabilities and degeneracy factors have been either measured or computed for many or all of these states²⁰⁻²⁵, no level cross section measurements have been obtained. This entails measuring the photon flux from transitions into and out of the selected states, and emission from the 5d levels lies in the range of 2 to 4 microns. Many of the cascade transitions into the 5d levels are in the visible region, however, as are most of the spontaneous emissions from the lower laser levels. Furthermore, examining transitions with similar quantum numbers (except for n) will yield information regarding the shape of the cross section with respect to electron energy.

The scope of the experiment is to measure the strongest of the visible lines cascading into the 5d levels, and also measure the cross section for populating the lower laser levels by electron collision. Ultimately it is desired to measure directly the absolute level cross sections of the 5d states.

2. RESULTS

The apparatus used in the experiment is a crossed electron and atomic beam device designed for measuring excitation and ionization.¹³ The chamber was pumped down with a turbo molecular pump

and then sealed off to obtain a relatively high (1-50 millitorr) static xenon gas pressure for this type of measurement. Spectra from 6000 to 9000Å were taken with the electron gun accelerating voltage set at 14, 18, and 33 eV. The data counts are electronically divided by the electron current, so that the spectra are automatically corrected for the change in electron current as a function of accelerating energy. In this spectral region, the response of the detection system is approximately flat (Figure 19), so that comparison of the line intensities at different electron energy gives a good value for the relative apparent cross sections of the transitions obtained without correction for detector sensitivity. Table 1 gives the most prominent transitions between 8900 and 6600Å obtained in this way. The second column gives the level designations in Racah notation. The third column gives the relationship designation to a prominent lasing line in the fourth column. Here PL indicates that the transition populates the lower laser level, DU is a transition which depopulates the upper laser level, etc. The relative apparent cross sections in the fifth, sixth, and seventh columns are given in counts per second.

Figure 20 is the excitation function of the Xe 8819Å $6s[1-1/2]_3 - 6p[2-1/2]_2$ transition obtained by fixing the monochromator on the peak of the line and sweeping the accelerating voltage of the electron gun. The cross section has a maximum at approximately 13 volts. Similar in shape are the 8231Å $6s[1-1/2]_2 - 6p[1-1/2]_2$ and 7336Å $6p[2-1/2]_2 - 5d'[2-1/2]_3$ lines given in

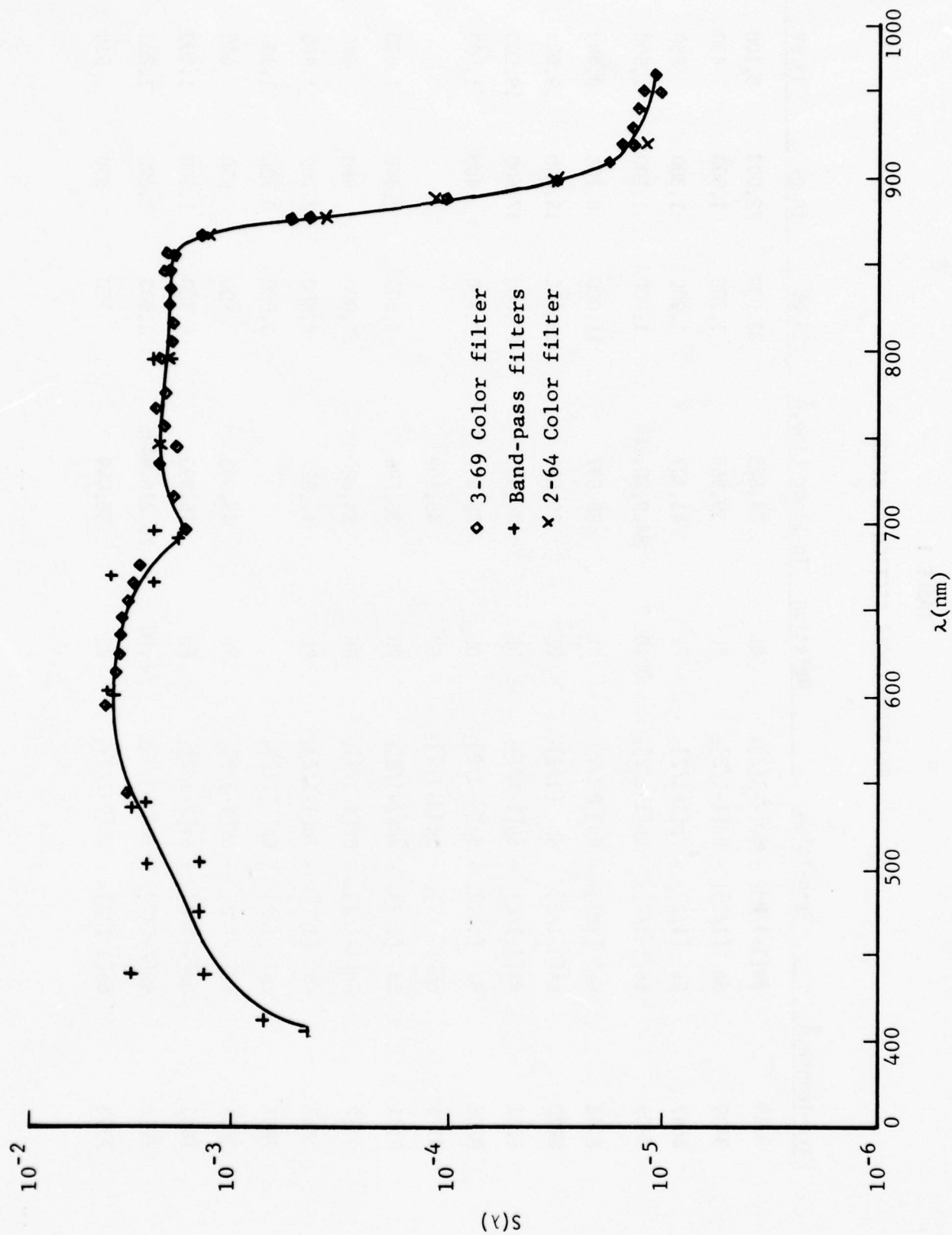


FIGURE 19 - Quantum efficiency of detection system vs. wavelength

TABLE 1
RELATIVE CROSS SECTION IN XENON

Wave-length, Å	Transition	Relation	To Laser Line, Å	14 eV	18 eV	33 eV
8819	6s[1-1/2] ₂ - 6p[2-1/2] ₃	DL	24,825	33,000	22,000	8,100
8739	6p [1/2] ₁ - 6d[1-1/2] ₂	PL	39,966	1,700	1,800	430
8647	6s' [1/2] ₁ - 7p[1-1/2] ₁	PL	41,427	1,900	1,300	850
8409	6s[1-1/2] ₂ - 6p[1-1/2] ₁	DU, DL	8409, 20,262	1,900	1,100	1,500
8346	6s' [1/2] ₁ - 6p'[1-1/2] ₂	DL	38,697	11,000	8,100	9,400
8280	6s[1-1/2] ₁ - 6p [1/2] ₀	DL	26,511	15,000	15,000	39,000
8231	6s[1-1/2] ₂ - 6p[1-1/2] ₂	DL	36,859	29,000	17,500	19,000
8206	6s' [1/2] ₀ - 6p'[1-1/2] ₁	DL	38,697	2,700	1,400	1,000
8171	6p[1-1/2] ₂ - 5d'[1-1/2] ₂	DU	46,109			
8171	5d [1/2] ₁ - 8p[2-1/2] ₂	PU	36,798	3,500	2,300	1,000
8057	5d[3-1/2] ₃ - 5f[4-1/2] ₄	PU	35,080	1,900	950	680
7967	6s' [1/2] ₀ - 7p[1-1/2] ₁	DL	41,527	4,500	2,700	1,900
7887	6s' [1/2] ₁ - 6p' [1/2] ₀			3,800	3,500	11,400
7664	5d[1-1/2] ₂ - 5f[1-1/2] ₂	PU	45,393	900	650	600
7643	5d[1-1/2] ₂ - 5f[2-1/2] ₃	PU	45,393	4,900	1,300	1,100
7501	6p[2-1/2] ₂ - 5d'[1-1/2] ₂	PL, PU	26,276, 9405	1,500	1,000	1,200
7393	6p[1-1/2] ₂ - 7d[2-1/2] ₃	PL	36,859	150	830	510

TABLE 1 (cont'd)
RELATIVE CROSS SECTION IN XENON

Wave-length, Å	Transition	Relation	To Laser Line, Å	14 eV	18 eV	33 eV
7336	6p[2-1/2] ₂ - 5d'[2-1/2] ₃	PL, PU	26,276,9405	3,000	2,100	2,400
7285	6p[1-1/2] ₁ - 7d[2-1/2] ₂	PL, PU	20,262,8409	1,900	1,000	770
7119	6p[2-1/2] ₃ - 7d[3-1/2] ₄	PL	24,825	1,700	920	600
6882	6p[2-1/2] ₂ - 7d[3-1/2] ₃	PL	26,276	1,300	1,000	2,100
6778	5d [1/2] ₁ - 6f[1-1/2] ₁	PU	36,798		280	
6728	5d[1-1/2] ₂ - 10p[2-1/2] ₂	PU	45,393			
6728	6p [1/2] ₁ - 7d [1/2] ₁	PL	39,966		260	850
*6668	6p [1/2] ₁ - 7d [1/2] ₀	PL	39,966	1,500	680	
6632	6p[1-1/2] ₂ - 8d[1-1/2] ₂	PL	36,859		230	
6595	6p[1-1/2] ₂ - 8d[2-1/2] ₃	PL	36,859		380	850

* Quantum numbers same as laser transition except for n.

Figure 21 and 22 respectively. The 8346\AA $6s'[1/2]_1 - 6p'[1-1/2]_2$ transition, Figure 23, has its maximum at 16 eV and has a slower fall-off at higher energy. Figures 24 and 25 give the 8280\AA $6s[1-1/2]_1 - 6p[1/2]_0$ and 7887\AA $6s'[1/2]_1 - 6p[1/2]_0$ transitions. These excitation functions are noteworthy for three reasons. First, the principle maximum is at 26 eV, unlike the other transitions observed. Furthermore, excepting for the total angular momentum of the core, the configuration of these two transitions are the same. Since it is unlikely that the $6p'$ levels are affected by cascade to the same degree as the $6p$ levels, the indication is that the double maximum excitation is a characteristic of the level cross section (see Figure 26). Comparison with the data of Fel'tsan²⁶ and Rostovikova²⁷ indicate that this shape is indeed characteristic of all terms with this quantum configuration. Lastly, the excitation function at 8280\AA is proportional to the cross section for populating the lower laser level of the $26,511\text{\AA}$ line. The maximum occurring at higher energy may account for the cw inversion observed in a xenon-helium discharge.

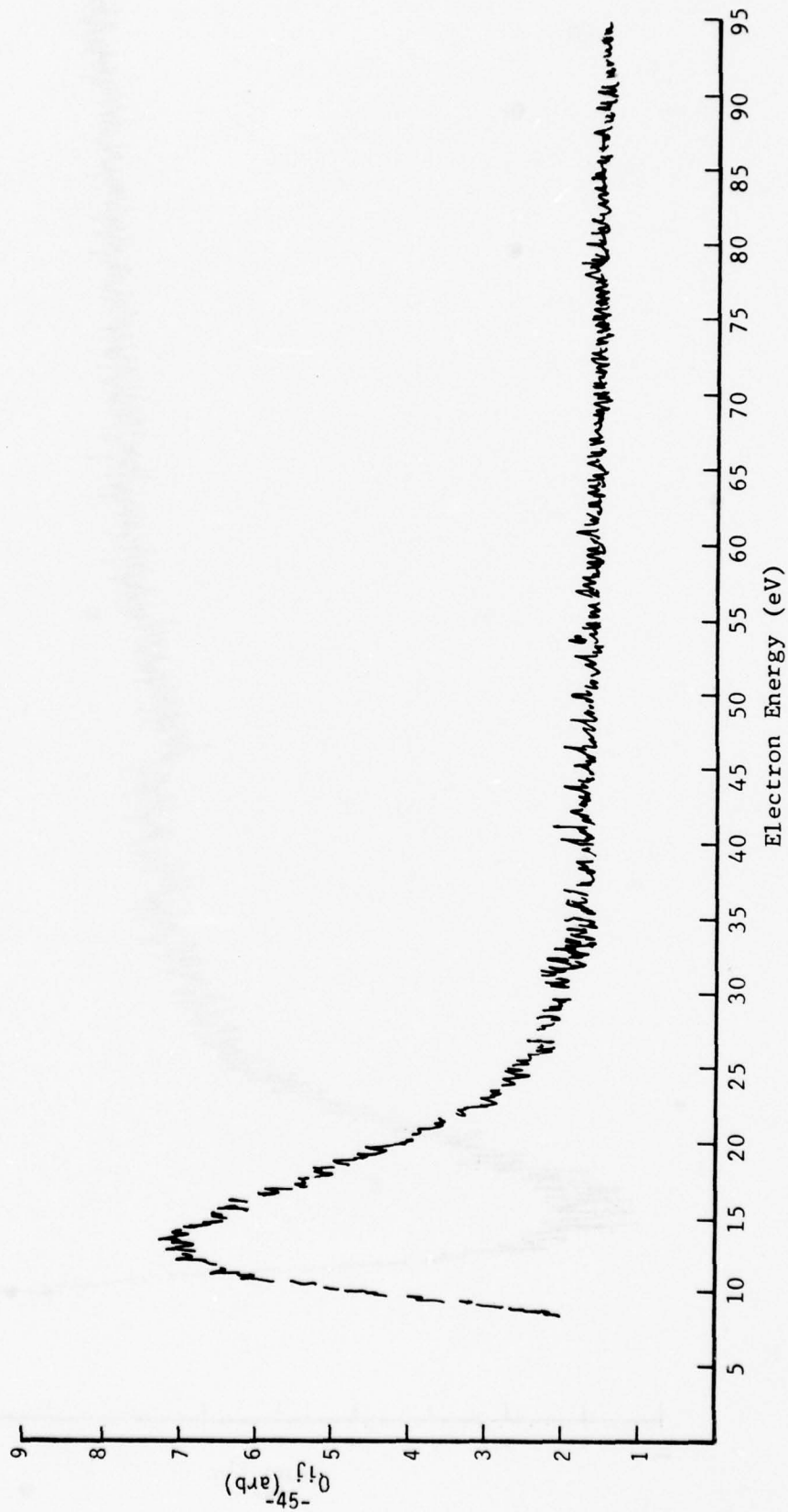


FIGURE 20 - Xe 8819 Å 6s [3/2]₂ - 6p [3/2]₃

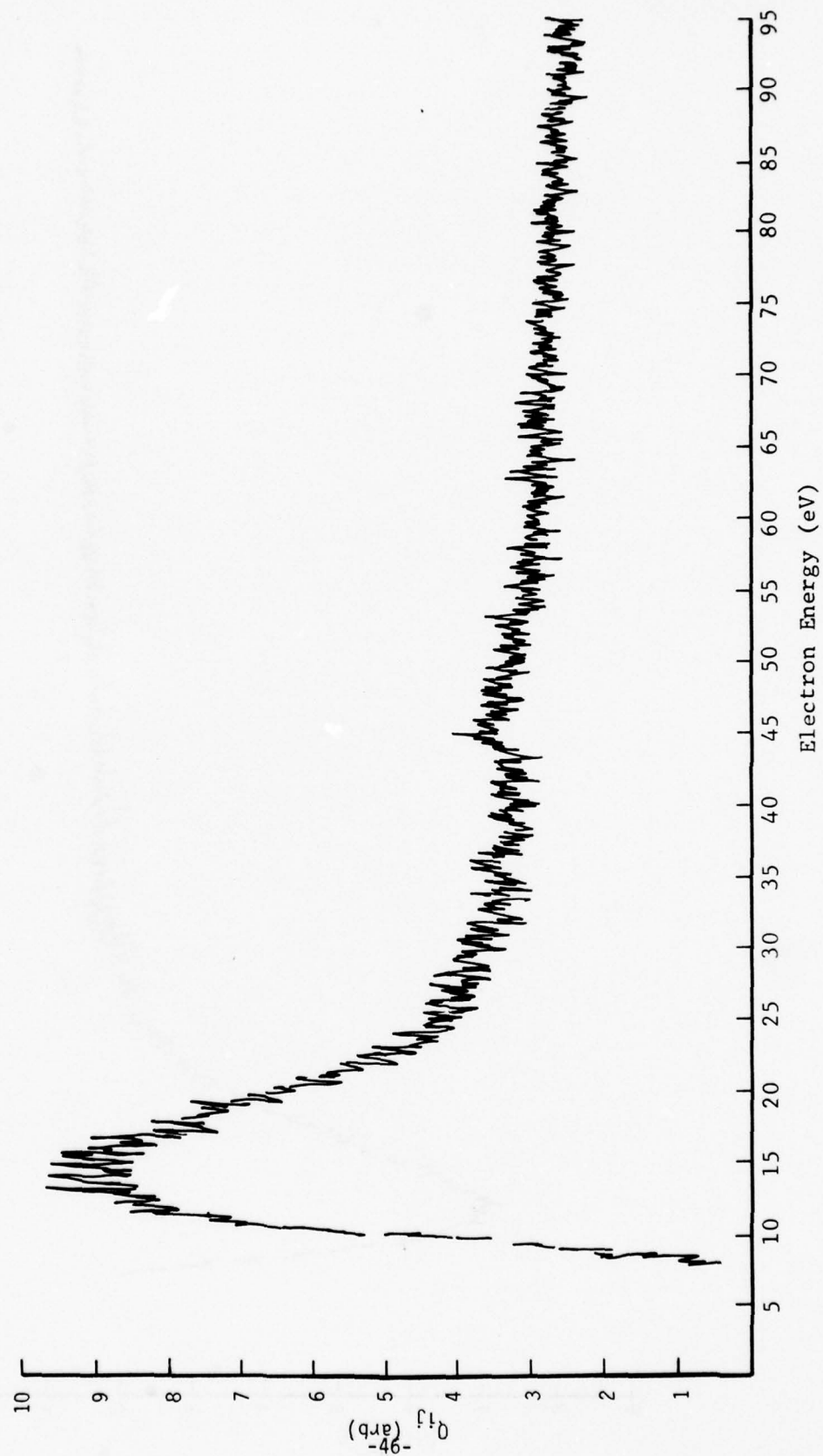


FIGURE 21 - Xe 8231 Å $6s[3/2]_2 - 6p[3/2]_2$

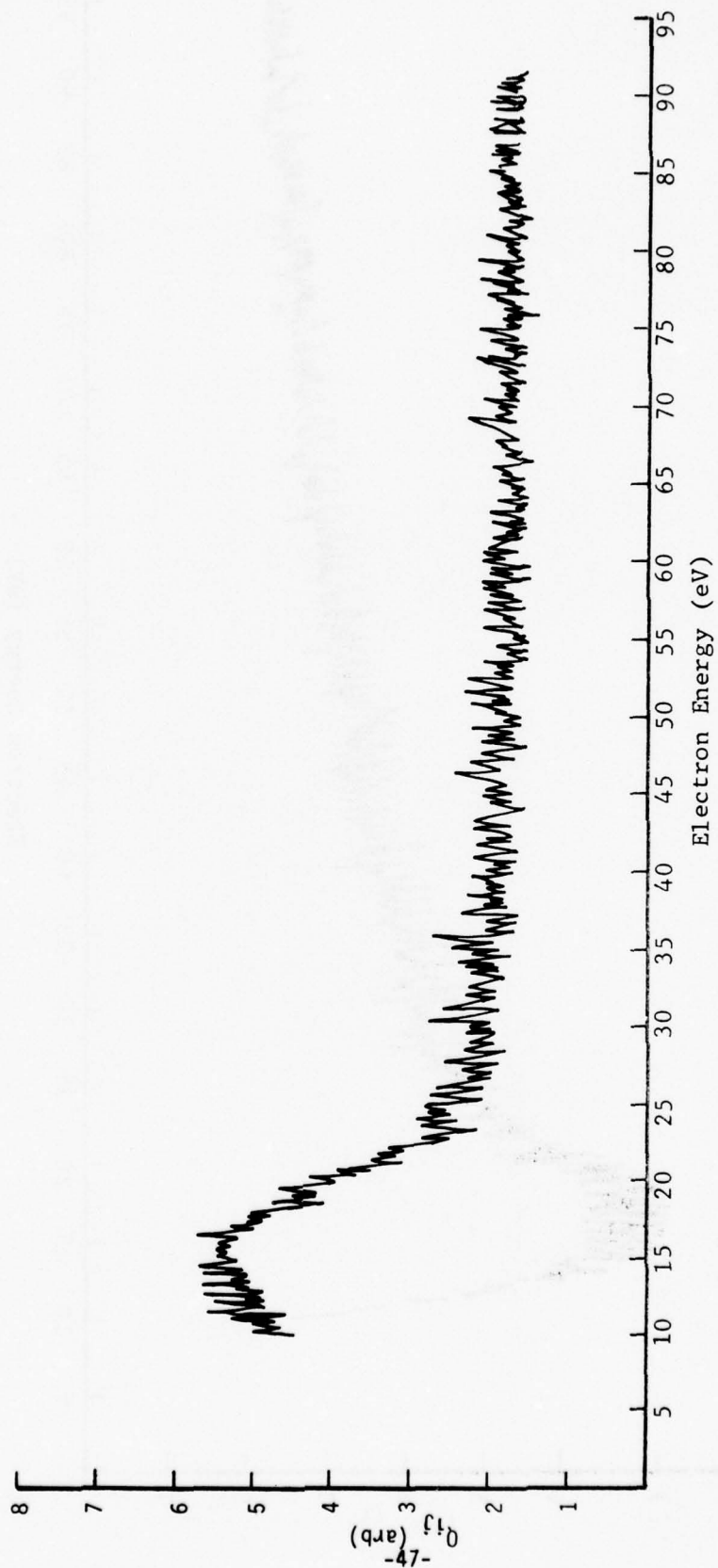


FIGURE 22 - Xe 7336 Å $6p[5/2]_2 - 5d'[5/2]_3$

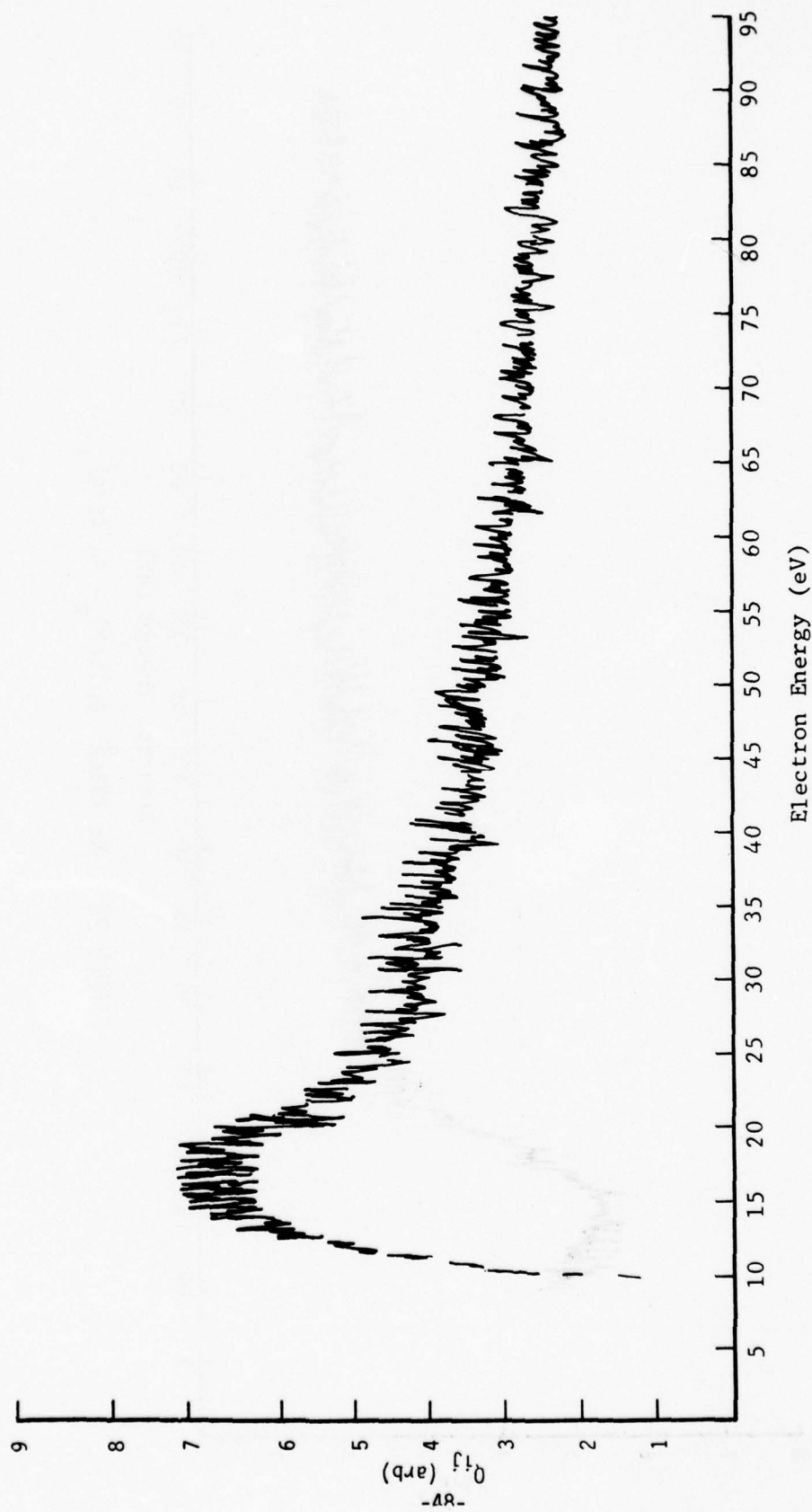


FIGURE 23 - Xe 8346 Å $6s'[1/2]_1 - 6p'[3/2]_2$

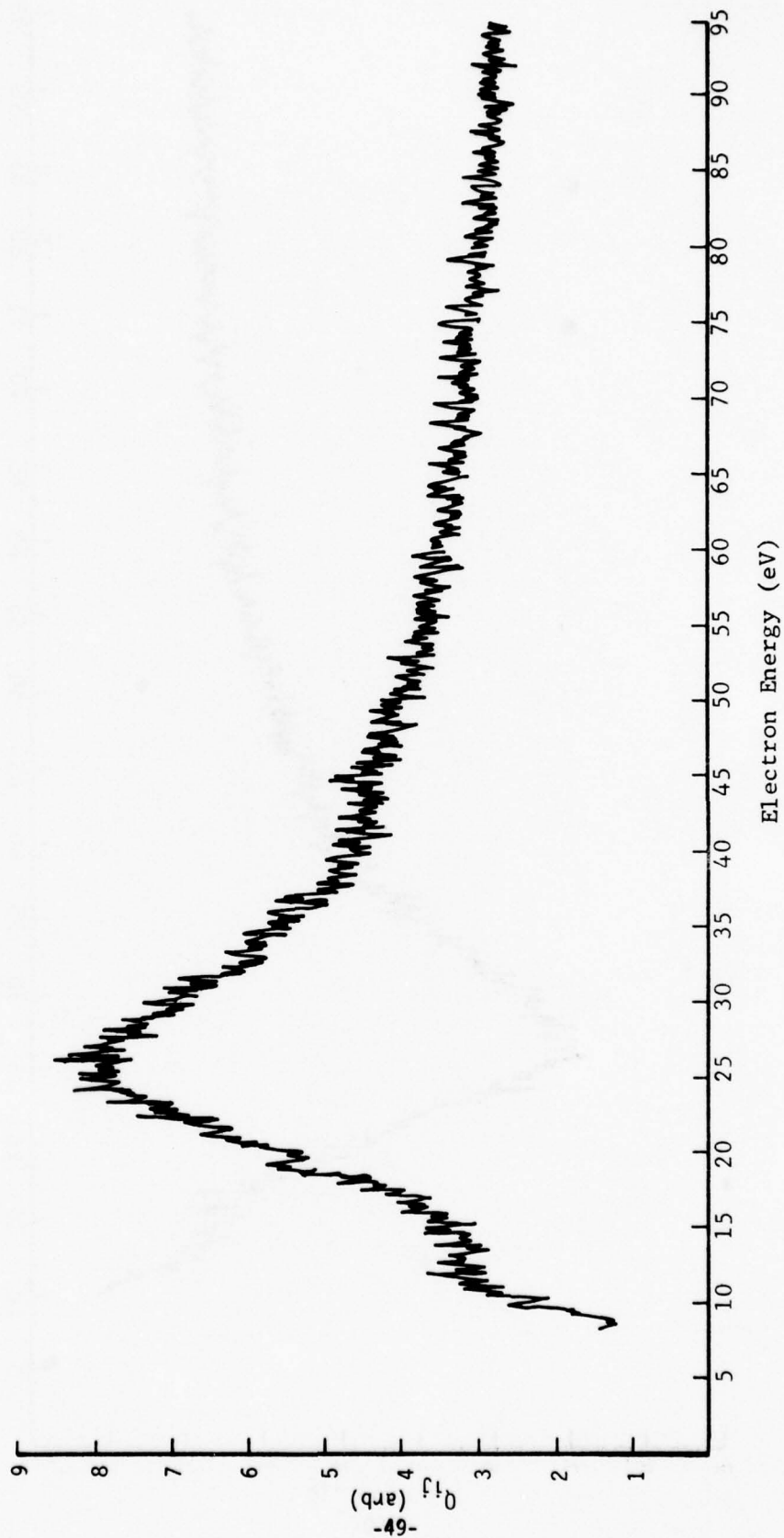


FIGURE 24 - Xe 8280 Å 6s[3/2]₁ - 6p[1/2]₀

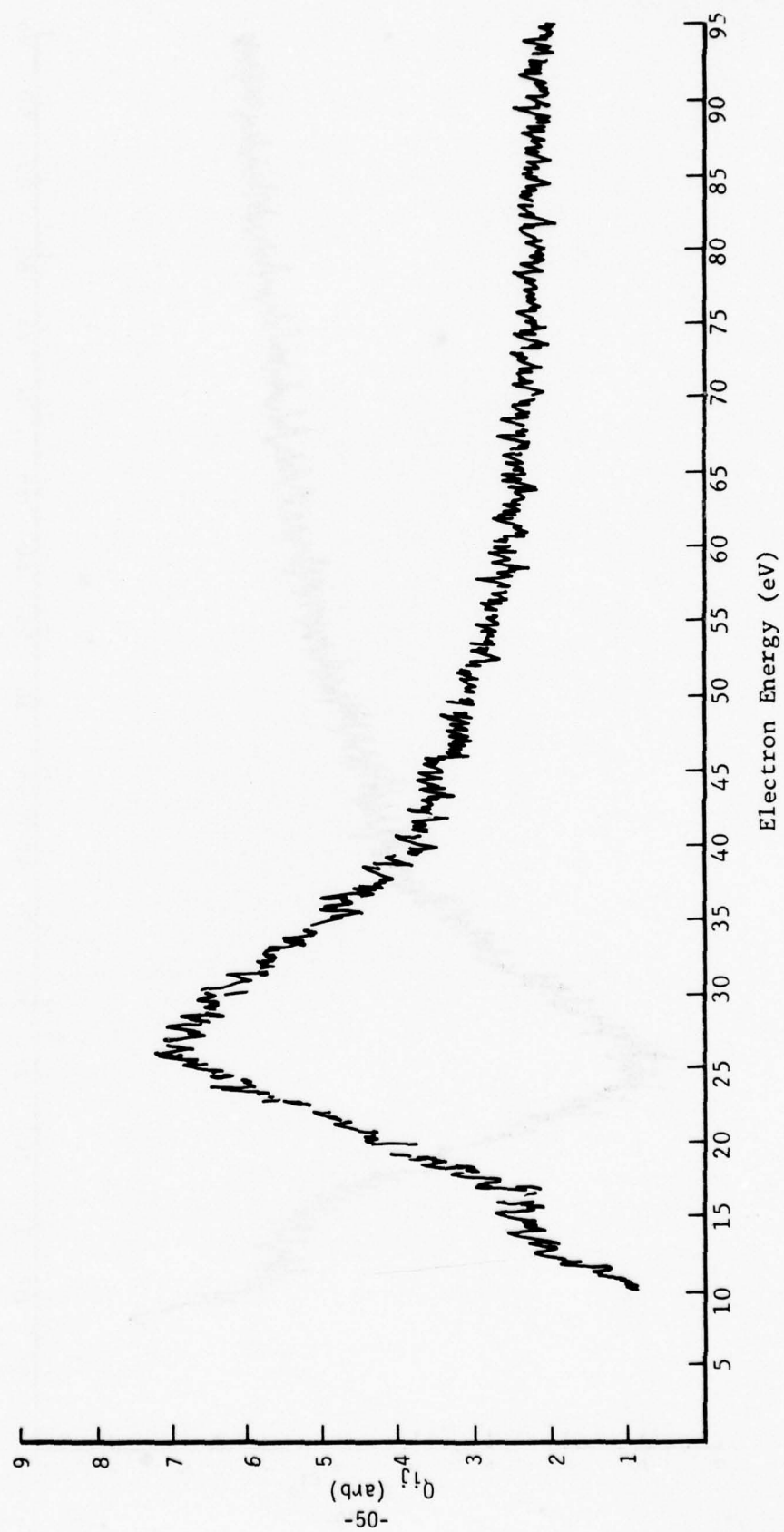


FIGURE 25 - Xe 7887 Å $6s'[1/2]_1 - 6p[1/2]_0$

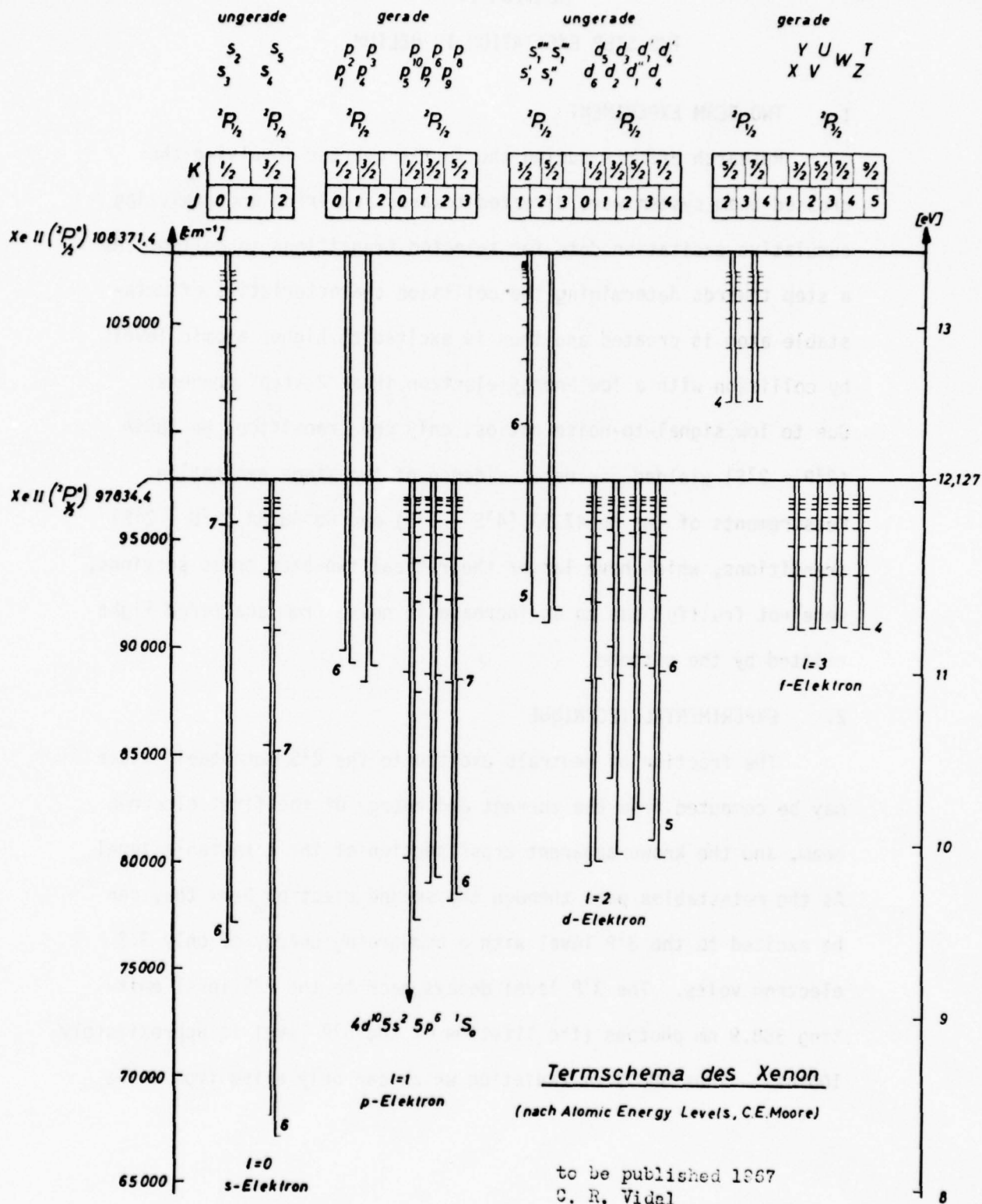


FIGURE 26 - Energy level diagram of xenon
-51-

SECTION IV

TWO-STEP EXCITATION IN HELIUM

1. TWO BEAM EXPERIMENT

Research efforts during the fourth quarter involving the crossed beam system were directed towards acquiring and analyzing cumulative excitation data for selected transitions in helium. As a step towards determining the collision characteristics of metastable atom is created and then is excited to higher atomic levels by collision with a low energy electron in a "2-step" process. Due to low signal-to-noise ratios, only one transition, He 3889Å ($3^3P - 2^3S$) yielded concrete evidence of two stage excitation. Measurements of the He 4713Å ($4^3S - 2^3S$) and He 5876Å ($3^3D + 2^3S$) transitions, which have larger theoretical two-step cross sections, were not fruitful due to an increase in noise from scattered light emitted by the cathode.

2. EXPERIMENTAL TECHNIQUE

The fraction of neutrals excited to the 2^3S metastable state may be computed from the current and energy of the first electron beam, and the known apparent cross section of the metastable level. As the metastables pass through the second electron beam they can be excited to the 3^3P level with a bombarding energy of only 3.2 electron volts. The 3^3P level decays back to the 2^3S level emitting 388.9 nm photons (the lifetime of the 3^3P level is approximately 100 ns). Thus 388.9 nm radiation which can only arise from a two

stage process can be monitored while sweeping the lower electron beam from 3.2 to 19.8 volts.

Above 19.8 volts it is possible to observe excitation of metastables created in the lower beam, and also direct excitation of the 3^3P level from the high energy tail of the electrons in the beam (Figure 27; the direct signal plotted here is divided by a factor of 10^7). These signals cannot be effectively discriminated against, and impose an upper limit of 20 volts on the useful energy range for measuring the desired cross section. Additionally, as a result of the current dependence on accelerating voltage, there is insufficient current below 8 eV to yield an interpretable signal. In practice therefore, unambiguous signals are only obtainable between 8 and 20 eV.

The apparent cross section for excitation from the metastable level to an upper level is obtained from the two-step signal in the following way. We first assume that the ratio between the number of metastables created in the upper beam, N_1^* , and the remaining neutrals, N_1 , does not change as the volume element containing them flows out of the first electron beam and into the second electron beam. Thus we have:

$$\frac{N_1^*}{N_1} = \frac{N_2^*}{N_2} \quad (24)$$

where the subscripts designate which electron beam the volume element is in. We assume this to be true even though the volume element is free to expand. This assumption is not strictly accurate

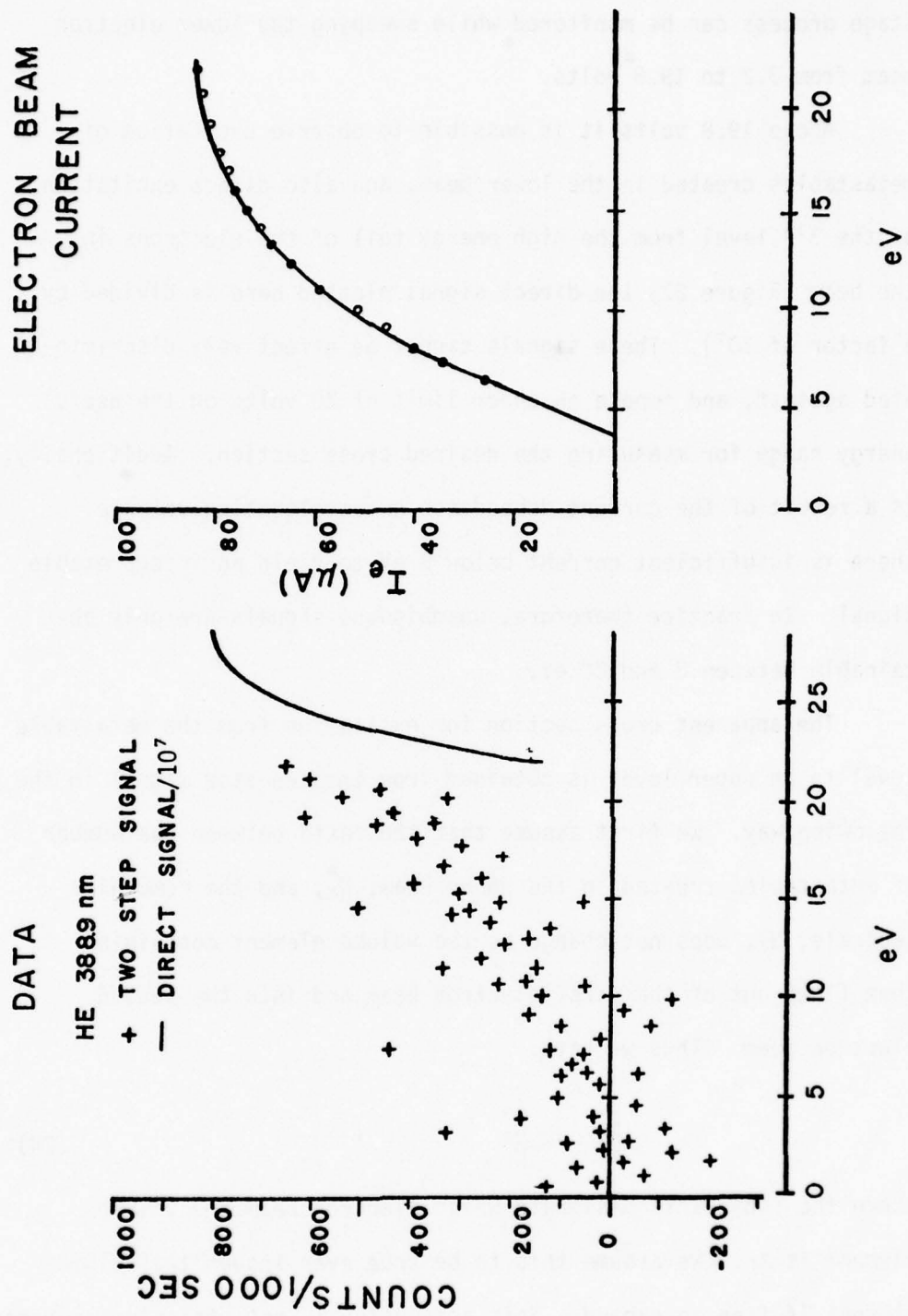


FIGURE 27 - Comparison of raw two-step excitation data of the function of the electron gun current vs. accelerating voltage

because the mean free path of the atoms is not sufficiently long that collisional deactivation and diffusion may be ignored. Conditions in the first electron beam can be controlled so that the following rate equation describes creation and loss terms.

$$\frac{dN_1^*}{dt} = N_1 Q_i' \Delta x_1 \frac{I_{e1}}{e} - N_1^* \bar{v} A = 0 \quad (25)$$

where Q_i' is the apparent cross section for populating the metastable level, Δx_1 is the path length of the electrons through the interaction volume, I_{e1} is the electron current in the first electron beam, e is the electron charge, \bar{v} is the average velocity of the atoms, and A is the exit area. Combining Equations (24) and (25) yields an expression for the metastable target density (composed of metastables created in the first electron beam) in the second electron beam interacting region.

$$N_2^* = \frac{N_2 Q_i' \Delta x_1 I_{e1}}{\bar{v} A e} \quad (26)$$

The photon flux from the single step excitation process is related to the product of the single step cross section and the neutral atom number density as follows:

$$F_{ki} = N_2 Q_{ki} \Delta x_2 \frac{I_{e2}}{e} \quad (27)$$

where F_{ki} is the photon flux for the k to i transition, Q_{ki} is the optical cross section for exciting the level k , Δx_2 is the length of path of the electrons in the second electron beam, and

I_{e_2} is the current in the second electron beam. Now it is seen that the metastable density in the second electron beam may be determined by measurements of the photon flux from a single excitation transition, the currents in both electron beams, and a knowledge of the pertinent cross sections and geometric factors.

$$N_2^* = \left(\frac{F_{ki} Q_{ik}' \Delta x_1 I_{e_1}}{Q_{ki} \Delta x_2 I_{e_2} \bar{v} A} \right) \quad (28)$$

Finally, for excitation from the metastable level to a short-lived upper level, the rate equation is

$$\frac{dN^{**}}{dt} = \frac{N_2^* Q_{ik}' \Delta x_2 I_{e_2}}{e} - \sum_j F_{kj}^+ \quad (29)$$

where Q_{ik}' is the apparent cross section for exciting the metastable to the level k_1 and $\sum_j F_{kj}^+$ is the sum of all two step photon fluxes out of the level k . By solving for Q_{ik}' and substituting Equation (28) for N_2^* , we have

$$Q_{ik}' = \frac{Q_{ki} \bar{v} A e \sum_j F_{kj}^+}{Q_{ki} \Delta x_1 I_{e_1} F_{ki}} \quad (30)$$

The signal observed at the output of the detection and recording system is related to the total photon flux as follows:

$$F_{ki} = \frac{4\pi}{\Omega} F_{ki}(\Omega) = \frac{4\pi}{\Omega} \frac{\Phi_{ki}}{S(\lambda)} \quad (31)$$

Similarly

$$\sum F_{kj}^+ = \frac{4\pi \sum \phi_{kj}^+}{\Omega S(\lambda)} \quad (32)$$

where Ω is the solid angle subtended by the detecting optics, $F_{ki}(\Omega)$ is the fraction of the total photon flux collected (assuming isotropic radiation), ϕ_{ki} is the recorded signal, and $S(\lambda)$ is the spectral response of the detection system. Also the total radiation out of a given level is related to one of the transitions by the ratio of the Einstein coefficients

$$F_{ki} = \frac{A_{ki}}{\sum_j A_{kj}} \sum_j F_{kj} \quad (33)$$

The ratio $\frac{A_{ki}}{\sum_j A_{kj}}$ is defined as the branching ratio, B_{ki} , for the k to i transition:

$$B_{ki} \equiv \frac{A_{ki}}{\sum_j A_{kj}} \quad (34)$$

Incorporating Equations (31) through (34) into Equation (30) yields

$$Q'_{ik} = \frac{\phi_{ki} Q_{k\epsilon} \bar{\nu} A_e}{B_{ki} \phi_{ki} Q_i \Delta x_i I_{e_1}} \quad (35)$$

This is the equation used to evaluate two-step excitation cross sections with the crossed beam systems.

3. RESULTS

The data acquired for the cross section $2^3S \rightarrow 3^3P$ indicates that the cross section has a maximum value of approximately 1 to 2×10^{-17} cm (Figure 28). Each data point plotted here represents the average of eight different integration periods of 1000 seconds. Flannery et al.^{29,30} have generated three theoretical calculations for the level cross section $2^3S \rightarrow 3^3P$. These are the Born approximation, the Eikonal approximation, and the Vainstein, Presnyakov and Sobel'man (VPS) approximation. At 14 eV there is an approximate factor of three difference between this experiment and the lowest of the theoretical treatments, the VPS. Poor signal-to-noise ratios prevented checking another noteworthy conclusion of Flannery's work, that at low energy 3D levels have the largest cross section from the 2^3S level, in contrast to cross sections from the ground state, which are larger for P levels. Considering the difficult nature of this experiment and the fact that even direct cross section measurements by different experiments commonly differ by factors of two, we feel that the experimental data is not in serious disagreement with theory. However, the data does favor theoretical treatments which give a lower value for the cross section, particularly in the threshold region.

4. MODIFICATIONS

Additional measurements in helium were attempted, but were not productive as a result of a poor signal strength. The conclusion drawn from these efforts directed that the system might

HELIUM $2^3S - 3^3P$

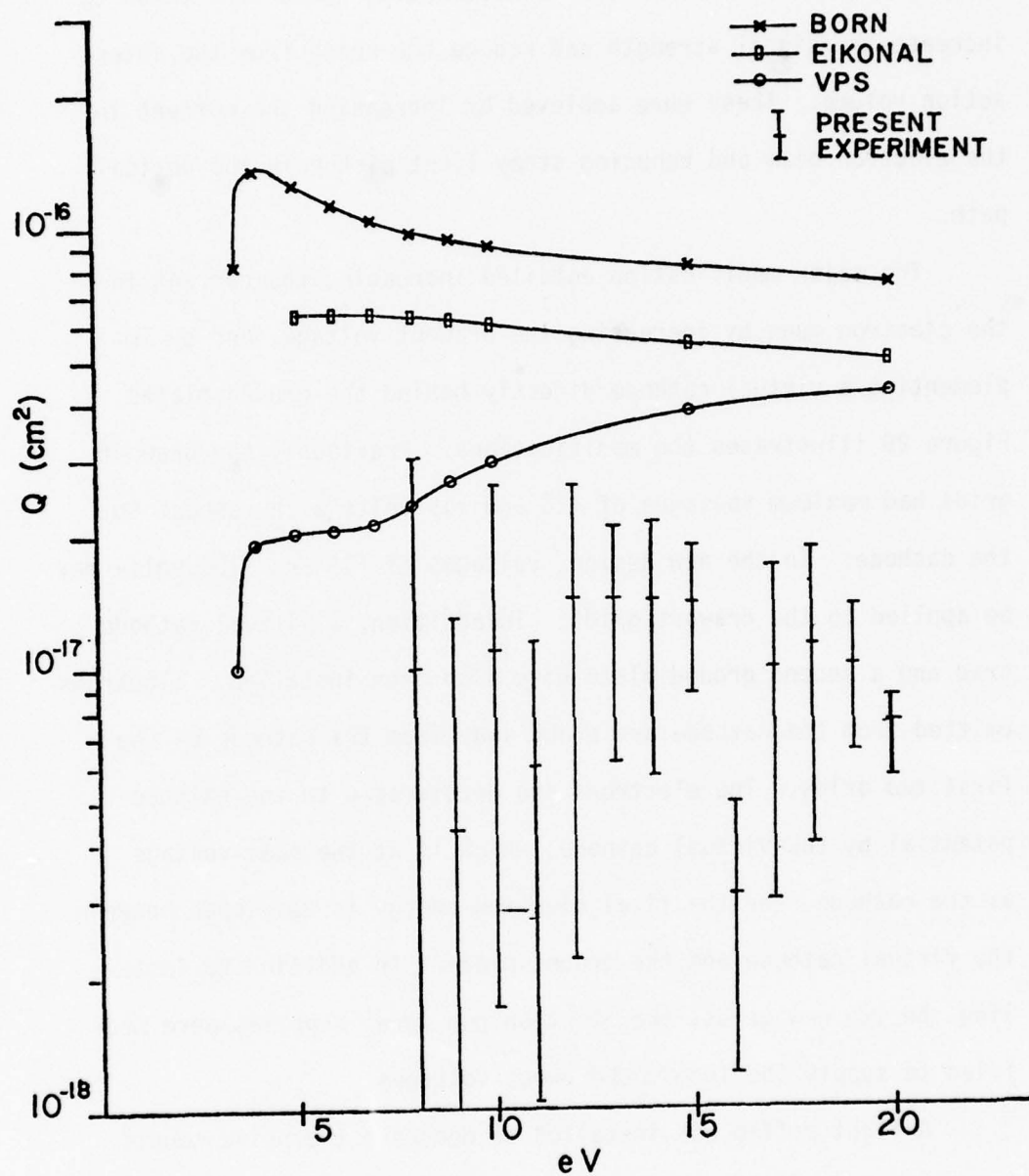
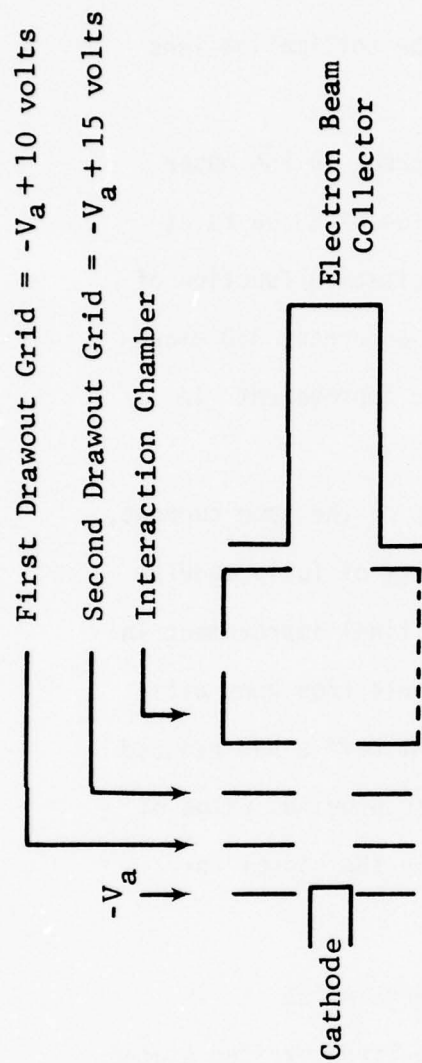


FIGURE 28 - Helium $2^3S \rightarrow 3^3P$

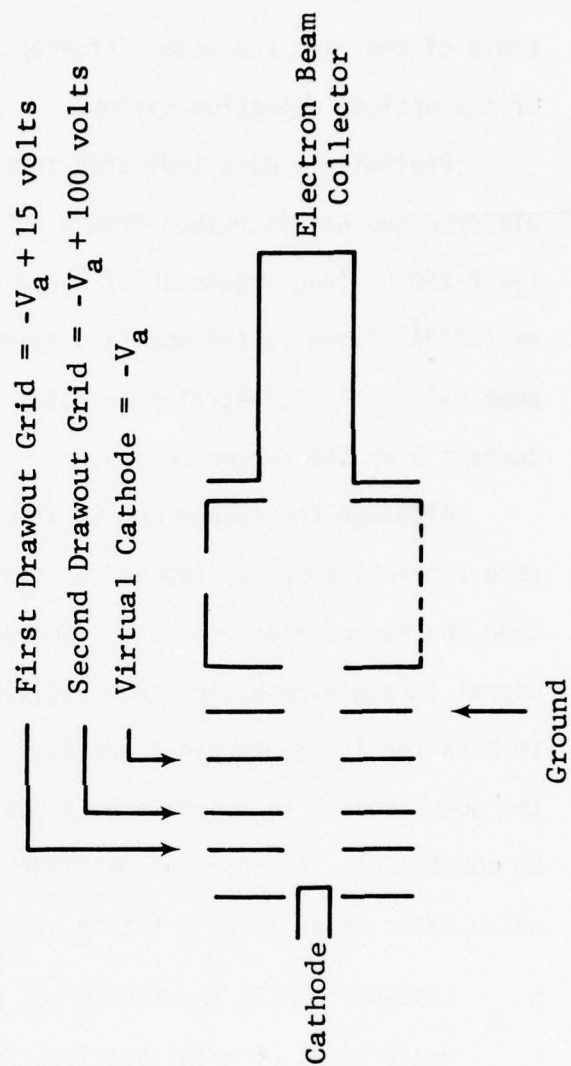
be most productively employed acquiring optical data from exciting metastable states, provided that improvements in the signal-to-noise ratio could be achieved. Consequently, steps were taken to increase the signal strength and reduce the noise from the interaction volume. These were achieved by increasing the current in the electron beam and reducing stray light pickup in the optical path.

The major modification entailed increasing the current in the electron guns by increasing the drawout voltage, and by implementing a virtual cathode directly behind the ground plates. Figure 29 illustrates the modifications. Previously the drawout grids had maximum voltages of +10 and +15 volts with respect to the cathode. In the new design, voltages of +15 and +100 volts may be applied to the drawout grids. In addition, a virtual cathode grid and a second ground plate have also been installed. Electrons emitted from the cathode are drawn away from the cathode by the first two grids. The electrons are decelerated to the cathode potential by the virtual cathode, which is at the same voltage as the cathode, and the final electron energy is developed between the virtual cathode and the ground plate. In addition to installing the two new grids, the electron gun power supplies were modified to supply the increased drawout voltages.

A light baffle was installed to decrease the noise counts contributed by the cathodes and the scattered radiation from the upper electron gun. The light baffle consists of a black anodized



OLD DESIGN



NEW DESIGN

FIGURE 29 - Modification of electron gun

aluminum plate with two apertures aligned with the electron beams. The solid angle of the apertures is slightly larger than the solid angle of the electron beams intercepted by the collimating lens of the optical detection system.

Preliminary data indicates that the current in the upper electron gun has increased from a typical value of 50 μ a to at least 250 μ a (see Figure 30 of the direct excitation function of He (3889Å) taken in the modified system with a current 350 microamperes). This illustrates a factor of seven improvement in current over the former design.

Although the second gun is also capable of the same current, some limitation may be imposed by the necessity of fully modulating the second electron gun. Therefore the final improvement in signal strength resulting from modifying the electron guns will be a factor lying between 5 and 25. The light baffle has reduced the noise counts to approximately 50% of their previous value of 50 counts/sec., so that the net improvement in the signal-to-noise ratio is at least a factor of ten.

5. LINEARITY TESTS AND SOURCES OF MISINTERPRETATION

Measurement of cross sections from long-lived excited states of an atom involves measuring a signal which is about six orders of magnitude smaller than signals resulting from direct electron impact on an atom in the ground state. This is because the production efficiency for the metastable target species is poor for conditions where the target number density can be determined from

its creation rate. Therefore instrumentation must be used which has the capability of discriminating against signals larger than or of comparable size to the desired signal. Direct cross sections of ground state atoms and molecules which are compatible with vacuum electronics can be measured with comparative ease. However, in the range between these signals and signals which are six orders of magnitude smaller, many effects manifest themselves with the conventional electron guns used to perform cross section measurements. Some of these effects can completely mask the desired signals. The cumulative cross section technique involves the use of two electron guns (one of which is current modulated) and the measurement of coupled modulated signal produced from stepwise excitation from the two guns. Therefore any other source of modulated signal will limit the ability to obtain true cumulative data.

Some sources of spurious modulated signal are (1) the energy spread of the electron beam folded with the direct excitation cross section, (2) direct population of the observed upper level outside the Faraday cage, leading to scattered radiation picked up by the detection system, (3) modulation of the potential shift in the unmodulated gun arising from introduction of ions, and (4) inadequate chopping of current in the modulated gun, leaving a weak beam of higher energy electrons during the "off" half-cycle of the electron beam.

It is believed that all of these effects have been observed to some degree in the electron guns before the addition of the

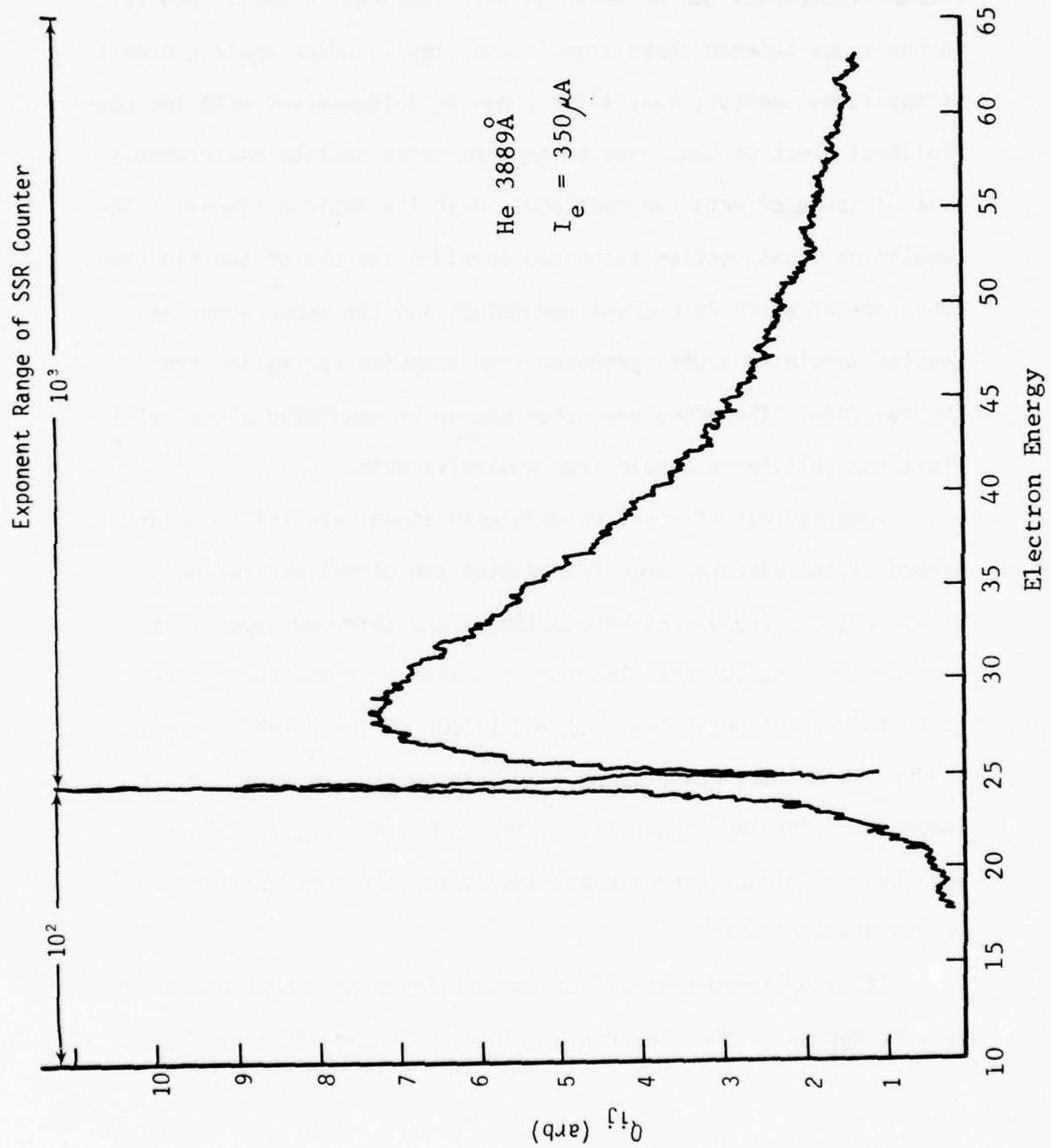


FIGURE 30 - Helium 3889 Å

virtual cathode. The grid voltages and the accelerating voltage for which these spurious signals appeared were identified, allowing for a study of cumulative excitation without ambiguous results. Since the addition of the virtual cathodes and the resulting increase in current might alter the onset potentials of these undesirable effects, recent experimental work has been conducted with attention given to identifying these sources of modulated signal. Figure 31 is a relative excitation function of the helium 3889Å line, taken under typical operating conditions but at modest sensitivity. This curve and other excitation functions presented here are uncorrected for the change in electron current with electron energy, nor are they corrected for potential shift.

Figure 32 gives the response of current as a function of accelerating voltage. When operating the system with only modest sensitivity, the excitation function in Figure 31 shows no abnormal features which might be attributed to any of the four sources of spurious in-phase signal mentioned above. Figure 33 is the same transition as in Figure 31 in helium monitored under similar conditions but with three orders of magnitude increase in sensitivity. This is achieved by increasing the pressure in the gas reservoir, the slit width on the monochromator, and the integration time of the detection system. The three peaks between 24 and 25 eV come about from auto-ranging of the counter, as the count rate goes from 10^2 /per second up to 10^5 /per second. Below the onset of direct excitation at 24 eV (uncorrected for potential shift) there

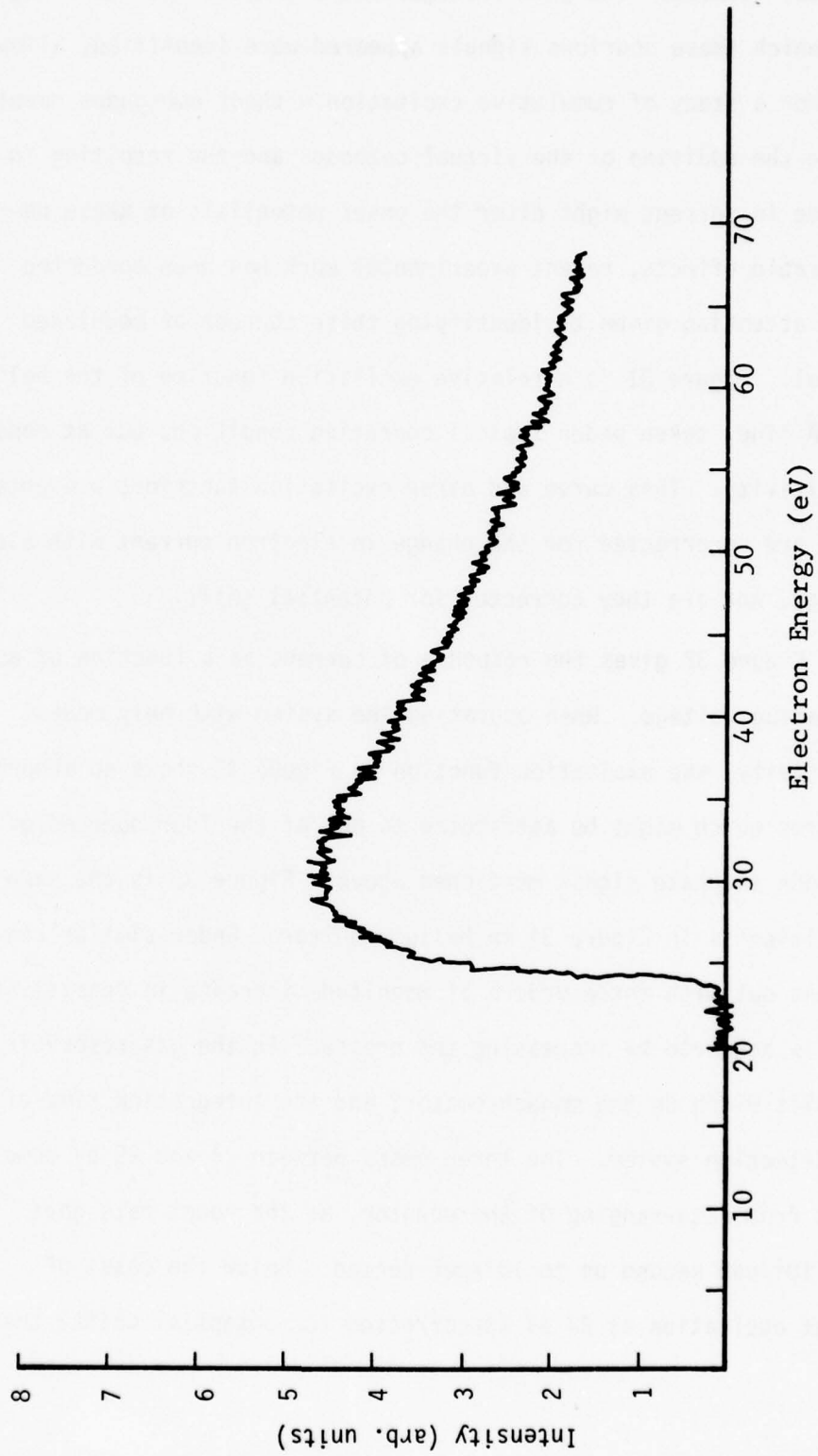


FIGURE 31 - Helium 3889Å

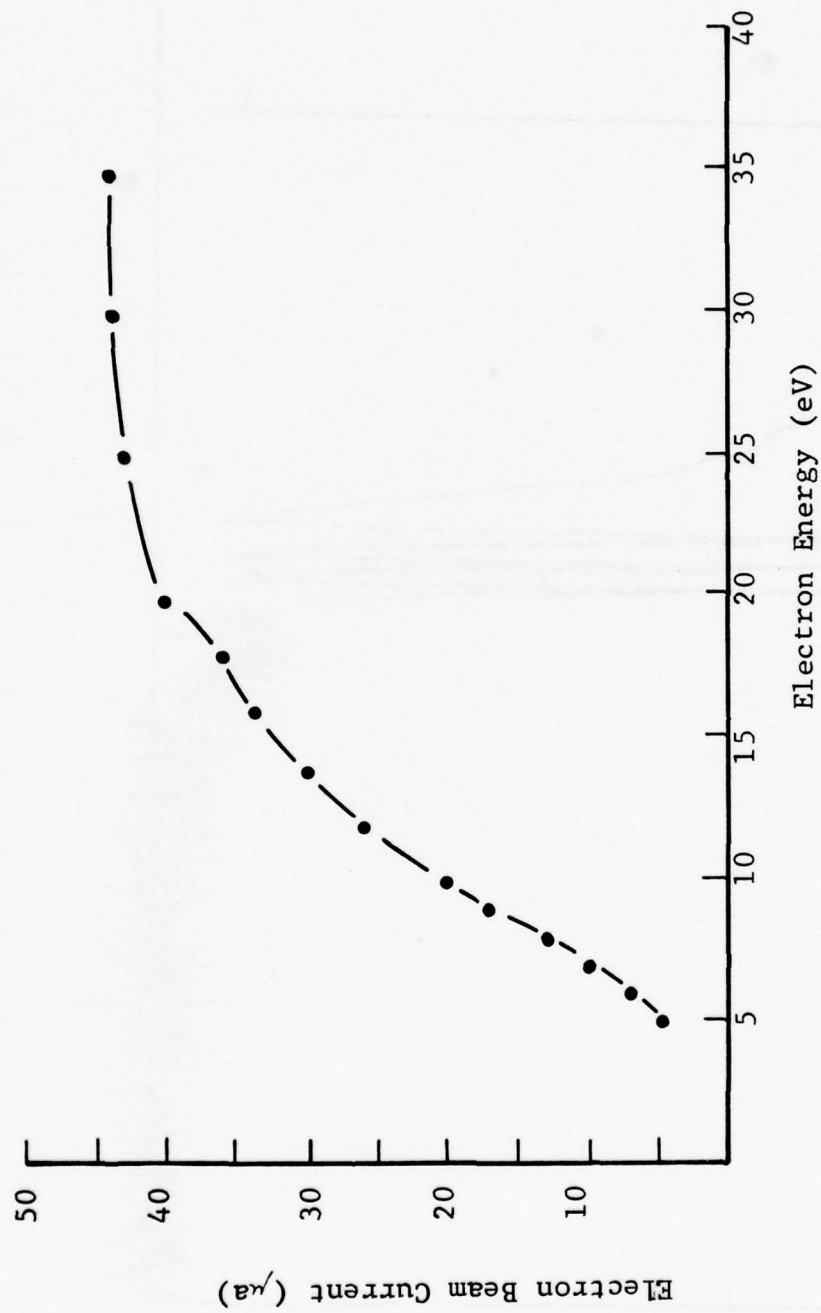
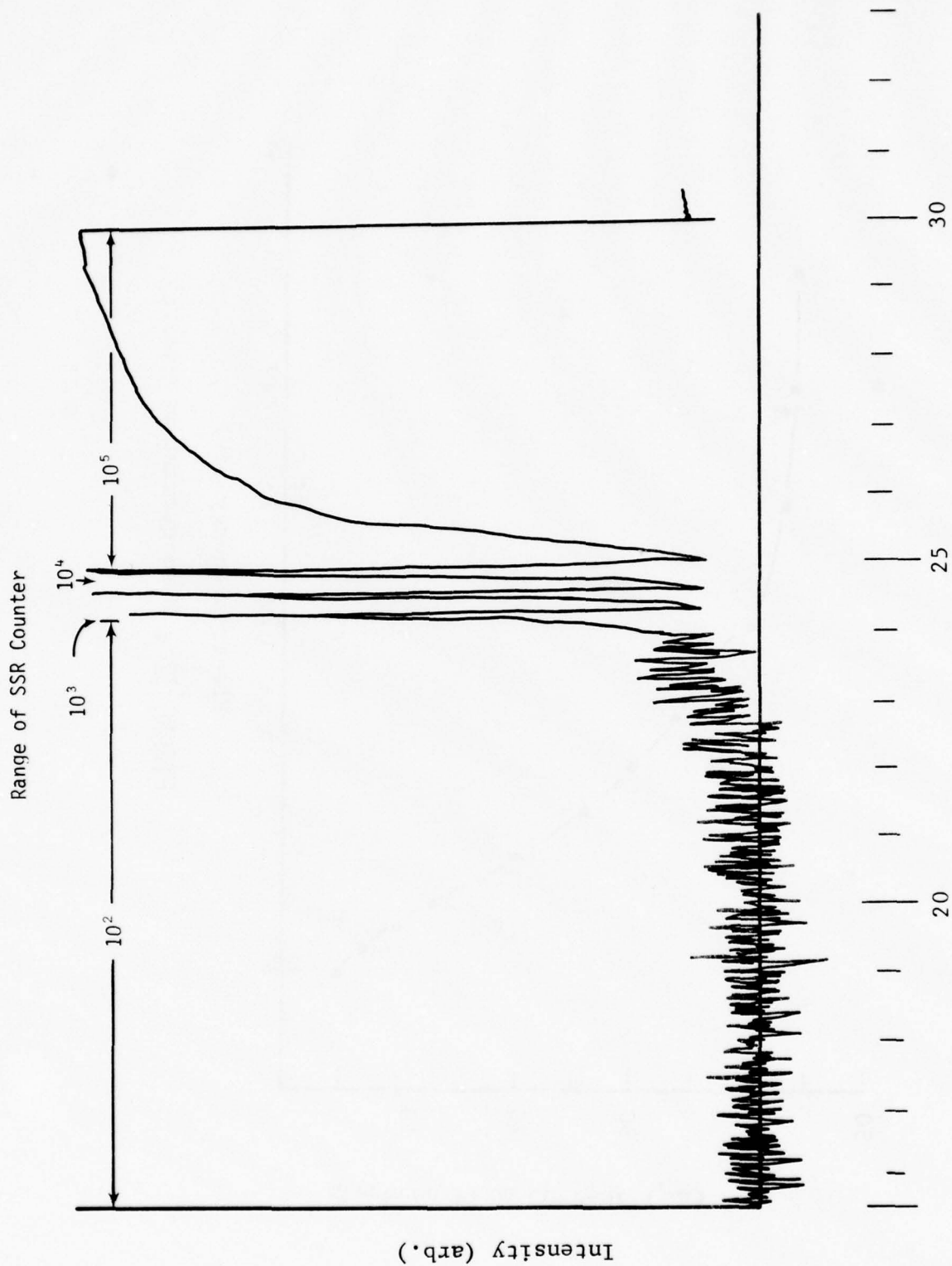


FIGURE 32 - Beam current vs. energy



Electron Energy (eV)

FIGURE 33 - Helium 3889Å

appears a very weak in-phase signal beginning at about 22 eV. The metastable source gun was not operating, but this weak signal could be cumulative excitation from metastables produced when the electron beam energy exceeded 19.8 eV. On the other hand, it could be $1^1S \rightarrow 3^3P$ excitation observable from the high energy tail of the electron beam. The threshold for direct excitation becomes ambiguous when examined with high sensitivity due to the distribution of electron energies in the electron beam. Another possibility is illuminated by Figure 34. While the accelerating voltage, V_{acc} is developed between the virtual cathode and the last grid, the collector voltage, V_c , is applied with respect to ground, so that the total electron energy beyond the Faraday cage is $(V_{acc} + V_c)$. Since this region is not in the viewing area of the detection system, ordinarily the effect of the added accelerating voltage would not be observable. But if even a minute fraction of radiation from the region between the Faraday cage and the collector made its way through optical reflection into the detection system, true cumulative data would be compromised.

Figure 35 is the He 3889Å transition monitored at a sensitivity similar to Figure 33, but with collector voltage set at eleven volts. In-phase signal now appears at 20 eV. This signal was eliminated by reducing the monochromator slit height to 3 mm and by lowering the collector voltage to 4 volts. Reducing the slit height was also beneficial in lowering noise counts from the

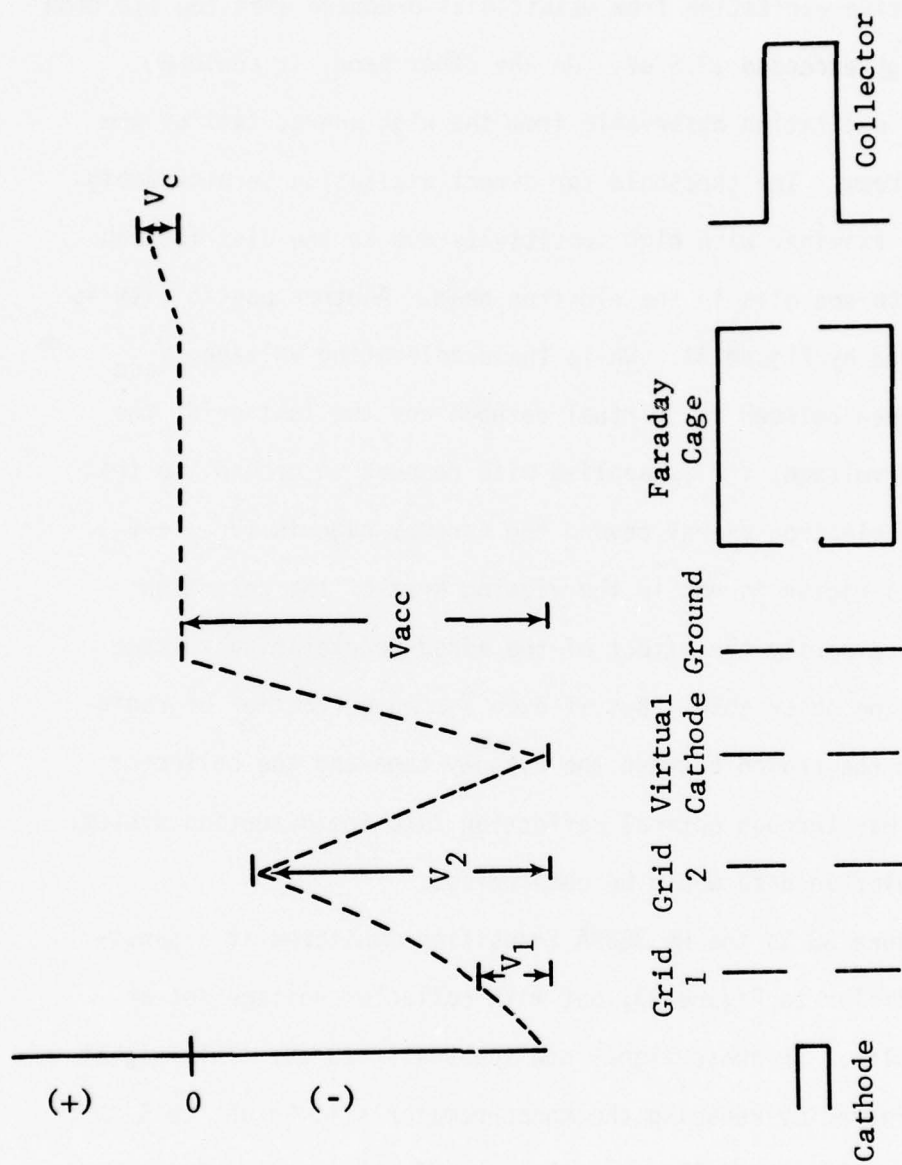


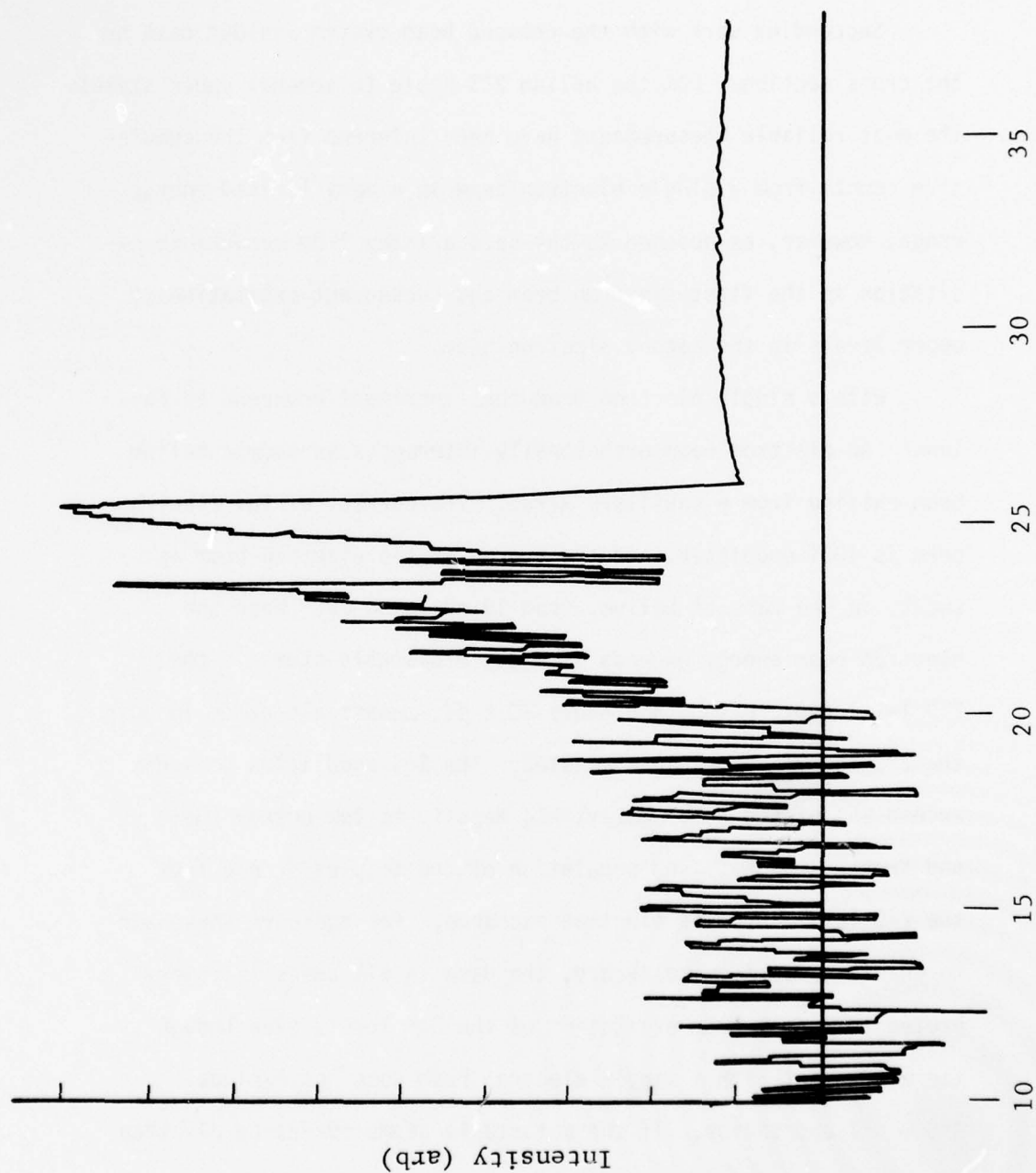
FIGURE 34 - Voltage configuration of electron beam

cathode. Figure 36 shows the 3889\AA transition following these measures.

6. SINGLE BEAM EXPERIMENT

Succeeding work with the crossed beam system yielded data on the cross sections from the helium 2^3S state to several upper states. The most reliable measurements have been inferred from the cumulative counts from a single electron beam in a very limited energy range, however, as opposed to the data arising from metastable excitation in the first electron beam and subsequent excitation to upper levels in the second electron beam.

With a single electron beam the experiment proceeds as follows: An electron beam orthogonally intersects an atomic helium beam exiting from a capillary array. The current of the electron beam is 100% modulated, and the energy of the electron beam is swept, in the case of helium, from 15 eV to 30 eV. When the electron beam energy exceeds 19.8 eV, metastable atoms in the 2^3S level are created, and above 20.6 eV, metastable atoms in both the 2^3S and 2^1S levels are created. The 2^1S population does not exceed 25% of the total metastable density at low energy (Holt and Krotkov, 1966)³¹, and population of the triplet scheme from the 2^1S level involves electron exchange. For these reasons, and to enable comparison to theory, the data in all cases is interpreted to result from excitation of the 2^3S level, even though the experiment with a single electron beam does not exclude $2^1\text{S} \rightarrow n^3\text{1}$ excitation. If the metastable atoms suffer an electron



Electron Energy

FIGURE 35 - Helium 3889 Å

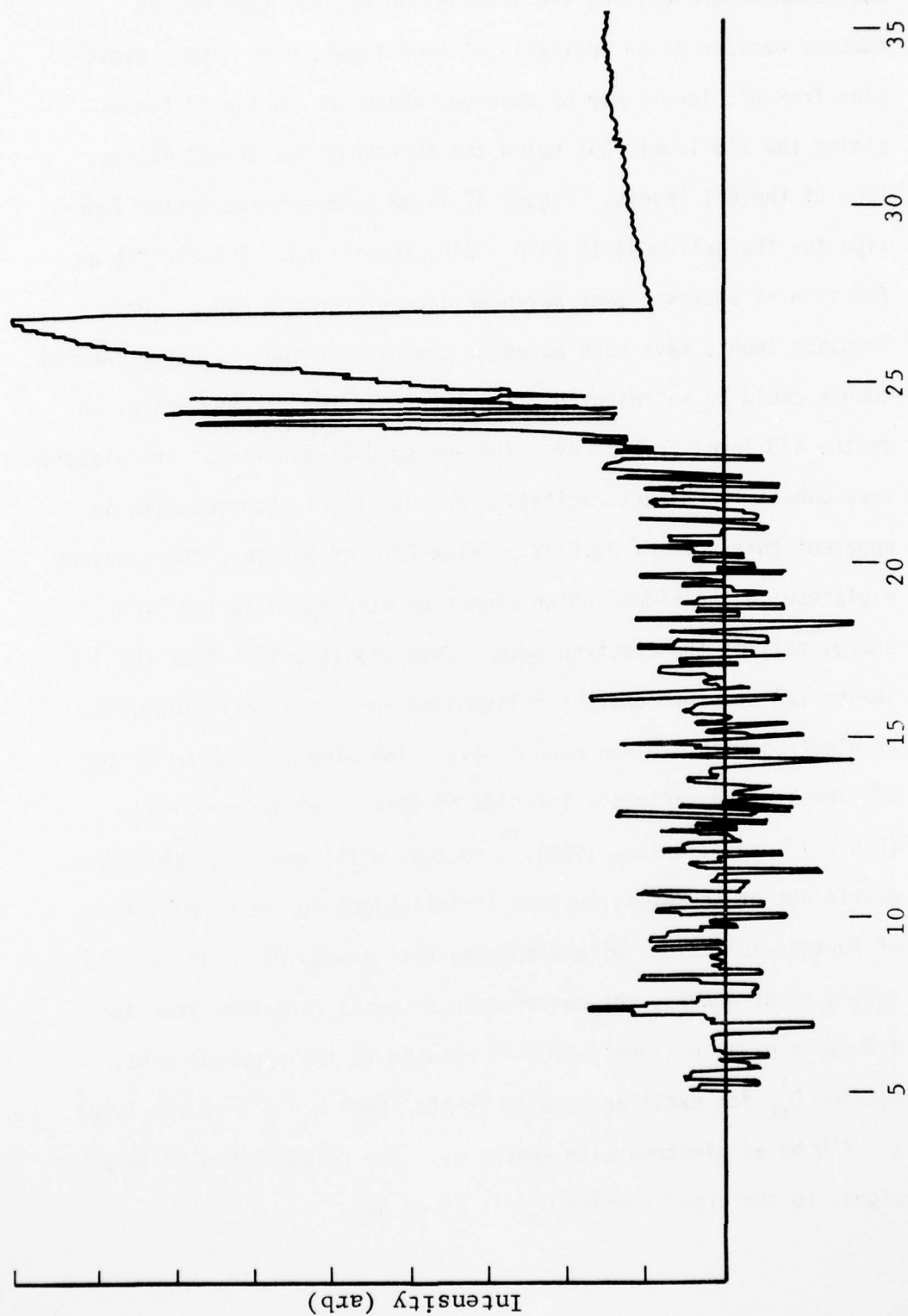


FIGURE 36 - Helium 3889Å

collision before exiting the interaction region, they may be further excited to an optically allowed level, n^31 . Thus, radiation from n^31 levels may be observed above the threshold for exciting the 2^3S level, but below the threshold for direct excitation of the n^31 levels. Figure 37 is an apparent excitation function for the helium 4471\AA ($4^3D \rightarrow 2^3P$) transition. The excitation function is observed over seven decades of dynamic range. One thousand counts have been added to the data so that negative (noise) counts could be represented. The threshold for direct excitation to the 4^3D level is 23.7 eV. The energy distribution of the electron beam causes the direct excitation process to be observed with an apparent threshold of 23.0 eV. Below 23.0 eV however, there exists a plateau in the signal which cannot be attributed to the high energy tail of the electron beam. This signal arises from the following two-step process: a helium atom suffers a collision with an electron with a given energy, eV_1 . The atom is excited to the 2^3S level. The radiative lifetime of this level is very long (2.5×10^4 sec., Griem, 1969),³² so that until the metastable atom drifts out of the electron beam it is subject to the probability of further collisions with electrons with energy eV_1 . If this second event occurs, the observation of decay radiation from the 4^3D state gives a signal which is related to the apparent cross section Q'_{mk} for exciting an atom in the level $m = 2^3S$ to the level $k = 4^3D$ by an electron with energy eV . The relationship of this signal to the cross section Q'_{mk} is given by

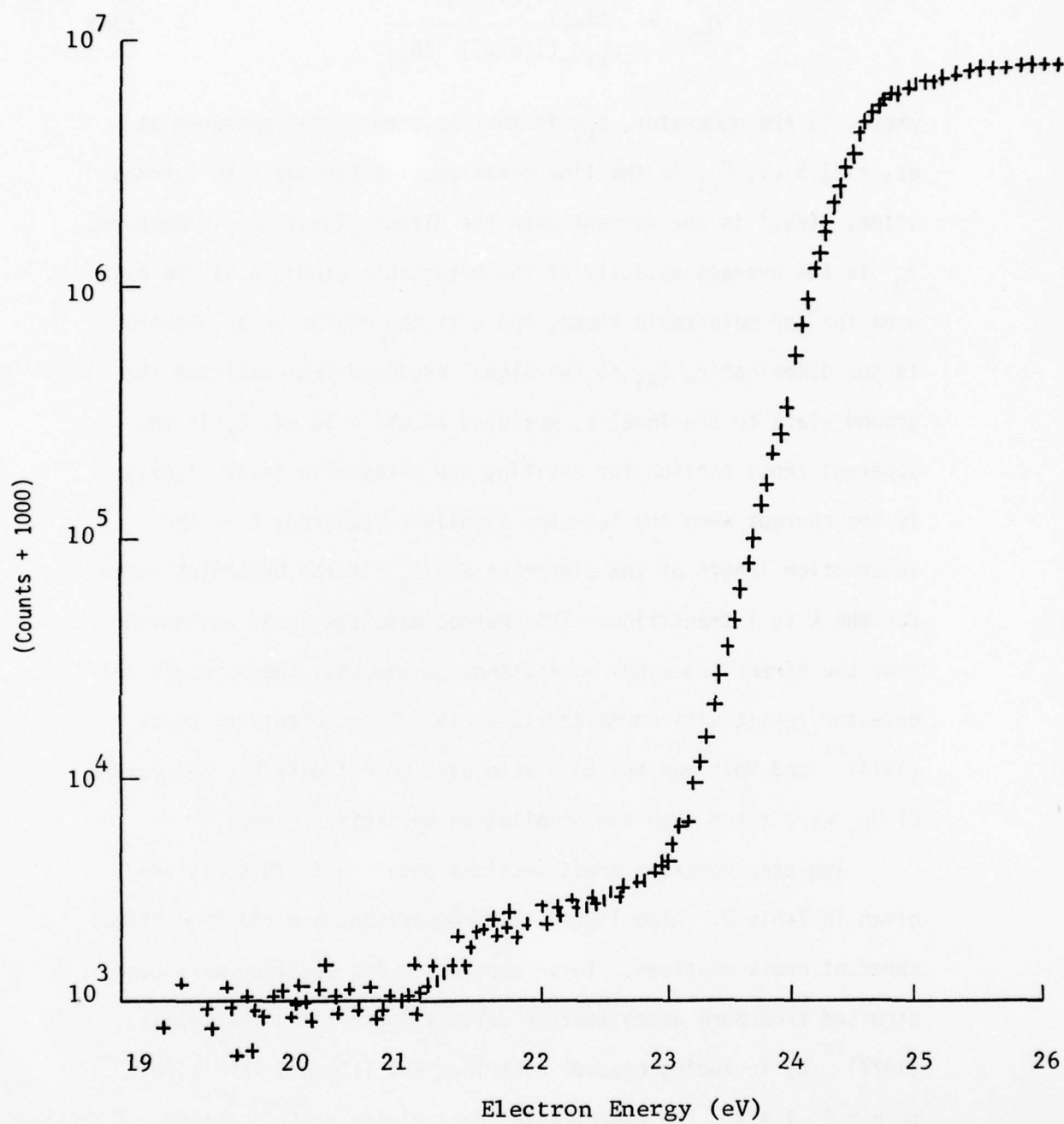


FIGURE 37 - Excitation function of the He 4471^oÅ
(4³D → 2³P) line

$$Q_{mk}' = \frac{\phi_{ki}^* Q_{ki} I(eV_2) \bar{v} A e}{\phi_{ki} Q_m' (I(eV_1))^2 \ell B_{ki}} \quad (36)$$

where, in the numerator, ϕ_{ki}^* is the two-step signal measured at $eV_1 = 21.5$ eV, Q_{ki} is the line cross section for the k to i transition, $I(eV_2)$ is the current when the direct signal ϕ_{ki} is measured, \bar{v}_m is the average velocity of the metastable atoms, A is the exit area for the metastable atoms, and e is the charge on an electron. In the denominator, ϕ_{ki} is the signal produced from exciting the ground state to the level k , measured at $eV_2 \approx 30$ eV, Q_m' is the apparent cross section for exciting the metastable level, $I(eV_1)$ is the current when the two-step signal is measured, ℓ is the interaction length of the electrons and B_{ki} is the branching ratio for the k to i transition. This method uses the decay radiation from the direct processes as a standard, and thus the pressure and detector sensitivity normalize to unity. Measurements by Borst (1974)²⁸ and Holt and Krotkov³¹ were used to estimate Q_m' , and values of Q_{ki} were taken from the compilation by Kieffer (1969).¹

Two-step apparent cross sections obtained in this way are given in Table 2. Also listed, for comparison, are the theoretical apparent cross sections. These apparent cross sections were constructed from Born approximation calculations of Ton That et al. (1977)¹² by including cascade contributions from $n^3 1$ levels up to $n = 5$, $l = 3$. The experimental data yields cross sections three to five times larger than the Born apparent cross sections.

TABLE 2
COMPARISON OF APPARENT CROSS SECTIONS OF THIS EXPERIMENT
WITH APPARENT CROSS SECTIONS CONSTRUCTED FROM THE BORN
APPROXIMATION VALUES OF TON THAT ET AL.

	3^3S	3^3P	3^3D	4^3S	4^3D
Q_{mk}' (10^{-16} cm 2) at 21.5 eV This experiment	7	4	16	1.6	2.8
Q_{mk}' (10^{-16} cm 2) at 20 eV Born approximation	1.7	1.15	3.26	.32	.79

The data for the 3^3P , 3^3S , 4^3S and 4^3D measurements show scatter ranging from 18% in the case of the 4^3D measurement to 60% in the case of the 4^3S measurement. The signal-to-noise ratio for the 3^3D measurement was considerably better. The value quoted for the apparent 3^3D cross section is an average of five different runs whose standard deviation is 23%.

The second way to observe two-step signal is to use two parallel electron beams perpendicular to and sequentially intersecting an atomic helium beam. The first electron beam has an accelerating voltage only sufficient to excite the 2^3S level, but not higher levels directly. Metastable atoms thus produced in the beam are intersected by the second electron beam, where they may be excited to upper n^3l levels with impact energies as low as 3 eV. Sweeping the energy of the second electron gun from 3 eV to 19.8 eV produces an excitation function of the apparent $2^3S \rightarrow n^3l$ cross section. However, the target density in the second electron beam, composed of metastables created in the first electron beam, cannot be determined precisely. The excitation function may be placed on an absolute scale by normalizing the excitation function at 19 eV with the absolute two-step cross section obtained from the single beam experiment at 21.5 eV. Using this procedure, the absolute apparent excitation cross sections for the $2^3S \rightarrow 3^3P$ and $2^3S \rightarrow 3^3D$ transitions were obtained in the energy range from 7 eV to 19 eV. Below 7 eV the electron beam current was insufficient to yield a reliable, measurable signal. Figure 38 shows the data points for the

$2^3S \rightarrow 3^3P$ excitation. Each data point represents the average of eight 1000 second integration periods. Also shown in Figure 38 are the level $2^3S \rightarrow 3^3P$ cross sections calculated by Flannery et al.²⁹ using the VPS and the Born approximations and Flannery and McCann³⁰ using the Eikonal treatment. Noise in the experimental data makes detailed comparison to the shapes difficult. Figure 39 gives the same results for the $2^3S \rightarrow 3^3D$ transition. As a result of a much stronger two-step signal, this experimental excitation function is more favorable for comparison. The excitation function appears to decrease gradually after a maximum close to threshold. The shape of the excitation function compares best to the Eikonal treatment. The disagreement in shape for Mityureva and Penkin's⁵ data and the present experiment (the latter being favored by the available theory) cannot be explained. Also at variance with present results and theory is the observation by Mityureva and Penkin that the lines which undergo the most intensive step-wise excitation are the strongest lines of the direct excitation spectrum. Our experiments indicate that the 3D levels have the largest cross section from the 2^3S levels. While errors due to the calibration procedure affect the absolute scale of the cross sections, these errors do not affect the relative values of the observed two-step cross sections.

These results for the excitation of the upper helium states from the metastable state are much different from the distribution that would result from their direct excitation from the ground

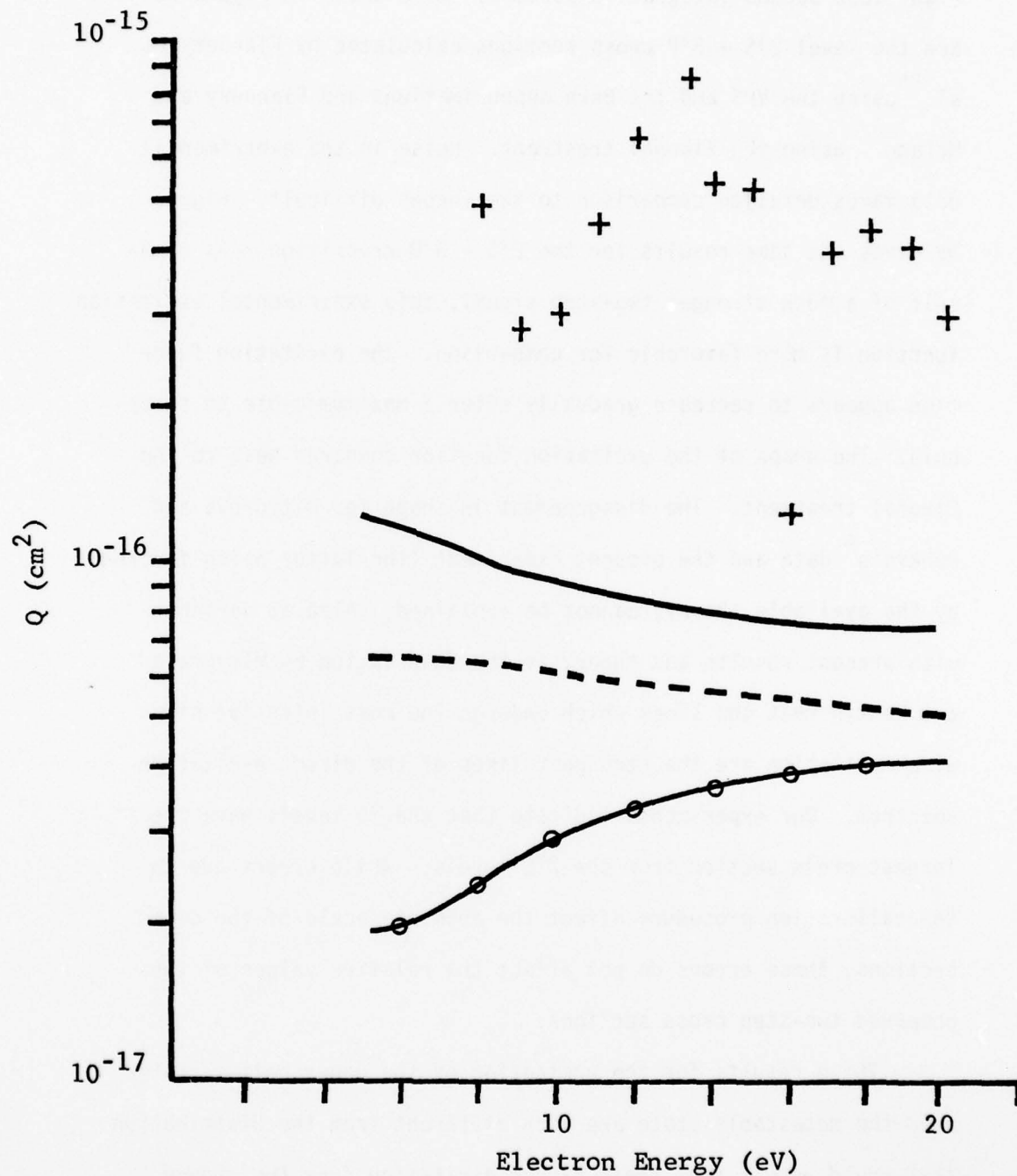


FIGURE 38 - Apparent $2^3S \rightarrow 3^3P$ cross section of this experiment (+) compared to the level cross sections of Flannery and McCann using the Eikonal (---) approximation and of Flannery et al. using the Born (—) and VPS (○) approximations

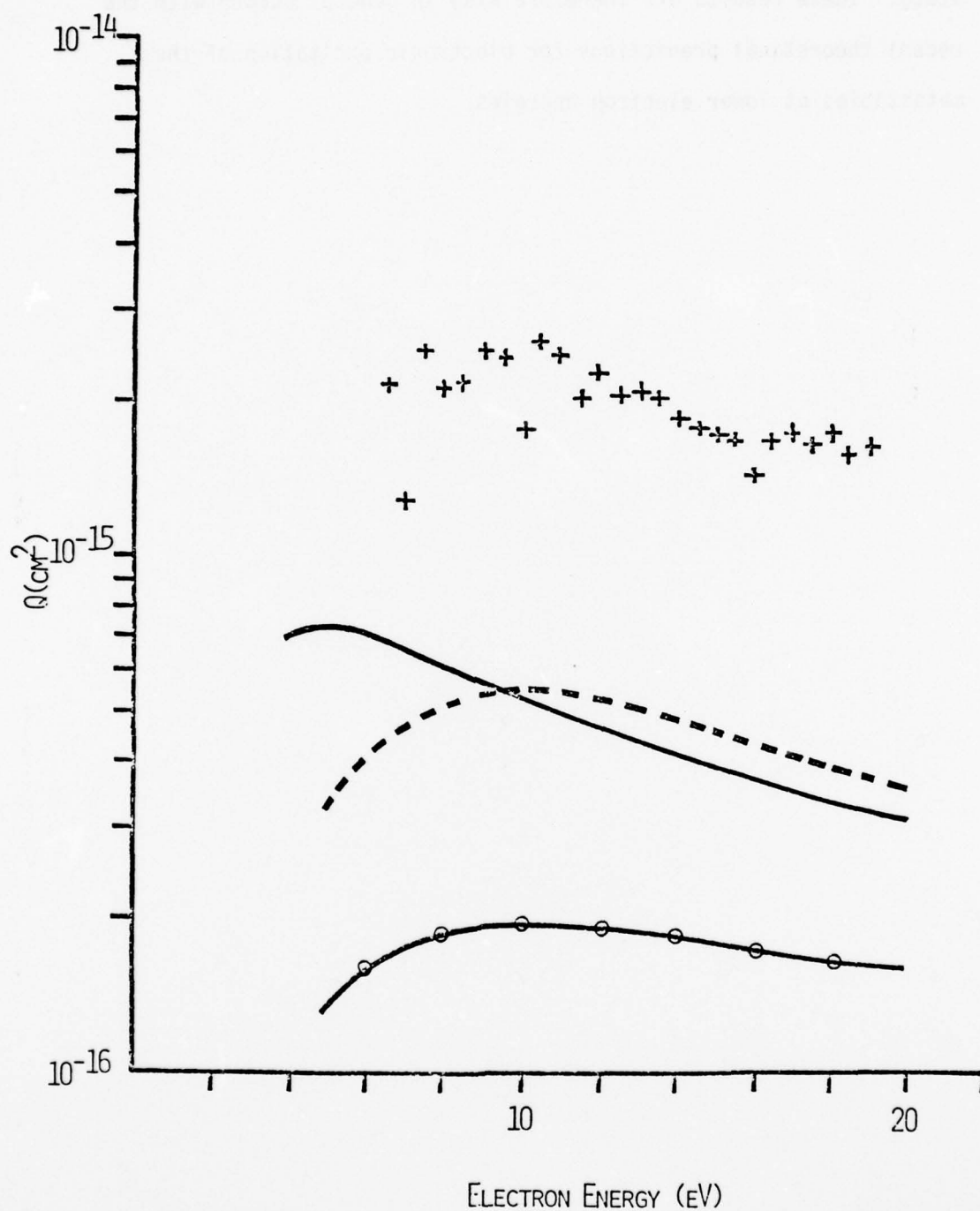


FIGURE 39 - Apparent $2^3S \rightarrow 3^3D$ cross section of this experiment (+) compared to the level cross sections of Flannery and McCann using the Eikonal (---) approximation and of Flannery et al. using the Born (—) and VPS (—○—) approximations

state. These results are therefore also in general accord with the recent theoretical predictions for electronic excitation of the metastables at lower electron energies.

SECTION V

EXCITATION OF KRYPTON BY SINGLE ELECTRON IMPACT

1. BACKGROUND

A considerable wealth of knowledge has been amassed regarding transitions from the ground state to upper electronic levels, represented in Figure 40 by process number two. Of the rare gases, the lightest elements, particularly helium, have received by far the most attention, so that there exist gaps in the literature for electron impact cross sections of krypton and xenon. The primary objective of this research effort is to measure cross sections of the third type in Figure 40. In this experiment the first two types of cross sections are used to calibrate signals from the third type. Cross sections to the metastable level provide an estimate of the metastable number density created by an electron beam. The decay radiation resulting from excitation of ground state atoms whose cross sections are known is used as a standard for photons arising from excitation from the metastable level, for which the cross section is to be measured. Therefore, cross sections from the ground state to optically allowed levels in krypton were measured using the optical technique. This is a result of the lack of ground state cross sections in krypton and the requirement for this data to evaluate metastable cross section phenomena.

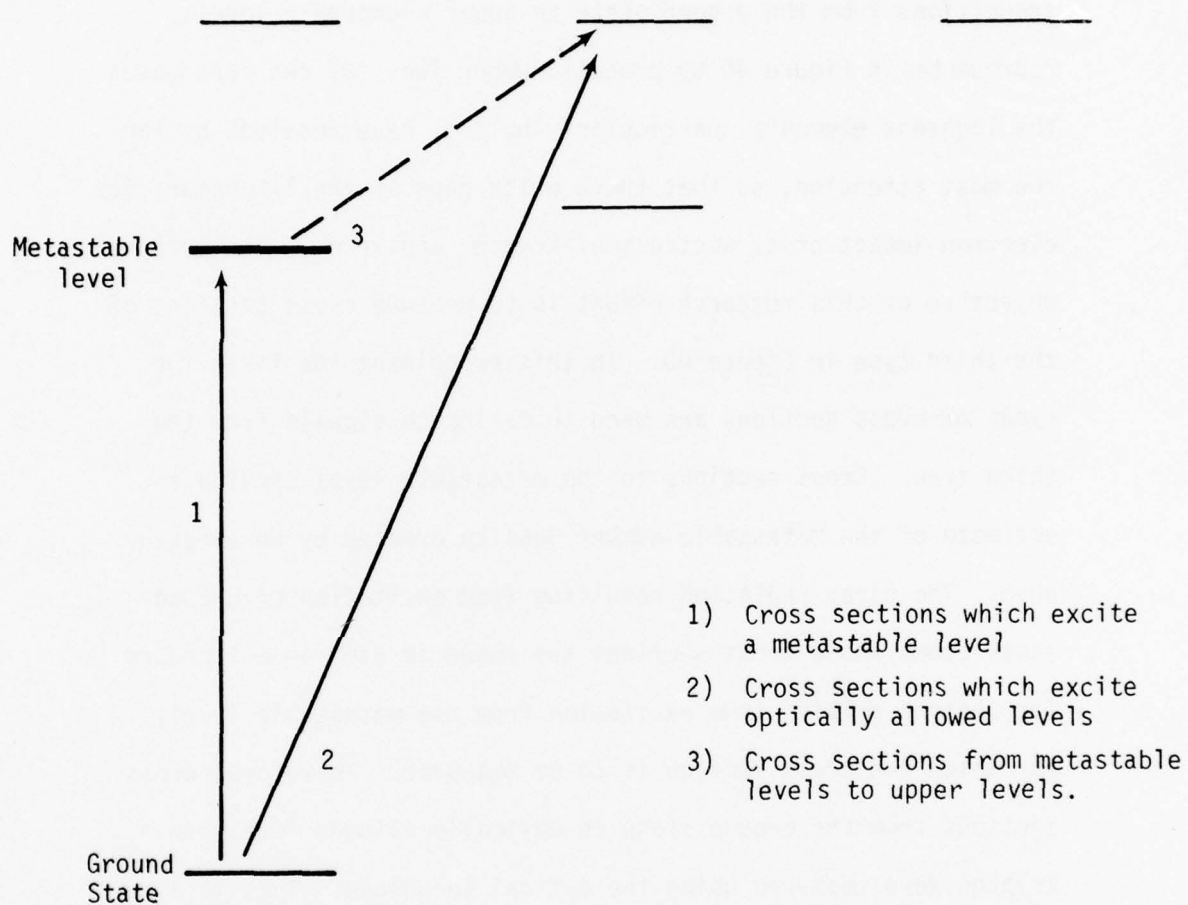


FIGURE 40 - Electron impact cross sections

2. RESULTS

The most prominent transitions in the range of the detection system arise from excitation of the 5p levels (Figure 41). These yield radiation which is in the 7000\AA to 9000\AA range. The strongest 6s to 5p and 4d to 5p lines are too far into the infrared to be measurable.

In 1967, P.V. Fel'tsan³³ published a paper in the Ukrainian Journal of Physics which contained an experimental determination of 33 of the major optical cross sections in krypton. Fel'tsan's work did not find itself in any of the recent review articles on cross sections, and this is part of the reason krypton was investigated again. Figure 42 shows the excitation functions of several transitions as determined by Fel'tsan. The excitation functions in general have a peak close to 20 eV. Figures 43 and 44 show corresponding excitation functions measured in our experiment. These are unretouched products of the data acquisition system, uncorrected for a 1.5 volt potential shift in the accelerating voltage, but not subject to errors in current and pressure changes, nor subject to detector non linearities. The spike near onset shows where the exponent of the data changes from the 100's range to the thousands range. These excitation functions, as well as the following ones from this experiment, are not normalized to each other. The functions are taken at a constant pressure and are electronically corrected for the change in electron beam current as a function of accelerating voltage. The excitation

AD-A063 306

UNIVERSAL ENERGY SYSTEMS INC DAYTON OHIO
EXPERIMENTAL MEASUREMENTS OF CUMULATIVE EXCITATION AND IONIZATION--ETC(U)
DEC 77 M L LAKE

F/G 20/10

F33615-75-C-1082

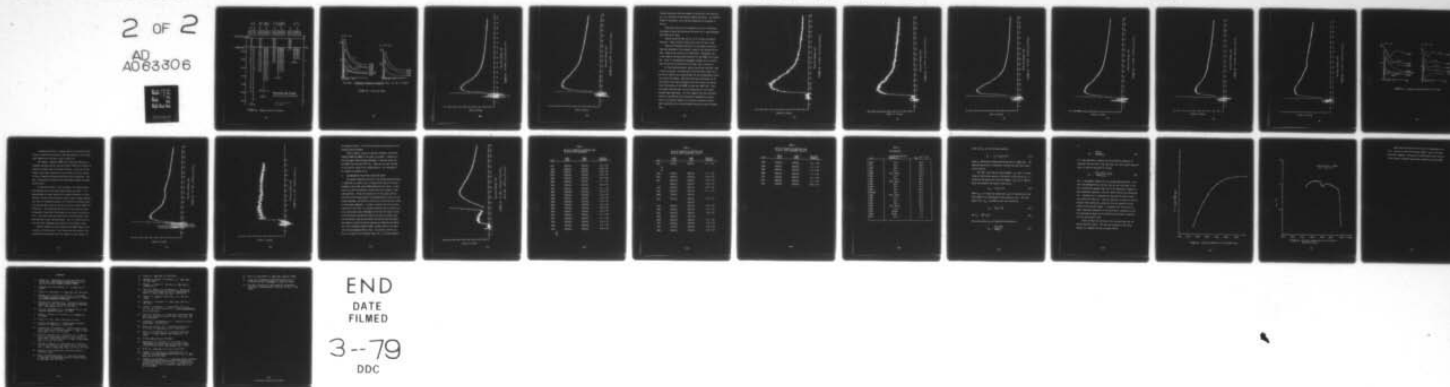
UNCLASSIFIED

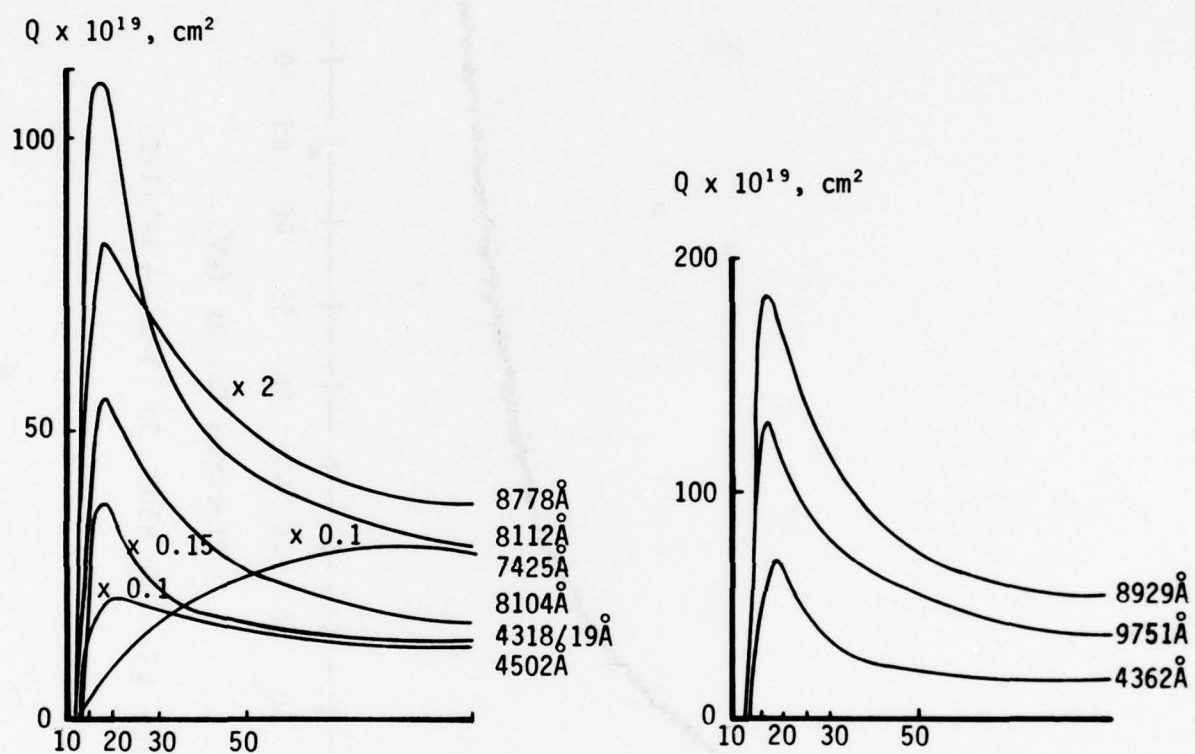
AFAPL-TR-77-84

NL

2 OF 2

AD
A063306





Fel'tsan. Ukranian Journal of Physics, Vol. 12, No. 9 (1967)

FIGURE 42 - Fel'tsan data

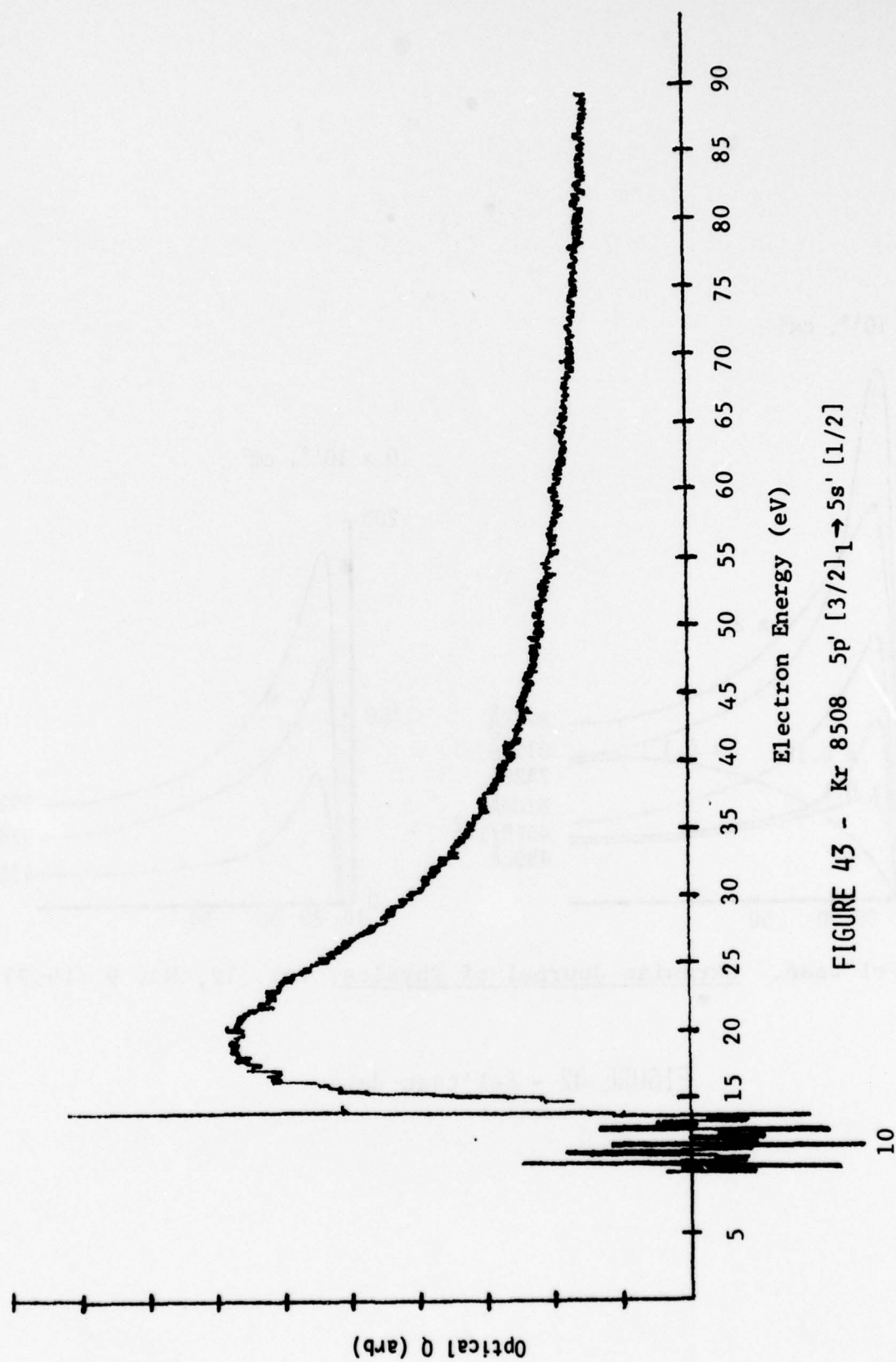


FIGURE 43 - Kr 8508 $5p' [3/2]_1 \rightarrow 5s' [1/2]$

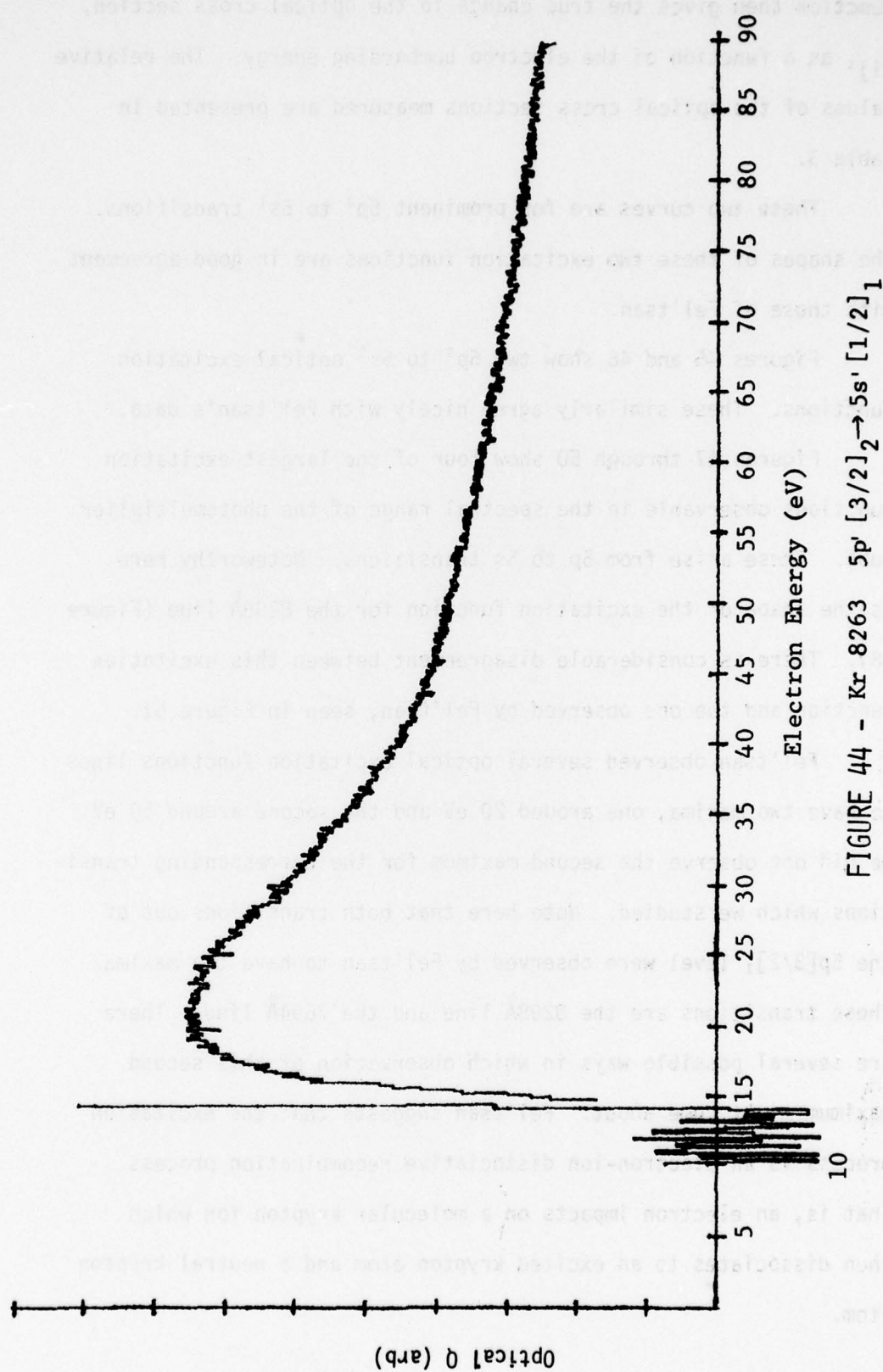


FIGURE 44 - Kr 8263 $5p [3/2]_2 \rightarrow 5s' [1/2]_1$

function then gives the true change in the optical cross section, Q_{ij} , as a function of the electron bombarding energy. The relative values of the optical cross sections measured are presented in Table 3.

These two curves are for prominent $5p^1$ to $5s^1$ transitions. The shapes of these two excitation functions are in good agreement with those of Fel'tsan.

Figures 45 and 46 show two $5p^1$ to $5s^1$ optical excitation functions. These similarly agree nicely with Fel'tsan's data.

Figures 47 through 50 show four of the largest excitation functions observable in the spectral range of the photomultiplier tube. These arise from $5p$ to $5s$ transitions. Noteworthy here is the shape of the excitation function for the 8298\AA line (Figure 48). There is considerable disagreement between this excitation function and the one observed by Fel'tsan, seen in Figure 51.

Fel'tsan observed several optical excitation functions lines to have two maxima, one around 20 eV and the second around 50 eV. We did not observe the second maximum for the corresponding transitions which we studied. Note here that both transitions out of the $5p[3/2]_1$ level were observed by Fel'tsan to have two maxima. These transitions are the 8298\AA line and the 7694\AA line. There are several possible ways in which observation of this second maximum might come about. Fel'tsan suggests that the excitation process is an electron-ion dissociative recombination process. That is, an electron impacts on a molecular krypton ion which then dissociates to an excited krypton atom and a neutral krypton atom.

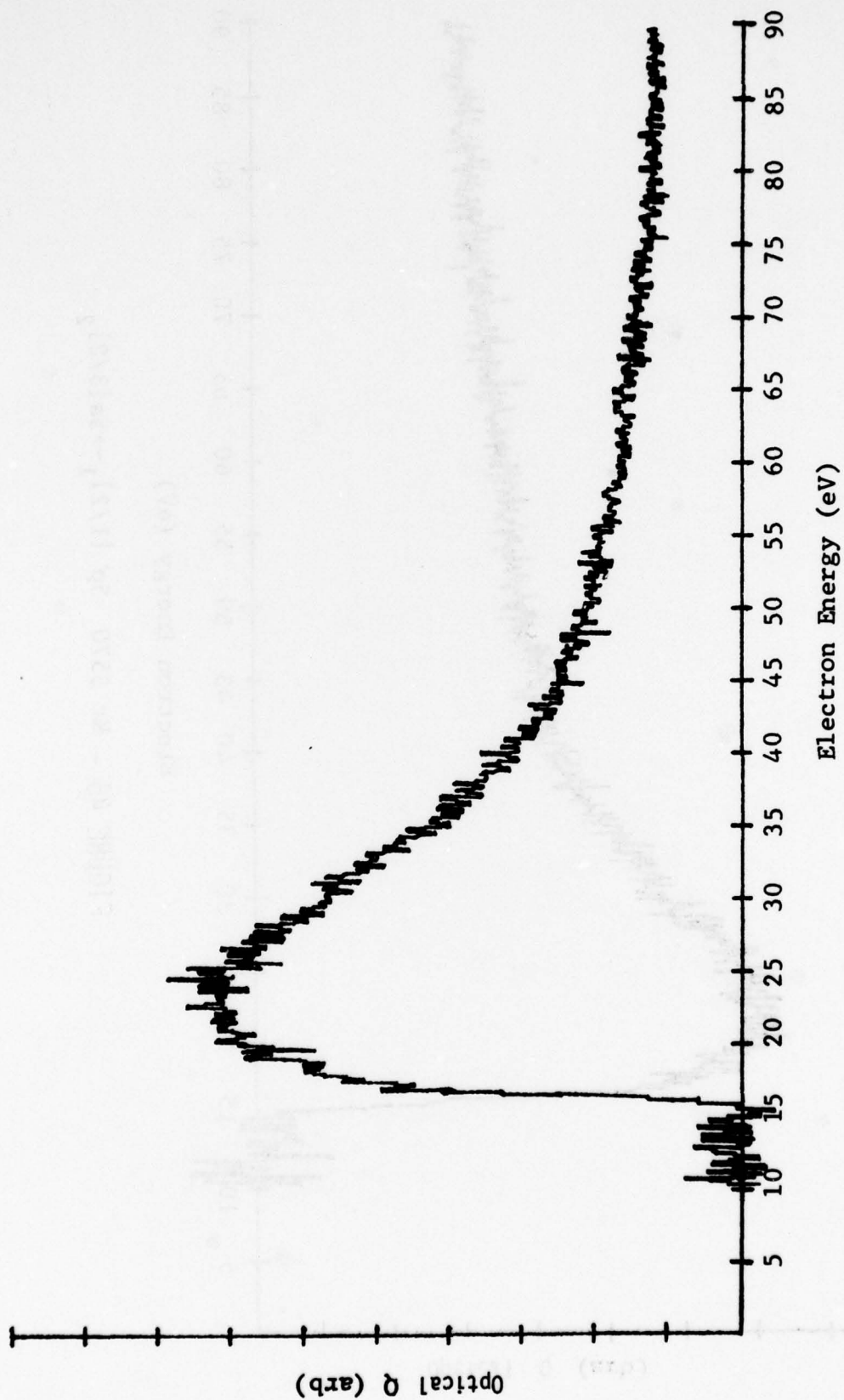


FIGURE 45 - Kr 5871 $5p'[3/2]_2 \rightarrow 5s[3/2]_1$

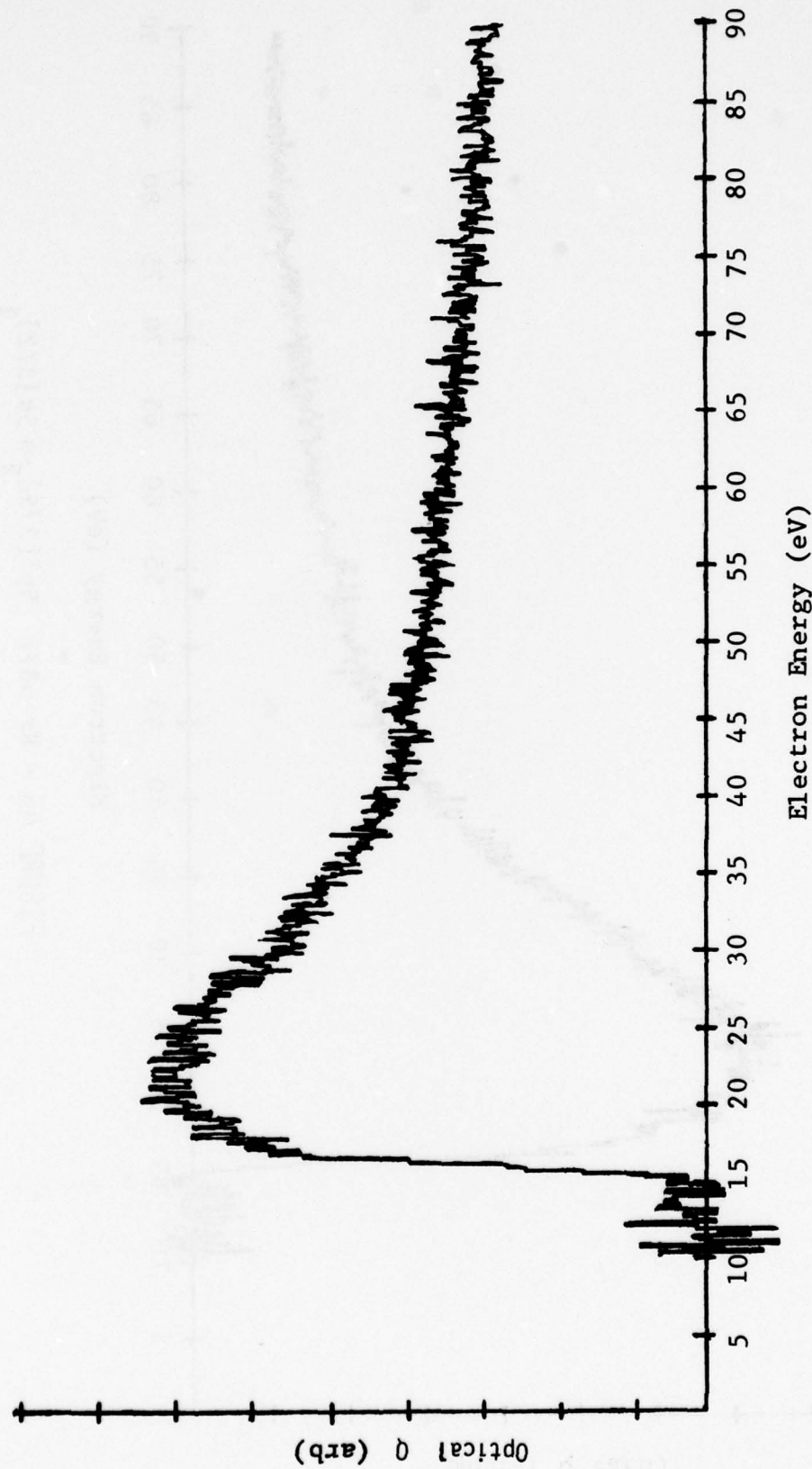


FIGURE 46 - Kr 5570 5p' [1/2]₁ → 5s [3/2]₂

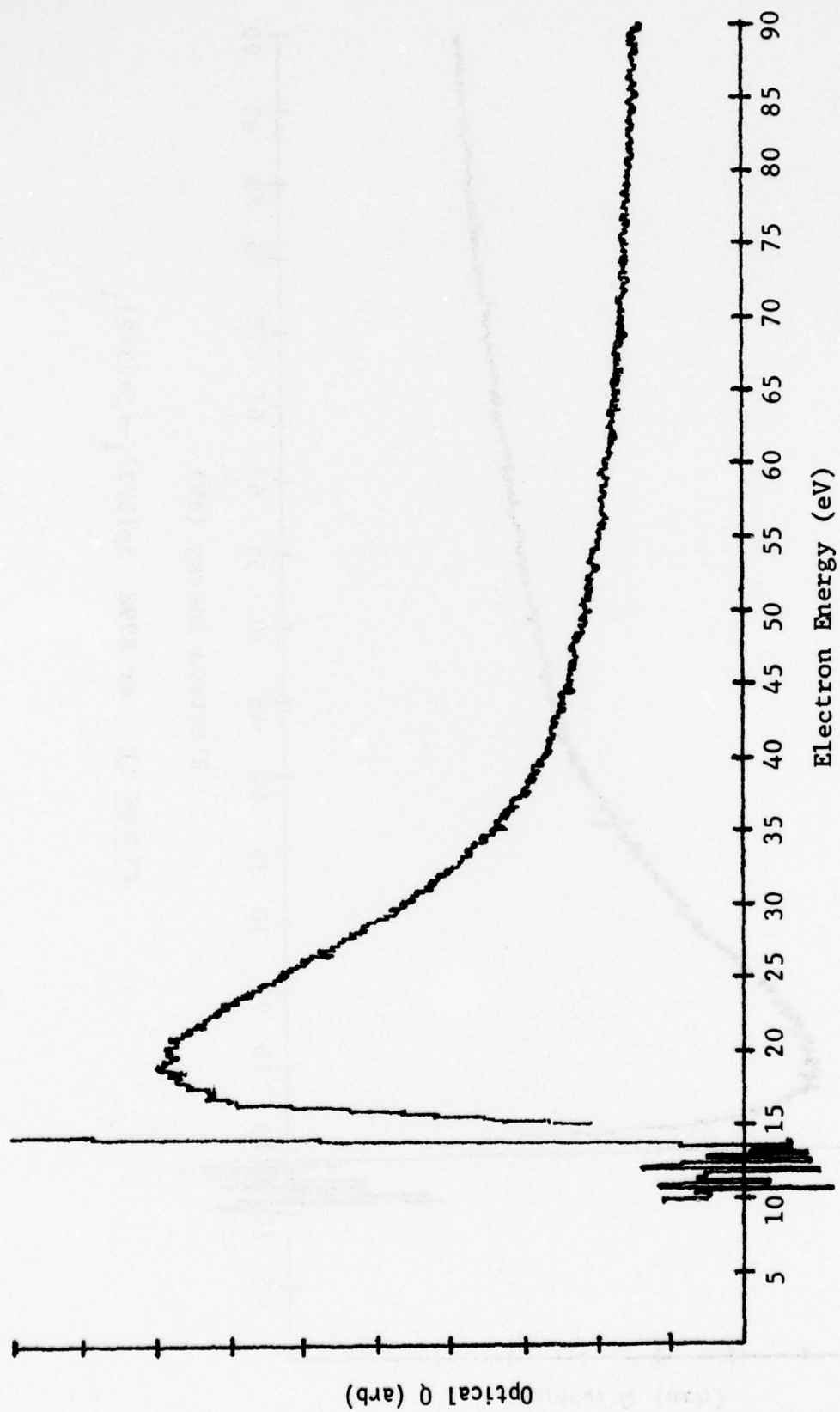


FIGURE 47 - Kr 8112 $5p[5/2]_3 \rightarrow 5s[3/2]_2$

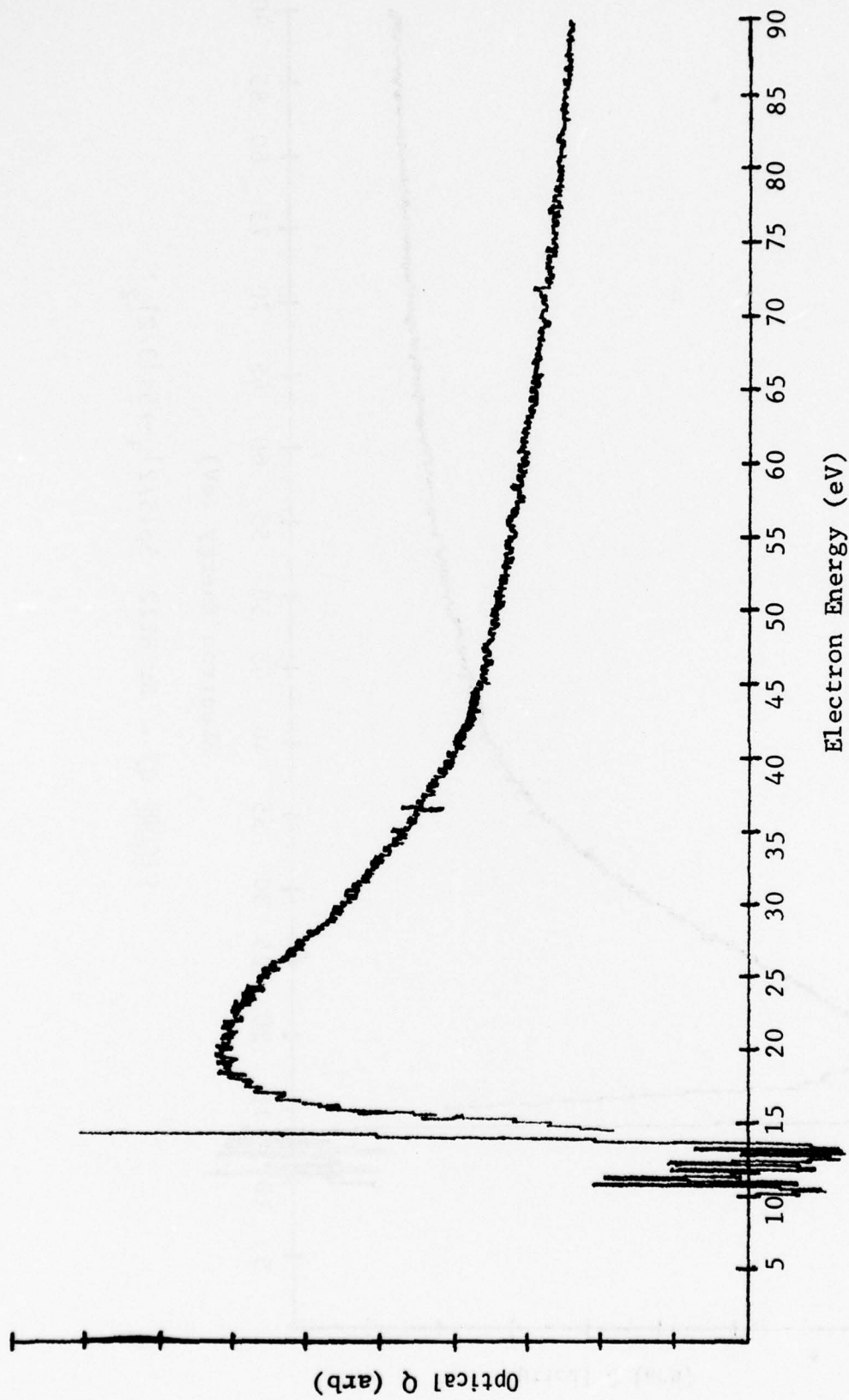
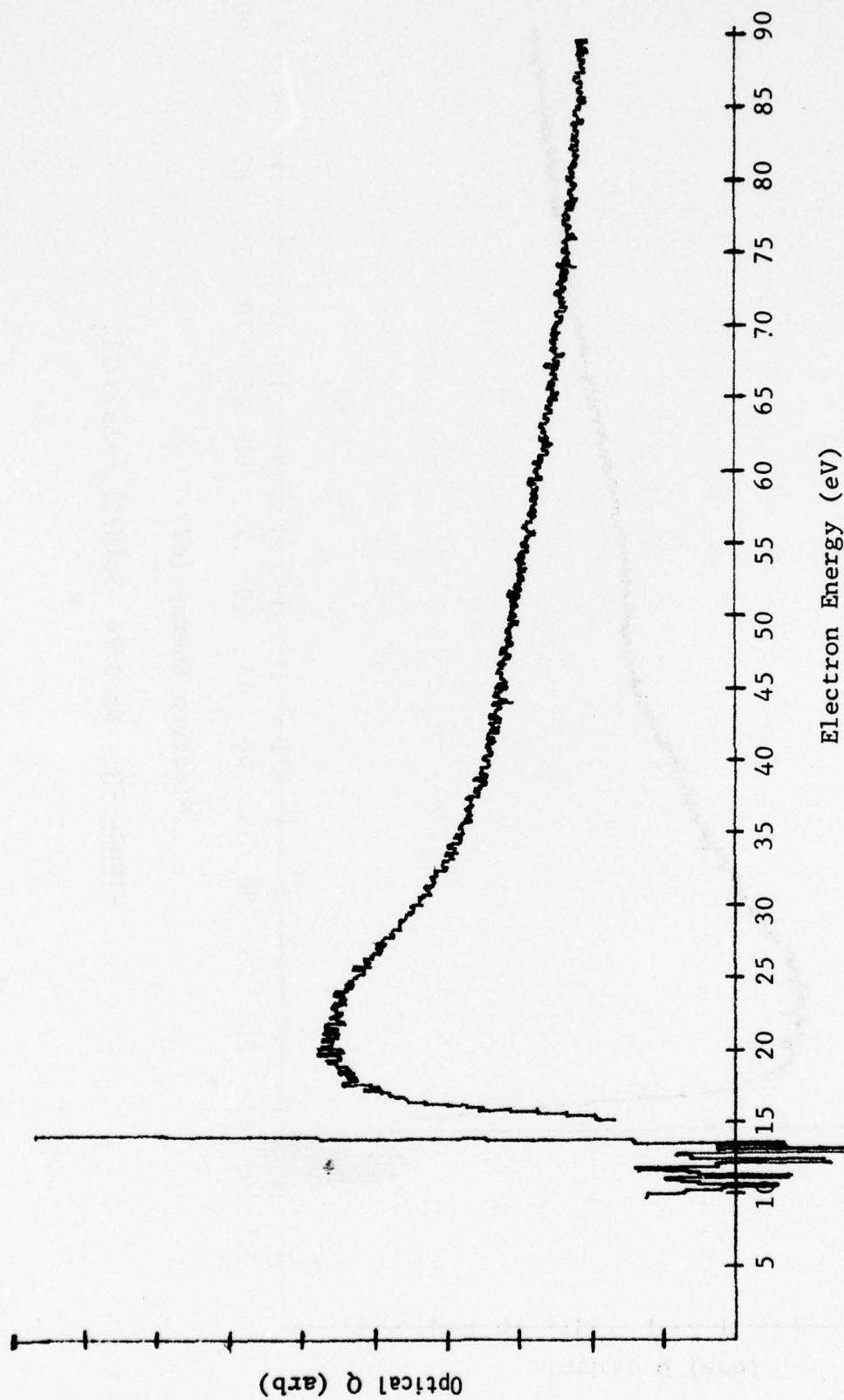


FIGURE 48 - Kr 8298 $5p[3/2]_1 \rightarrow 5s[3/2]_1$



Electron Energy (eV)

FIGURE 49 - Kr 8190 $5p[3/2]_2 \rightarrow 5s[3/2]_1$

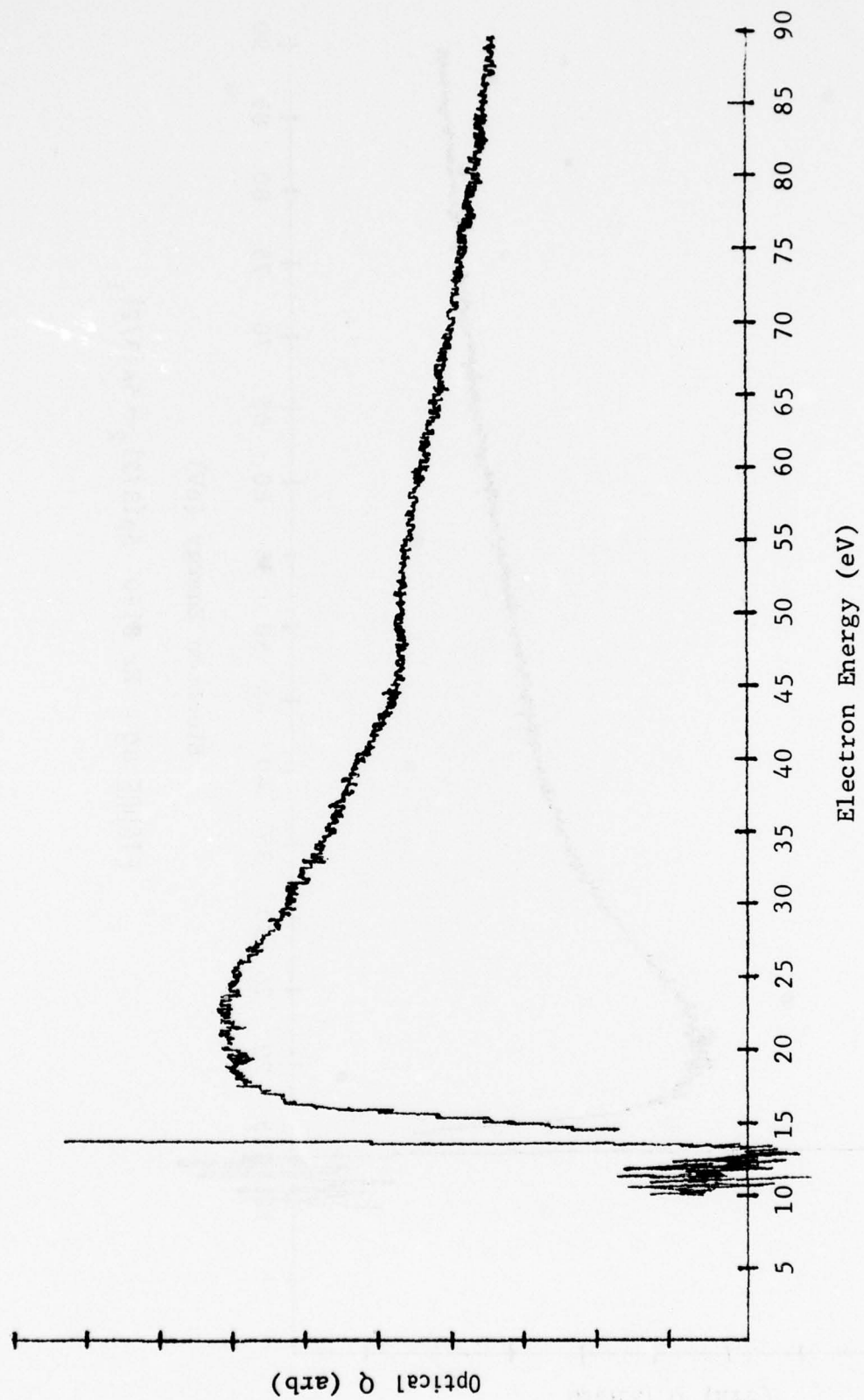


FIGURE 50 - Kr 8776 $5p[5/2]_2 \rightarrow 5s[3/2]_1$

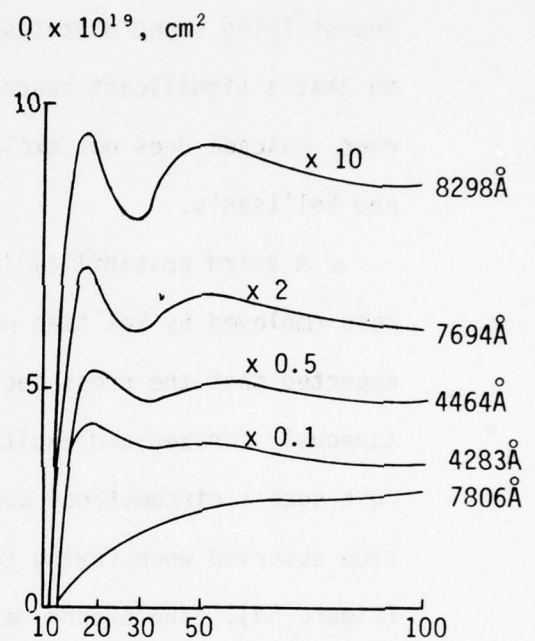
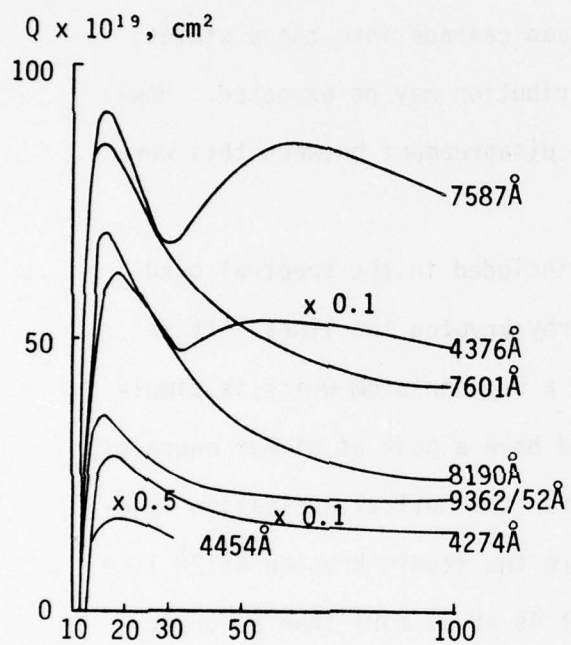


FIGURE 51 - Krypton measurements by Fel'tsan

A second possibility is cascade radiation from upper levels. Figures 52 and 53 are excitation functions measured in this experiment showing an s-to-p and a d-to-p transition.

The $7s[3/2] \rightarrow 5p[3/2]_2$ 7982Å line (Figure 52) does have a secondary maximum at 50 eV, and the $5d[1/2] \rightarrow 5p[3/2]_1$ 7913Å line (Figure 53) exhibits an almost level excitation function. These are not the lowest lying s and d states which can cascade into the p states, so that a significant cascade contribution may be expected. However, cascade does not explain the disagreement between this work and Fel'tsan's.

A third possibility is that included in the spectral band-pass employed by Fel'tsan were nearby krypton ion lines. It is expected that the cross section of a krypton atom which is simultaneously ionized and excited would have a peak at higher energies. Just such a circumstance accounts for the optical excitation function observed when trying to measure the atomic krypton 4812Å line (Figure 54). The second maximum at 45 eV is more than an order of magnitude larger than the maximum for the atomic excitation at 20 eV. But recall that both transitions from the $5p[3/2]_1$ state were observed to have the double peak. This is consistent with a true excitation phenomenon associated with the $5p[3/2]_1$ state.

When an attempt was made to measure the 8298Å transition as a function of the pressure, it was found that the portion of the excitation function above 30 eV did indeed rise with respect to

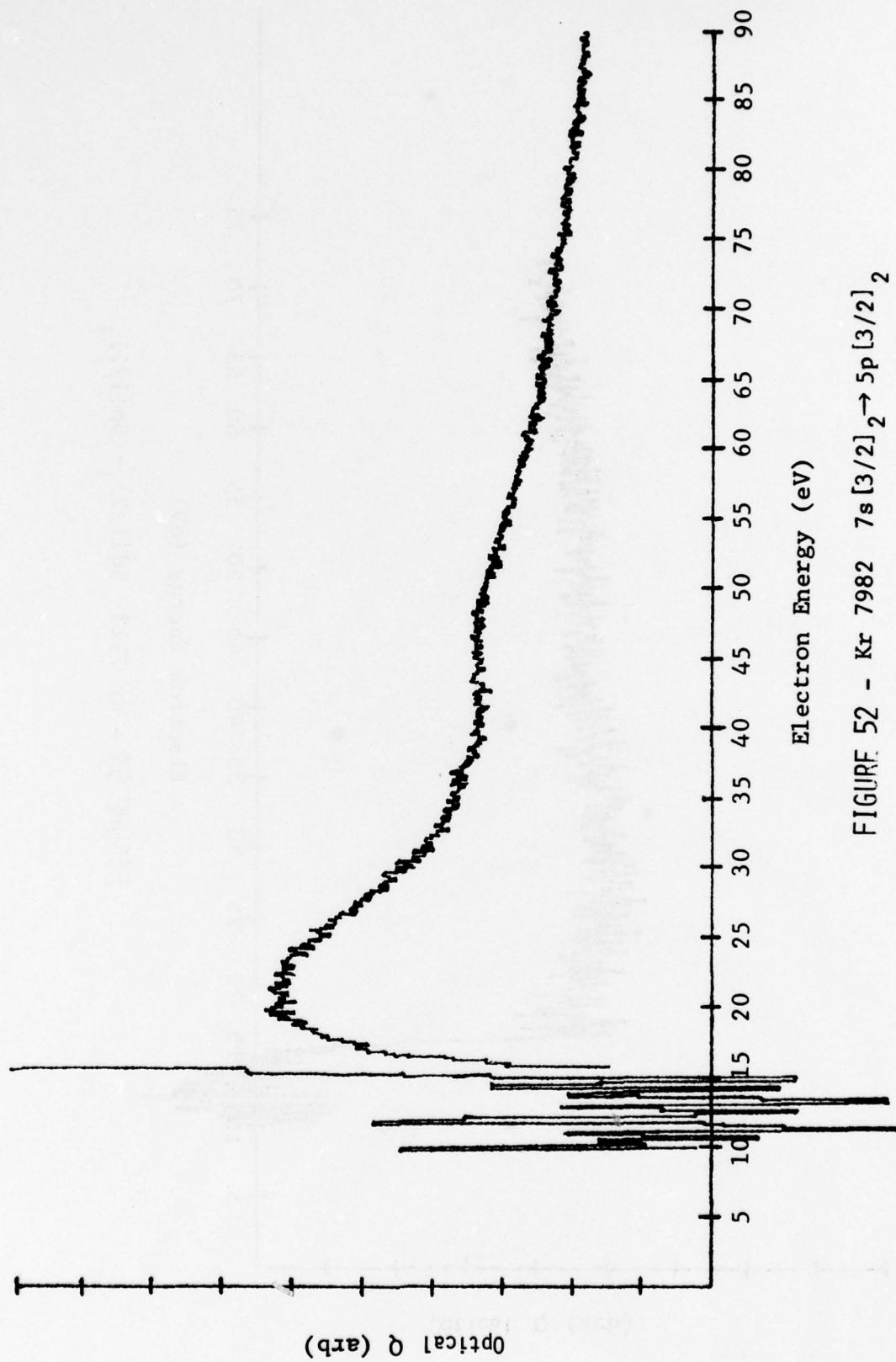
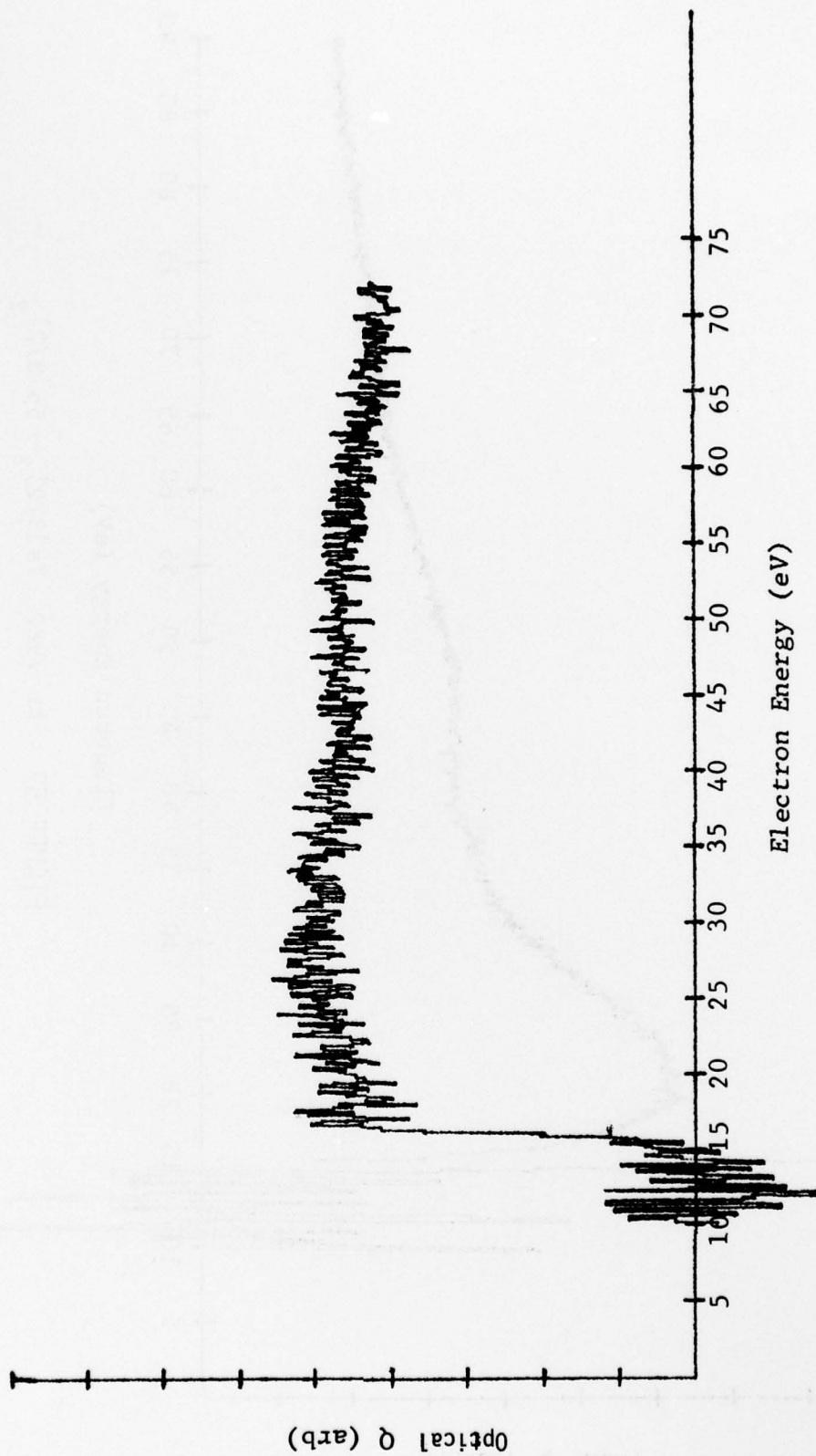


FIGURE 52 - Kr 7982 $7s[3/2]_2 \rightarrow 5p[3/2]_2$



Electron Energy (eV)

FIGURE 53 - Kr 7913 $5d[1/2]_1 \rightarrow 5p[1/2]_1$

the maximum at 20 eV. Fel'tsan's excitation function was not reproduced exactly however.

Table 3 shows a listing of the most prominent transitions between 5500Å and 9000Å in the order of strength. Comparing to the 1967 paper, (Table 4), good agreement is observed except for the 8929Å line and the 8777Å line. These two are near the edge of the spectral range of our photomultiplier, and consequently are subject to greater error.

3. CALIBRATION OF THE OPTICAL DETECTION SYSTEM

The optical detection system for the crossed beam experiment is comprised of a quartz lens, a quarter-meter Jarrell Ash monochromator, and an RCA type 31034Å photomultiplier tube, in addition to cut-off and band-pass filters which may be used in some configurations. Since the transmission of the optics and the efficiency of the monochromator and photomultiplier tube are wavelength dependent, the spectral sensitivity of the detection system is wavelength dependent. In order to analyze the true relative intensity of the lines in a selected spectrum, and in order to obtain a more-nearly exact knowledge of the electron impact excitation efficiency, the spectral sensitivity must be removed from the raw spectral data obtained with the crossed beam experiment. The spectral sensitivity may be measured by comparing the photon flux from a tungsten ribbon-filament standard lamp to the count rate from the photomultiplier tube. The spectral sensitivity, $S(\lambda)$, is related to the standard lamp flux, I_{S_1} and the detector

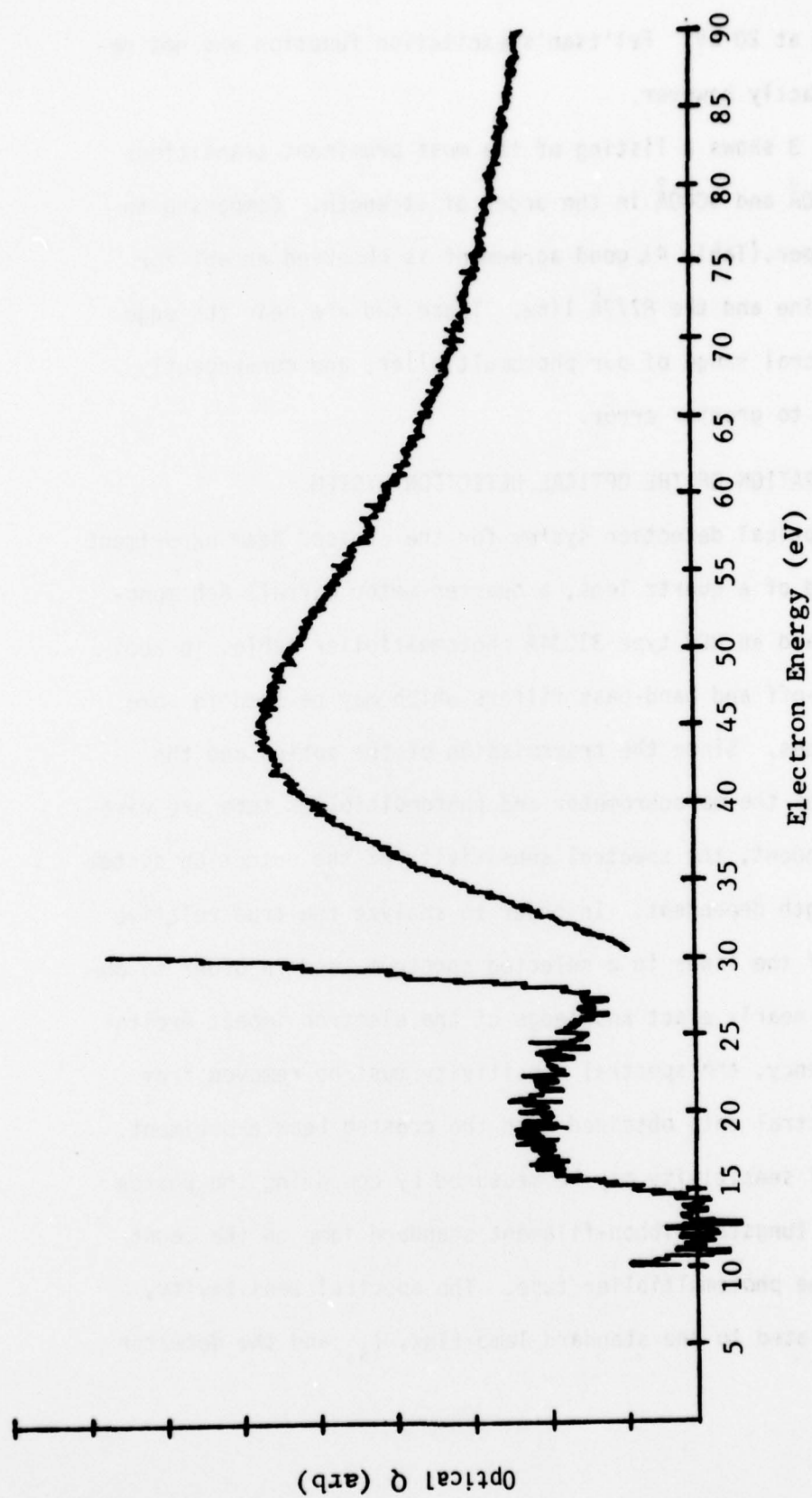


FIGURE 54 - Kr 4812 $4f[3/2]_1 \rightarrow 5s_1[1/2]_0$
 (KrII 4811 $5p^4S^{\circ}_{3/2} \rightarrow 5s P_{1/2}$)?

TABLE 3
RELATIVE INTENSITY OF KRYPTON LINES
AT 20 eV (THIS EXPERIMENT)

$\lambda(\text{\AA})$	UPPER LEVEL	LOWER LEVEL	RELATIVE INTENSITY
8112	5p[5/2] ₃	5s[3/2] ₂	1.02×10^5
7601	5p[3/2] ₂	5s[3/2] ₂	4.98×10^4
8929	5p[1/2] ₁	5s[3/2] ₂	4.89×10^4
8776	5p[5/2] ₂	5s[3/2] ₁	4.87×10^4
8263	5p ¹ [3/2] ₂	5s ¹ [1/2] ₁	4.03×10^4
8298	5p[3/2] ₁	5s[3/2]	3.7×10^4
8104	5p[5/2] ₂	5s[3/2] ₂	3.69×10^4
7587	5p[1/2] ₀	5s[3/2] ₁	3.4×10^4
7685	5p ¹ [1/2] ₀	5s ¹ [1/2] ₁	1.66×10^4
7854	5p ¹ [1/2] ₁	5s ¹ [1/2] ₀	1.35×10^4
8190	5p[3/2] ₂	5s[3/2] ₁	1.34×10^4
8508	5p ¹ [3/2] ₁	5s[1/2] ₁	1.31×10^4
8059	5p ¹ [3/2] ₁	5s ¹ [1/2] ₀	1.25×10^4
8281	5p ¹ [1/2] ₁	5s ¹ [1/2] ₁	8.63×10^3
7694	5p[3/2] ₁	5s[3/2] ₂	6.62×10^3
6456	6d[3/2] ₄	5p[5/2] ₃	5.6×10^3
5871	5p ¹ [3/2] ₂	5s[3/2] ₁	3.5×10^3
7928	5d[7/2] ₃	5p[3/2] ₂	3.16×10^3
7982	7s[3/2] ₂	5p[3/2] ₂	3.0×10^3
6415	6e[3/2] ₃	5p[5/2] ₃	2.96×10^3

20
24

TABLE 3
RELATIVE INTENSITY OF KRYPTON LINES
AT 20 eV (THIS EXPERIMENT) (Cont'd)

$\lambda(\text{\AA})$	UPPER LEVEL	LOWER LEVEL	RELATIVE INTENSITY
5827	7d[7/2] ₄	5p[5/2] ₃	2.8 x 10 ³
27			
32			
7486	7s[3/2] ₂	5p[5/2] ₃	2.5 x 10 ³
8132	5d ¹ [5/2] ₃	5p ¹ [3/2] ₂	2.46 x 10 ³
6012	9s[3/2] ₂	5p[3/2] ₂	2.25 x 10 ³
	6d[3/2] ₂	5p[1/2] ₁	2.25 x 10 ³
7746	5d[1/2] ₀	5p[1/2] ₁	2.25 x 10 ³
7913	5d[1/2] ₁	5p[1/2] ₁	2.2 x 10 ³
5500	7d[1/2] ₁	5p[1/2] ₁	
5504	7d[1/2] ₀	5p[5/2] ₂	2.17 x 10 ³
		5p[1/2] ₂	
7224	5d[3/2] ₂	5p[1/2] ₁	2.16 x 10 ³
5490	7d[3/2] ₂	5p[1/2] ₁	1.87 x 10 ³
6652	6d[5/2] ₂	5p[3/2] ₁	1.85 x 10 ³
5516	6p[3/2] ₁	5s ¹ [1/2] ₀	
5520	8d[7/2] ₄	5p[5/2] ₃	1.8 x 10 ³
6813	6d[3/2] ₂	5p[3/2] ₂	1.72 x 10 ³
7425	7s[3/2] ₁	5p[5/2] ₂	1.69 x 10 ³
6056	6d[1/2] ₁	5p[1/2] ₁	1.65 x 10 ³

TABLE 3

RELATIVE INTENSITY OF KRYPTON LINES
AT 20 eV (THIS EXPERIMENT) (Cont'd)

$\lambda(\text{\AA})$	UPPER LEVEL	LOWER LEVEL	RELATIVE INTENSITY
6236	8s[3/2] ₂	5p[5/2] ₃	1.5×10^3
6035	7d[5/2]	5p[3/2] ₂	1.2×10^3
6699	6d[5/2] ₃	5p[3/2] ₂	1.14×10^3
6082	6d[1/2] ₀	5p[1/2] ₁	1.1×10^3
6151	7d[3/2] ₂	5p[3/2] ₂	1.0×10^3
6373	6d[5/2] ₂	5p[7/2] ₂	9.5×10^2
7993	5d ¹ [3/2] ₁	5p ¹ [3/2] ₁	8.48×10^2

TABLE 4
FEL'TSAN DATA

$\lambda(\text{\AA})$	EXCITATION FUNCTION MAXIMUM, eV	$Q_{\text{max}} \text{ cm}^2 \times 10^{19}$
8929	18.5	184.6
8777	20.0	166.2
9752	18.0	132.0
8112	20.0	111.3
8298	20.5, 48-50	110.0
8263	21.0	103.5
7601	20.0	92.9
7587	20.0, 60-65	86.5
8190	20.0	69.4
8104	20.0	55.8
8509	20.0	49.6
9362/52	18.5	36.0
7685	20.5, 48-52	31.0
8059	19.0	30.2
7854	20.5	28.8
8281	20.5	22.1
7694	20.5, 49-52	15.9
5871	21.0	4.9
7425	90-100	3.0
7806	80-90	2.7
5570	20.5	1.6

count rate ϕ_{s_1} by the following equation:

$$\phi_{s_1} = I_{s_1} \Delta\lambda A_{s_1} \Omega_{s_1} S_0(\lambda) \quad (37)$$

where ϕ_{s_1} photons per second steradian per mm^2 of ribbon area. The spectral sensitivity is defined to include lens and filter transmission factors.

The count rate from the vacuum chamber, ϕ_{ij} , which is proportional to the desired quantity, the optical cross section Q_{ij} , is related to the photon flux from the chamber, $F_{ij}(\Omega)$ by an equation which also contains the spectral sensitivity.

$$\phi_{ij} = F_{ij}(\Omega) S(\lambda) \quad (38)$$

where ϕ_{ij} is in counts per second and $F_{ij}(\Omega)$ is the portion of the total photon flux intercepted by the collecting lens. The total photon flux, F_{ij} , is related to the cross section by:

$$F_{ij} = NQ_{ij}\Delta x \frac{I_e}{e} \quad (39)$$

$$\text{and } F_{ij} = \frac{4\pi}{\Omega} F_{ij}(\Omega) \quad (40)$$

The cross section Q_{ij} can therefore be obtained by:

$$Q_{ij} = \frac{4\pi F_{ij}(\Omega)e}{\Omega N \Delta x I_e} \quad (41)$$

or

$$Q_{ij} = \frac{4\pi\phi_{ij}e}{\Omega S(\lambda)N\Delta x I_e} \quad (42)$$

If it were possible to measure all the quantities appearing in Equations (37) and (42) at the same time, the cross section equation could be usefully expressed as follows:

$$Q_{ij} = \frac{4\pi e I_{s_1} \Delta\lambda A_{s_1} \Omega_{s_1} \phi_{ij}}{\Omega N \Delta x I_e I_{s_1}} \quad (43)$$

This is the general formula for the crossed beam experiment. However, the photomultiplier cooling lines are too rigid when in service to allow the standard lamp flux to be immediately compared to each transition intensity, since this entails moving the monochromator. Therefore $S(\lambda)$ is measured over the desired spectral region and plotted for later use. Then the quantities in Equation (43) are measured under appropriate conditions with the detection system aligned on the electron beams. To determine the influence of unknown, unmeasured parameters on the experiment, repeatability must be established by measuring the quantities described in Equations (37) and (43) several times.

Figure 55 shows the radiance of the standard lamp over the desired spectral region. This data was supplied by the Eppley Company for standard lamp serial number 7430-8.

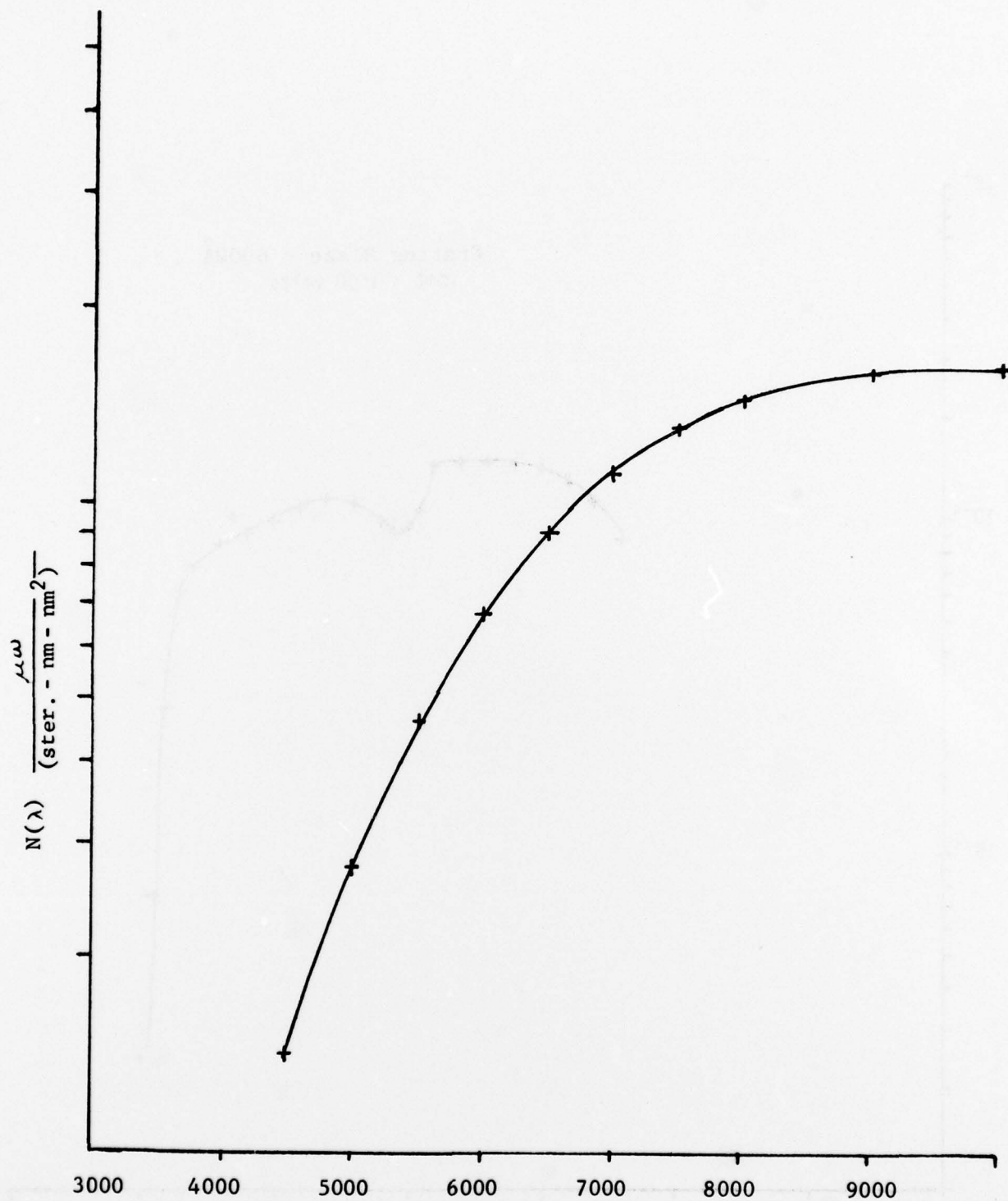


FIGURE 55 - Spectral radiance of the standard lamp

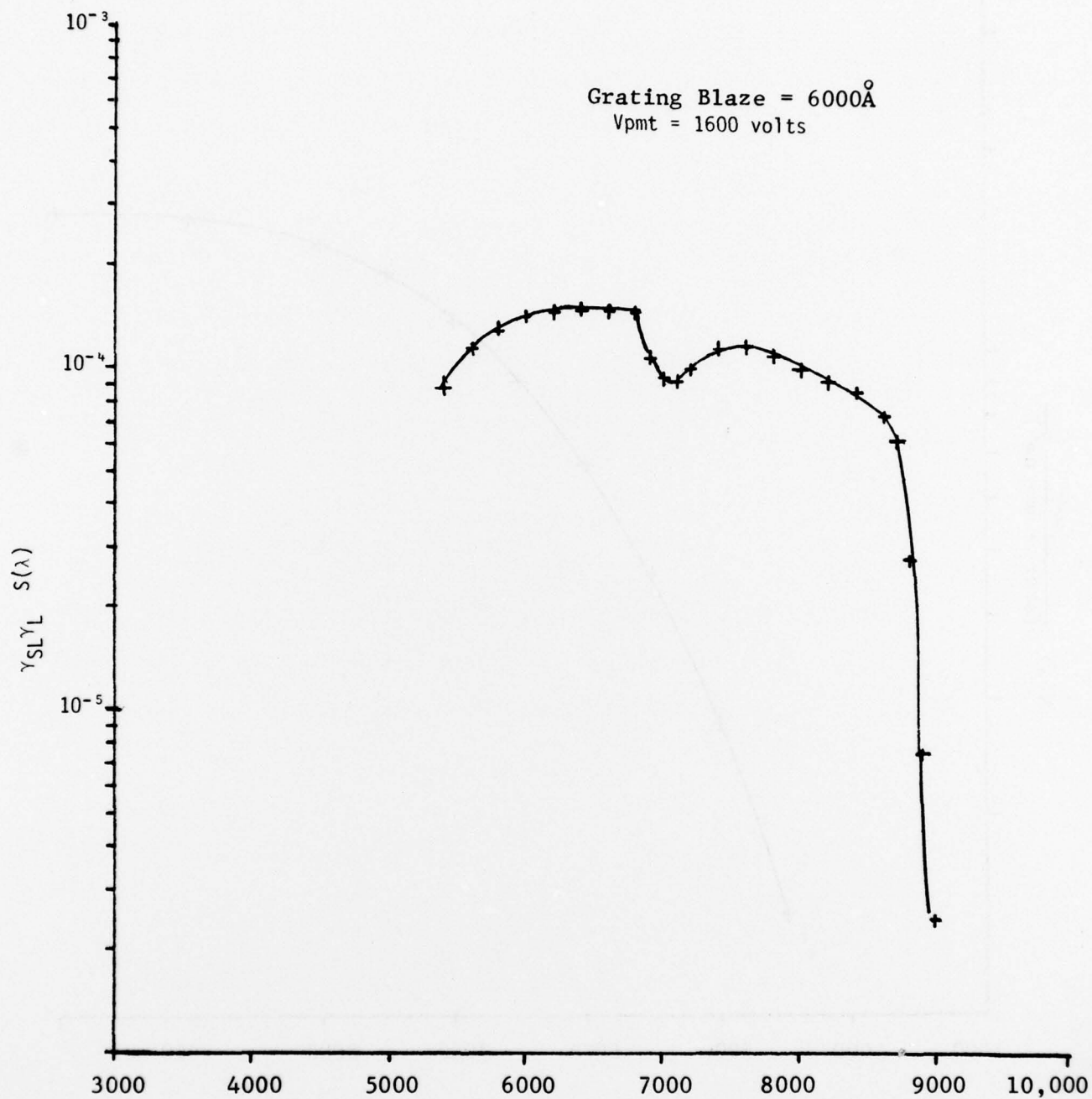


FIGURE 56 - Spectral sensitivity of the optical detection system

Figure 56 gives the result of one set of measurements for $S(\lambda)$. The dip in sensitivity around 7000\AA is due to the photomultiplier response. The cut-on is established by the long pass filter used to eliminate second order transmission below 4500\AA .

REFERENCES

1. Kieffer, L.J. "Compilation of Low Energy Electron Cross Section Data", JILA Information Center Report #7, University of Colorado, Boulder, Colorado, (1969).
2. Latyscheff, G.D. and Leipunsky, A.I., Z. Phys., 65, 111 (1930).
3. Phelps, A.V. and Molnar, J.P., Phys. Rev., 89, 1202 (1953).
4. Neynaber, R.H., Trujillo, S.M., Marino, L.L., and Rothe E.W., Atomic Collision Processes, edited by M.R.R. McDowell, North Holland, Amsterdam, 1089 (1964).
5. Mityureva, A.A. and Penkin, N.P., "Excitation of Neon and Helium Lines in Collision between Electrons and Metastable Atoms", Opt. Spectry., 38, No. 2, 229 (1975).
6. Fite, W.L. and Brackman, R.T., "Proceedings 6th Int. Conf. Ionization Phenomena in Gases", 21 (1963).
7. Vriens, L., Bonson, T.F.M. and Smit, J.A., Physica, 40, 229 (1968).
8. Koller, H.H., Ph.D. Thesis, University of Zurich.
9. Long, D.R. and Geballe, R., "Electron-Impact Ionization of He(2s ³S)", Phys. Rev. A, 1, 260 (1970).
10. Shearer-Izumi, W. and Botter, R., "Electron Impact Ionization of Long-Lived Excited Helium Atoms", J. Phys. B: Atom. Molec. Phys., 7, No. 4, L125 (1974).
11. Dixon A.J., Harrison, M.F.A. and Smith A.C.H., "A Measurement of the Electron Impact Ionization Cross Section of Helium Atoms in Metastable States", J. Phys. B: Atom. Molec. Phys., 9, No. 15, 2617 (1976).
12. Ton-That, D., Manson, S.T. and Flannery M.R., "Cross Sections for Excitation and Ionization in e-He(2^{1,3}S) Collisions", J. Phys. B: Atom. Molec. Phys., 10, No. 4, 621 (1977).
13. Tannen P.D., Ph.D dissertation, Air Force Institute of Technology, (1973).
14. Rapp, D. and Englander-Golden, P., "Total Cross Sections for Ionization and Attachment in Gases by Electron Impact." J. Chem. Phys., 43, 1464 (1965).

15. Borst, W.L., Phys. Rev. A, 5 648 (1972).
16. Olmstead, J., Newton, A. and Street, K., J. Chem. Phys., 42, 2321 (1965).
17. Kurzweg, L., Egbert, C.T. and Burns, J., Phys. Rev. A, 7, 1966 (1973).
18. Hall, R.I., Mazeow, J.R. and Schemann, C., "Electron Impact Threshold Excitation of N_2 by the Trapped-Electron Method", J. Phys. B: Atom. Mol. Phys., 3 991 (1970).
19. Levine, A.K., Lasers 2, Marcel Hekler, Inc., New York, (1968).
20. Chenevier, M. and Nguyen, T.A., Phys. Lett., 39A, No. 3, 186 (1972).
21. Husson, X. and Margerie, J., "Hanle Effect of $2p_3$, $2p_6$, $2p_7$, $2p_8$, $2p_9$, and $3p_8$ Levels of Xe I", Optics Communications, 5, No. 3, 139 (1972).
22. Davis, C.C. and King, T.A., "Upper Level Lifetimes of High-Gain Laser Transitions in Neutral Xenon", Phys. Lett., 39A No. 3, 186 (1972).
23. Verolainen, F. and Osherovich, A.L., "Lifetimes of Certain Xenon Levels", UDC 539.184.52.
24. Miller, M.H. and Roig, R.A., "Transition Probabilities of Xe I and Xe II", Phys. Rev. A, 8, No. 1, 480 (1973).
25. Chen, C.J. and Garstang, R.H., "Transition Probabilities For Xe I", J. Quant. Spectry. Rad. Transfer, 10, 1347 (1970).
26. Feltsan, UKR Fiz Zh, 13, 205 (1968).
27. Rostovikova, G.S., Samoilov, V.P. and Smirnov, Yu. M., "Measurements of Cross Section for Excitation of Xenon Lines by Electron Impact", Opt. Spectry., 34, 7 (1973).
28. Borst, W.L., Phys. Rev. A, 9, No. 3, 1195 (1974).
29. Flannery, M.R., Morrison, W.F. and Richmond, B.L. "Excitation in Electron-Metastable Helium Collisions", J. Appl. Phys., 46, No. 3 1186 (1965).
30. Flannery, M.R. and McCann, K.J., "Ten-Channel Eikonal Treatment of Electron-Metastable-Helium Collision: Differential and Integral Cross Sections for $2^{1,3}P$ and $n = 3$ Excitations from He ($2^{1,3}S$) and the (λ, χ, II) Parameters", Phys. Rev. A, 12 No. 3 846 (1965).

31. Holt, H.K. and Krotkov, R., Phys. Rev., 144, 82, (1966).
32. Griem, H.R, "Spontaneous Single-Photon Decay of $2\ ^3S_1$ in Helium-Like Ions", Astrophys. J., 156, 103 (1969).
33. Fel'tsan, "Excitation of Inert Gases by Electron-Atom Collisions", Ukranian Journal of Physics, 12, No. 9, 1425 (1967).